

# **Estimating Aboveground Biomass/Carbon Stock and Carbon Sequestration using UAV (Unmanned Aerial Vehicle) in Mangrove Forest, Mahakam Delta, Indonesia**

EKO KUSTIYANTO

February 2019

SUPERVISORS:

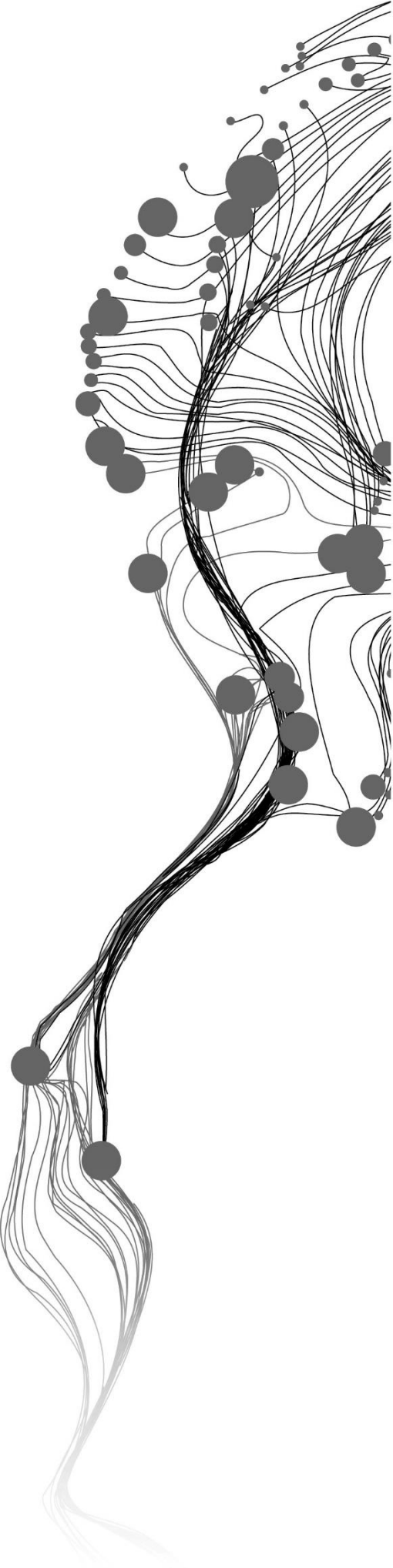
Dr. Yousif A. Hussin

Dr. Iris C. van Duren

ADVISOR:

Dr. Y. Budi Sulistioadi

University of Mulawarman, Samarinda, Indonesia



# **Estimating Aboveground Biomass/Carbon Stock and Carbon Sequestration using UAV (Unmanned Aerial Vehicle) in Mangrove Forest, Mahakam Delta, Indonesia**

Thesis submitted to the Faculty of Geo-Information Science and Earth Observation of the University of Twente in partial fulfilment of the requirements for the degree of Master of Science in Geo-information Science and Earth Observation.

Specialization: Natural Resources Management

## **SUPERVISORS:**

Dr. Yousif A. Hussin

Dr. Iris C. van Duren

## **ADVISOR:**

Dr. Y. Budi Sulistioadi

University of Mulawarman, Samarinda, Indonesia

## **THESIS ASSESSMENT BOARD:**

Dr. Ir. C. A. de Bie (Chair)

Prof. Dr. T.L.U. Kauranne (External Examiner, Lappeenranta  
University of Technology, Finland)



#### DISCLAIMER

This document describes work undertaken as part of a programme of study at the Faculty of Geo-Information Science and Earth Observation of the University of Twente. All views and opinions expressed therein remain the sole responsibility of the author, and do not necessarily represent those of the Faculty.



## ABSTRACT

Mangrove forest which provides ecosystem services plays a pivotal role to storage a large amount of carbon than any other tropical forest. However, the existing mangrove forests are threatened by deforestation and forest degradation. Mahakam Delta mangrove forest, East Kalimantan, Indonesia is one of the most extensive mangrove forests in Southeast Asia which has lost a massive part of its area due to conversion into aquaculture, agriculture, mining, oil exploration and settlement. UNFCCC thought REDD+ program and its MRV mechanism is doing its best to reduce greenhouse gases emission, which is addressed to IPCC for using earth observation data to mitigate climate change. UAV is one of promising advanced technology of remote sensing which has many benefits such as, very-height spatial resolution data, cost-effectiveness, reliable data quality, and multi-temporal. UAV images can be used for forest monitoring and management.

This research aimed to assess aboveground biomass (AGB)/carbon stock using UAV images of 2017 and 2018 as well as calculate carbon sequestration over a one-year period in a part of mangrove forest in Mahakam Delta, East Kalimantan, Indonesia. Fieldwork was done to collect biometric mangrove tree parameters such as diameter at breast height (DBH) and trees height to calculate aboveground biomass/carbon stock and carbon sequestration using UAV images of October 2017 and December 2018. These results were compared with biometric data collected in the field to assess its accuracy.

The results show that there was a significant relationship between crown diameter derived from crown projection area of UAV images and the ground truth DBH of both 2017 and 2018. The results reveal that there was a strong relationship between trees height derived from canopy height model (CHM) of UAV images and trees height derived from terrestrial laser scanner (TLS) data in 2017 and 2018. AGB modelled from UAV images were 102 Mg/ha and 112 Mg/ha in 2017 and 2018, while ABG from biometric (i.e., ground truth) data in 2017 was 104 Mg/ha and in 2018 was 114 Mg/ha. According to the results from UAV images in the period from October 2017 to December 2018, sequestered carbon was 6 Mg/ha/year compared to 5 Mg/ha/years of carbon sequestration assessed using biometric ground truth data.

**Keywords:** Mangrove, UAV, ground truth data, aboveground biomass, carbon sequestration.

## ACKNOWLEDGEMENTS

First and foremost, I would like to acknowledge my supervisors, Dr. Yousif A. Hussin and Dr. Iris C. van Duren for the constructive remarks, encouragement and discussion during the thesis research period. I believe that I have been exceptionally fortunate to have them as my supervisors.

I highly acknowledge and appreciate my advisor, Dr. Y. Budi Sulistioadi and the Faculty of Forestry University of Mulawarman, Samarinda, Indonesia for facilitating our research work, helping us with the logistic, collecting image and ground truth data in Tani Baru mangrove forest. I highly appreciate the support of the team of Dr. Y. Budi Sulistioadi: Mita Priskawanti and Muhammad Lutfi Hamdani for their continuous help during October 2018. I acknowledged the UAV data collection by Dr. Y. Budi Sulistioadi in 2017 and 2018. Without data and support, our research would not have been done.

I would like to express my gratitude to Dr. Ir. C.A.J.M de Bie as the Chairman of the thesis assessment board for the pivotal and valuable suggestions as well as discussions during the proposal and mid-term defence which assist me to enhance my research method.

I would also like to thank the NRM course director Drs. R. G. Nijmeijer, for coordination of the coursework and facilitating the thesis mechanism. I am very fortunate to have him as my course director.

I highly acknowledge and appreciate the support of the Indonesian Ministry of Science and Technology and Higher Education by offering our team a research permit to execute our research activities and our fieldwork in Indonesia. I would like to express my gratitude to the Ministry of Science and Technology and Higher Education (Kemenristekdikti) through Riset-Pro scholarship for giving me funding and opportunity to study in ITC, University of Twente.

Great honour to give thanks to the Agency for the Assessment and Application of Technology (BPPT) of The Republic of Indonesia for giving me the opportunity and permission to study overseas in order to enhance and expand knowledge of geospatial science and technology.

I would also like to thank all the NRM staff and NRM 2017/2019 batch classmate from all over the world for sharing ideas, knowledge and experiences. I would like to appreciate to my NRM fieldwork mates of Kalimantan group for participation and cooperating during the fieldwork ground truth data collection.

Great honour to acknowledge and appreciation to ITC Indonesian students, especially batch 2017/2019 for the wonderful time spent. The Netherlands feel like home due to their presence, and it could release the tension into happiness through togetherness.

I highly express my gratitude to my parents, my sister and my relatives for their lovely and moral support by putting me in their prayers to achieve my dream. Without their support, it is difficult to finish the thesis and manage my physiological issue.

# TABLE OF CONTENTS

---

Abstract.....	i
Acknowledgment.....	ii
Table of Contents.....	iii
List of Figures.....	vi
List of Tables.....	viii
List of Acronyms.....	ix
1. Introduction.....	1
1.1. Background.....	1
1.2. Problem statement.....	2
1.3. Research objectives.....	4
1.3.1. Main objectives.....	4
1.3.2. Specific objectives.....	4
1.3.3. Research question.....	4
1.3.4. Hypothesis.....	4
1.4. Conceptual diagram.....	5
1.5. Literature review.....	6
1.5.1. Biomass and carbon stock in mangroves forest.....	6
1.5.2. Unmanned Aerial Vehicle.....	6
1.5.3. The Crown cover of tree.....	7
1.5.4. Canopy height model.....	8
1.5.5. Error measurement of tree height using handheld laser instrument.....	9
2. Materials and Methodology.....	10
2.1 Study area.....	10
2.2 Materials.....	10
2.2.1 Data.....	11
2.2.2 Software.....	11
2.2.3 Equipment.....	12
2.3 Research method.....	13
2.4 Fieldwork planning.....	15
2.4.1 Sampling plot design.....	15
2.4.2 UAV flight planning.....	15
2.5 Field data collection.....	16
2.5.1 Ground truth data acquisition.....	16
2.5.2 UAV image data acquisition.....	18
2.6 Ground truth data processing.....	19
2.6.1 Ground truth data.....	19
2.6.2 Backward prediction.....	19
2.6.3 Wood density.....	19
2.7 UAV Image processing.....	20
2.7.1 Tree Reconstruction.....	20
2.7.2 Manual digitising of CPA.....	21
2.7.3 Extracting individual tree height of CHM.....	22
2.8 Data analysis.....	22

2.8.1	Relationship between DBH and crown diameter.....	22
2.8.2	Predicted DBH model and validation.....	23
2.8.3	Relationship between trees height and CHM.....	23
2.8.4	Calculation of aboveground biomass.....	23
2.8.5	Calculation of carbon stock and carbon sequestration.....	23
3.	Results.....	24
3.1	Statistics of field data collection.....	24
3.1.1	Biometric DBH field data collection.....	24
3.1.2	Biometric tree height measured Leica DISTO D510 laser ranger.....	25
3.1.3	Tree height derived from TLS point clouds data.....	26
3.1.4	Comparison biometric and TLS tree height.....	27
3.2	Backward prediction of 2017.....	28
3.2.1	The results of backward prediction of DBH 2017.....	28
3.2.2	The results of backward prediction of TLS tree height 2017.....	29
3.3	UAV image processing.....	29
3.3.1	UAV 2018 image processing.....	30
3.3.2	Orthomosaic, DSM and DTM of UAV 2018.....	30
3.3.3	Generating CHM 2018.....	32
3.3.4	UAV 2017 image processing.....	33
3.3.5	Orthomosaic, DSM and DTM of UAV 2017.....	33
3.3.3	Generating CHM 2017.....	35
3.4	Crown Projection Area.....	36
3.4.1	The crown projection area of 2018.....	36
3.4.2	The crown projection area of 2017.....	36
3.5	Crown Diameter.....	37
3.5.1	The crown diameter of 2018.....	37
3.5.2	The crown diameter of 2017.....	38
3.6	Crown Height Measurement.....	39
3.6.1	The crown height measurement of 2018.....	39
3.6.2	The crown height measurement of 2017.....	40
3.7	The relationship between DBH and CPA.....	41
3.7.1	The relationship between DBH and CPA of 2018.....	41
3.7.2	The relationship between DBH and CPA of 2017.....	41
3.8	The relationship between tree height derived TLS and tree height derived CHM of UAV.....	42
3.8.1	The relationship between tree height TLS and CHM of 2018.....	42
3.8.2	The relationship between tree height TLS and CHM of 2017.....	42
3.9	The relationship between DBH and CD.....	42
3.9.1	The relationship between DBH and CD of 2018.....	43
3.9.2	The relationship between DBH and CD of 2017.....	43
3.10	Model of predicted DBH.....	43
3.10.1	Model of predicted DBH 2018.....	43
3.10.2	Model of predicted DBH 2017.....	44
3.11	Validation of predicted DBH.....	44
3.11.1	Validation of predicted DBH 2018.....	44
3.11.2	Validation of predicted DBH 2017.....	44
3.12	Aboveground biomass.....	45

3.12.1 Comparison biometric and modelled of ABG 2018 .....	46
3.12.2 Comparison biometric and modelled of AGB 2017 .....	47
3.12.3 Comparison biometric and modelled of AGB sequestration .....	47
3.13 Carbon stock.....	48
3.13.1 Comparison biometric and modelled of carbon stock 2018.....	48
3.13.2 Comparison biometric and modelled of carbon stock 2017.....	49
3.13.3 Comparison biometric and modelled of carbon sequestration .....	51
4. Discussion .....	52
4.1 Uncertainties of fieldwork data measurement.....	52
4.2 Quality of point cloud and orthophoto of UAV .....	53
4.3 Estimated DBH using the crown diameter .....	55
4.4 Estimated tree heigh using CHM.....	56
4.4.1 Mangrove Blue carbon sedimentation affecting the assessment of DTM.....	58
4.5 AGB/Carbon stock estimation .....	58
4.6 Carbon sequestration estimation .....	60
4.7 Limitation.....	60
5. Conclusion .....	61
List of References.....	62
Appendices.....	64

## LIST OF FIGURES

---

Figure 1.1 Conceptual diagram of the research.....	5
Figure 1.2 Carbon flux in mangrove. ....	6
Figure 1.3 Structure from motion.....	7
Figure 1.4 Measuring crown projection area and crown diameter. ....	8
Figure 1.5 DSM and DTM. ....	8
Figure 1.6 Tree height error due to the stand distance position using handheld laser height measuring instrument.....	9
Figure 2.1 Location of the study area.....	10
Figure 2.2 Flowchart of research method. ....	13
Figure 2.3 Ground Control Points (GCP) used in the study area before UAV flight. ....	16
Figure 2.4 Measuring DBH using diameter type.....	17
Figure 2.5 Measuring tree height using Leica Disto D510 laser ranger(a) and using TLS RIEGL VZ400 (b).....	17
Figure 2.6 Some steps in collecting UAV images using DJI Phantom 4.....	18
Figure 2.7 Marking appeared GCP on image in PIX4D Mapper.....	20
Figure 2.8 Manual digitising of CPA 2017 and CPA 2018. ....	21
Figure 2.9 Example of individual tree height derived CHM 2017 and CHM 2018.....	22
Figure 3.1 Distribution of the number of trees in each plot. ....	24
Figure 3.2 Histogram distribution of biometric DBH measured in the field. ....	25
Figure 3.3 Histogram distribution of biometric trees height measured in the field. ....	25
Figure 3.4 Histogram distribution of trees height derived from TLS point cloud data.....	26
Figure 3.5 Trees height measured using Leica DISTO D510 laser Ranger and TLS trees height.....	27
Figure 3.6 Scatterplot of TLS and Leica DISTO measured trees height regression analysis.....	27
Figure 3.7 Histogram distribution of DBH of 2017 calculated using backward prediction. ....	28
Figure 3.8 Histogram of TLS trees height measurements in 2017 calculated using backward prediction. ..	29
Figure 3.9 UAV 2018 image processing. ....	30
Figure 3.10 Orthomosaic image of UAV 2018. ....	31
Figure 3.11 DSM and DTM UAV 2017.....	32
Figure 3.12 CHM of UAV 2018. ....	32
Figure 3.13 UAV 2017 image processing.....	33
Figure 3.14 Orthomosaic UAV image of 2017. ....	34
Figure 3.15 DSM and DTM images of UAV 2017.....	35
Figure 3.16 CHM image of UAV 2017.....	35
Figure 3.17 Histogram distribution of the crown projection area in 2018. ....	36
Figure 3.18 Histogram distribution of the trees crown projection area in 2017.....	37
Figure 3.19 Histogram distribution of crown diameter of trees in 2018.....	38
Figure 3.20 Histogram distribution of trees crown diameter in 2017.....	39
Figure 3.21 Histogram CHM 2018.....	40
Figure 3.22 Histogram distribution of trees height or CHM in 2017.....	40
Figure 3.23 Relationship of DBH and CPA of 2018.....	41
Figure 3.24 Relationship of DBH and CPA of 2017.....	41
Figure 3.25 Relationship between tree height TLS and CHM of 2018. ....	42
Figure 3.26 Relationship between tree height TLS and CHM of 2017. ....	42
Figure 3.27 Relationship between DBH and CD of 2018.....	43

Figure 3.28 Relationship between DBH and CD of 2017. ....	43
Figure 3.29 Relationship between CD and DBH of the model of predicted DBH 2018. ....	44
Figure 3.30 Relationship between CD and DBH of the model of predicted DBH 2017. ....	44
Figure 3.31 Relationship between CD and DBH of the validation of predicted DBH 2018. ....	45
Figure 3.32 Relationship between CD and DBH of the validation of predicted DBH 2017. ....	45
Figure 3.33 Comparison biometric and modelled AGB in 2018. ....	46
Figure 3.34 Relationship between biometric and modelled of AGB in 2018. ....	46
Figure 3.35 Comparison of biometric and modelled AGB in 2017. ....	47
Figure 3.36 Relationship between biometric and modelled of AGB in 2017. ....	47
Figure 3.37 Comparison biometric and modelled of AGB sequestration. ....	48
Figure 3.38 Relationship between biometric and modelled AGB sequestration. ....	48
Figure 3.39 Comparison biometric and modelled of carbon stock in 2018. ....	49
Figure 3.40 Relationship between biometric and modelled of carbon stock in 2018. ....	49
Figure 3.41 Comparison biometric and modelled of carbon stock in 2017. ....	50
Figure 3.42 Relationship between biometric and modelled of carbon stock in 2017. ....	50
Figure 3.43 Comparison biometric and modelled of carbon sequestration. ....	50
Figure 3.44 Relationship between biometric and modelled of carbon sequestration. ....	51
Figure 4.1 Number of overlapping images in UAV 2017 and UAV 2018. ....	54
Figure 4.2 Relationship between crown DBH and CD (A), relationship between CD and biomass (B). ....	56
Figure 4.3 A comparison of the growth of mangrove trees in approximately one-year (A) 2017 and (B) 2018. ....	57
Figure 4.4 Soil deposit and sedimentation on top of the mangrove floor. ....	58
Figure 4.5 Plot-5 as an example of high biomass plots that show high-density big trees. ....	59

## LIST OF TABLES

---

Table 2.1 Data and source of data used in this research.....	11
Table 2.2 Software used in this research.....	12
Table 2.3 Fieldwork equipment. ....	12
Table 2.4 UAV flight plan parameters used in this research.....	15
Table 2.5 UAV data collection of 2017 and 2018.....	18
Table 2.6 The mean annual increment of DBH and tree height. ....	19
Table 2.7 Wood density of mangrove tree species. ....	19
Table 3.1 Descriptive statistics of fieldwork data collection in all 30 plots.....	24
Table 3.2 The number of trees according to different species. ....	24
Table 3.3 Summary statistics of biometric trees height measured in the field. ....	25
Table 3.4 Summary statistics of trees height measured using TLS point clouds data.....	26
Table 3.5 Summary statistics of DBH of 2017 calculated using backward prediction. ....	28
Table 3.6 Summary statistics of TLS trees height in 2017 calculated using backward prediction. ....	29
Table 3.7 UAV 2018 imaging parameters. ....	30
Table 3.8 UAV 2018 images result.....	31
Table 3.9 GCPs of UAV 2018. ....	31
Table 3.10 UAV 2017 imaging parameters. ....	33
Table 3.11 UAV 2017 imaging parameters. ....	34
Table 3.12 GCPs of UAV 2018.....	34
Table 3.13 Statistics summary of crown projection area measured from UAV images of 2018.....	36
Table 3.14 Statistics summary of crown projection area in 2017. ....	37
Table 3.15 Statistics summary of crown diameter 2018.....	38
Table 3.16 Statistics summary of crown diameter 2017.....	38
Table 3.17 Statistics summary of CHM 2018. ....	39
Table 3.18 Statistics summary of CHM 2017. ....	40
Table 3.19 Statistics summary of aboveground biomass .....	45
Table 3.20 Statistics summary of carbon stock .....	49

## LIST OF ACRONYMS

---

AGB	Above Ground Biomass
CD	Crown Diameter
CF	Conversion Factor
CHM	Canopy Height Model
CPA	Crown Projection Area
DBH	Diameter Breast Height
DSM	Digital Elevation Model
DTM	Digital Terrain Model
FAO	Food and Agriculture Organization
GPS	Global Positioning System
IPCC	International Panel on Climate Change
MRV	Monitoring Reporting and Verification
REDD+	Reduce Emission from Deforestation and Degradation Measurement
RMSE	Root Mean Square Error
SfM	Structure from Motion
TLS	Terrestrial Laser Scanner
RTK	Real Time Kinematic
UAV	Unmanned Aerial Vehicle
UNFCCC	United Nation Framework Convention on Climate Change



# 1. INTRODUCTION

## 1.1. Background

Mangroves are coastal forests ecosystems which influenced by tides and can be found in tropic and sub-tropic countries. Generally, the habitats of mangroves are in saline and brackish environment where located in humid to temperate climatic zone, approximately in latitude from 25° N to 25° S as well as facing with permanent tidal inundation in fringe mangrove area close to the sea and temporary spring tide flooded habitat (Kauffman & Donato, 2012). Mangroves forest has unique trees and shrubs which adapted to the daily fluctuation of saline and freshwater, ocean tides, topographic structure, sedimentation and soil deposit. Thus most of them have aerial roots system for respiration in interphase ecosystem between land and saline water (FAO, 2007).

Mangrove forests have a lot of benefits for the local community up to national level which consists of the ecologic, ecosystem and social-economic value. According to ecological services, mangroves has functions as carbon storage/carbon sequestration, nursery, coastal protection and natural land expansion (Lee et al., 2014), while that environment also have ecosystem functions such as biodiversity, environment protection, adaptation and mitigation for climate change (Tuan et al., 2012). Mangrove ecosystem also can store three times higher than common terrestrial forest approximately 937 Mg C/ha on average (Alongi, 2002). Moreover, mangroves can generate social-economic value for the local community from tourism, recreation, education and scientific research as well revenue from carbon trade of REDD+ program (Barbier et al., 2011; Warren-Rhodes et al., 2011).

Generally, the mangroves forest illustrates two different concepts. Firstly, these ecosystems represent an ecological of evergreen plant species to several trees families which have similar biophysical characteristics and environmental adaptation and similar habitat preference. Secondly, mangroves are a complex community of trees which has a function as coastal protection. As communities, mangroves consist of trees and shrubs which grow in a muddy soil of the tidal zone and are influenced by marine and estuary ecosystems (Lee et al., 2014). Mangrove forest is also the home for many creatures, such as fishes, crabs, shrimps and different kind of molluscs and aquatic creatures, where all of this avifauna utilise mangroves as nursery and shelter during juvenile stage (Barbier et al., 2011).

FAO (2007), reported that there were 15.2 million hectares of mangroves in the world, where 42% is concentrated along of the coastline in South and South-east Asia (Gopal, 2013), and 3.1 million hectares are located and spreading in the archipelago of Indonesia (Giri et al., 2011). However, global destructions in mangroves areas occur due to economic and population growth such as urban expansion, aquaculture and agriculture, oil and mining, as well as overlogging (Alongi, 2002). Pendleton et al. (2012), counted that every year the global rate of converted mangrove is 1.9%, equal to 1.02-billion-tons of carbon dioxide emitted, which causes an economic loss of approximately 42 billion US\$. Indonesia as the largest mangroves country in the world is also lost those areas, for example in Mahakam Delta, 63% of 770 square km areas were converted to aquaculture, oil and mining exploration, palm oil plantation and human settlement between 1990 and 2000, which have direct negative effect in environmental, economic and social for local communities (A.S Sidik, 2010).

UNFCCC (United Nation Framework Convention on Climate Change) through REDD+ program has technical approach or a mechanism by measurement, reporting and verification (MRV) for reduction emission from deforestation and forest degradation, preservation of carbon storage, increment forest carbon stock and sustainable forest management which addressed to IPCC (Intergovernmental Panel on Climate Change/scientific expert) using remote sensing data to inventory greenhouse gases, field-based data

collection and land cover change (US Agency for International Development, 2014). Based on this approach, remote sensing can be applied to provide information to deal with the issues of destructions in the mangroves ecosystem related to REDD+.

Forest, which stores and sequesters carbon has an important role to cope with climate change and is more adaptable to reduce emission than another environment, where store carbon mostly in the aboveground biomass (AGB) of trees. This means forest is the most influenced cover types by deforestation and forest degradation (Gibbs et al., 2007). Estimating biomass give an overview in term of the potential of trees ecosystem to store or emit carbon to the atmosphere and carbon can be calculated by halving the value of biomass.

Gibb et al., (2007) also described that there are six methods to estimate biomass/carbon stock, which comprises biome averages, forest inventory, passive optical remote sensing, very-high spatial resolution airborne optical remote sensing, active remote sensing and laser remote sensing. Each one of the mentioned method has advantages and disadvantages as well as the level of its uncertainty. In general, biomass is estimated using a destructive method by cutting of the trees and weighted the dry biomass. Although it has high accuracy, it is time-consuming, expensive and field labours involved. Whereas the other method is non-destructive, which can be applied using a remote sensing technique (Rahman et al., 2017). These methods inventory trees biophysical parameters, such as diameter breast high (DBH), tree height, canopy cover and density, trees species and location of the trees in the field. This can be done by direct or indirect measurement. Then, using the allometric equation which is a mathematic equation representing the relationship between biomass and DBH, tree height as well as canopy cover to derive biomass/carbon stock.

Very high spatial resolution data acquired from the unmanned aerial vehicle (UAV) become more popular to derive proper data such as mapping, generated the 3D model, surveillance and inspection (Nex & Remondino, 2014). UAV technique to assess biomass is a combination of basic photogrammetry and computer vision employing a sequence of images by structure from motion (SfM), and the results of this process are generated point clouds, 3D model and orthophoto. UAV has several benefits such as cost-effective, very high spatial resolution image, alternative methodology generated 3D points cloud, fast acquired data, and bridging the gap between field data measurement and satellite imagery data. However, it also has limitation, for instances flight height, endurance of battery, payload, area extends to be captured, the number of generated points cloud, and unable to capture understorey (Zahawi et al., 2015).

## 1.2. Problem statement

Mangroves have an important role to cope with climate change and have ecosystem services such as carbon storage. In fact, mangroves are one of the most prominent carbon sink ecosystems, which store carbon approximately 1,023 ton/ha, including both above and below ground biomass (Donato et al., 2011). Komiyama (2008) reported that above ground biomass of mangroves reaches 436.4-ton carbon/ha are varying depending on age, species and location. It is almost double compared to a tropical forest, estimated 228.7 Mg C/ha (Baccini et al., 2012). However, estimating biomass/carbon stock in a unique mangroves ecosystem is challenging due to the structure of trees, habitat, location and accessibility.

UNFCCC has the initiative REDD+ program and its mechanism MVR to monitor, verify and report carbon emission base on ecosystem service to obtain global benefits using remote sensing data and field-base measurement (Stickler et al., 2009). Monitoring could be applied to get information related to the natural dynamic of forest and the changes in the forest area due to natural disturbance and human encroachment (Giri et al., 2007). On the other hands, monitoring has to deal with multi-temporal or spatio-temporal data to achieve information in term of dynamic changes.

One of the applications on monitoring, verification and reporting in term of REDD+ is using remote sensing data to estimate carbon stock in mangroves forest. The monitoring of mangrove requires accurate data to extract information to help to manage, such an important natural resource. Remote sensing is

essential as data source and technique to derive biometric mangrove trees parameters (e.g. DBH and height) to be used for biomass/carbon stock assessment and other management purpose (Boehm et al., 2013). The integration of remotely sensed data with ground truth would help to assess the mangrove its biomass, biophysical conditions and sustainable forest management.

There are several studies which have conducted in the mangroves area to assess biomass/carbon stock using different remote sensing data with some benefits and drawback. The majority of them is by using satellite data both active and passive sensor, as well as terrestrial and airborne LiDAR ( Le Toan et al., 2004; Boudreau et al., 2008; Dube & Mutanga, 2015). Those data have limitations, for instances, optical remote sensing has medium to coarse spatial resolution, and its energy cannot penetrate cloud and other atmospheric disturbance. Radar has a drawback such as coarse spatial resolution, error variation related to topographic, and other difficulties in complex canopy structure. While Lidar required field data calibration, expensive, time-consuming, and cannot penetrate leaves. Based on all issues mentioned, there are a lot of uncertainties using these sensors.

In contrast, there are few studies done in mangroves for forest inventory or biomass/carbon stock assessment using UAV (Zahawi et al., 2015; Tian et al., 2017; Otero et al., 2018). Surprisingly, those studies acknowledged that using UAV is a low-cost, rapid processing, time-effectiveness, reasonable accuracy and multi-temporal acquisition data, which is promising for monitoring application. UAV can capture a relatively large area with very high spatial resolution. It also flies with low altitude less than 100 m above the ground to minimise cloud and atmospheric disturbances as well as to get a higher quality of ground sample distance. Moreover, it can acquire data more rapid and frequent.

Furthermore, UAV captures areas of interest using different sensor and camera to obtain a specific characteristic of the object sensed. RGB sensor is generally assembled on UAV, while others sensor, such as (e.g. Sequoia and FirefLEYE) can be installed for a specific application such as forest, agriculture and urban area since they have infrared and red-edge spectral bands. Here, one of the applications of the multispectral sensor of Sequoia camera which has five bands namely green, red, red-edged, near infra-red and RGB, is to distinguish trees species by digital image classification.

The accuracy assessment of remotely sensed data can be done using ground truth data as a reference to validate the derived data from UAV. Structure for motion (SfM) is applied to reconstruct 3D space image from 2D scene base on consecutive overlapped images to generates data such as points cloud, digital surface model (DSM), digital retain model (DTM), orthophoto, mosaic and finally canopy height model (CHM) which is the tree height in the case of inland and mangrove forest (Remondino, et al., 2014). In this case, ground truth data of tree height is employed to assess the accuracy of crown height measurement (CHM) derived from DSM and DTM data. Whereas, crown projection area (CPA) which is obtained from UAV mosaic images, can be segmented automatically using the OBIA technique (Blaschke, 2010), assessed by manual on-screen digitation. CPA can also be used to model DBH since there is a relationship between these two parameters. Consequently, above ground biomass (AGB) and carbon stock can be assessed using the estimated height and modelled DBH with reasonable accuracy.

Therefore, this research will assess the application of UAV images to estimate above ground biomass/carbon stock and carbon sequestration in the mangrove area, where these areas comprise natural and planted mangrove ecosystem. The derived data (predicted DBH and trees height derived from CHM) from UAV images then will be evaluated with ground truth data for accuracy assessment. The main issues in this research are mangrove area which sequesters more carbon compared to another forest ecosystem. Thus, using two different years of UAV images data, monitoring carbon sequestration is possible. Meanwhile, the UAV data gives very high spatial resolution, cost-effectiveness, time-efficient and multi-temporal acquisition data serving the purpose REDD+ MRV approaches. Looking at the scientific published literatures, there is hardly any publication on the use of UAV images for assessing carbon sequestration in the mangrove forest. We believe that this research is an innovative one.

### **1.3. Research objectives**

#### **1.3.1. Main objectives**

The main objective of this research is to assess aboveground biomass/carbon stock using UAV (Unmanned aerial vehicle) images of 2017 and 2018 as well as calculate carbon sequestration over one-year period in a mangrove forest in part of Mahakam Delta, East Kalimantan, Indonesia.

#### **1.3.2. Specific objectives**

1. Assessing the relationship of crown diameter (CD) derived from the crown projection area (CPA) of UAV images and diameter at breast height (DBH) measured in the field.
2. Estimating trees height using point clouds of UAV images through canopy height model (CHM) and assessing its accuracy using trees height derived from terrestrial laser scanner (TLS) point clouds data.
3. Assessing above ground biomass (AGB)/carbon stock of the years 2018 and 2017 and assessing its accuracy using UAV images and ground truth data.
4. Assessing carbon sequestration of mangrove forest in the period of one year between the end of October 2017 and mid-December 2018.

#### **1.3.3. Research question**

1. What is the relationship between crown diameter derived from CPA of UAV images and DBH of ground truth data?
2. What is the relationship between trees height derived from CHM of UAV images and trees height derived from TLS point clouds data?
3. What are AGB/carbon stock modelled from UAV images in 2017 and 2018 in the study area and how accurate are these results compared to the biometric data?
4. What is the carbon sequestration modelled from UAV images of the years 2017 and 2018 and how accurate is it?

#### **1.3.4. Hypothesis**

1. Ho: There is no significant relationship between crown diameter derived from CPA of UAV images and DBH of ground truth data.  
H1: There is a significant relationship between crown diameter derived from CPA of UAV images and DBH of ground truth data.
2. Ho: There is no significant relationship between trees height derived from CHM of UAV images and trees height derived from TLS point clouds data.  
H1: There is a significant relationship between tree height derived CHM of UAV and trees height derive TLS point clouds data.
3. Ho: There is no significant relationship between AGB/carbon stock modelled from UAV images in 2017 and 2018 and AGB/carbon stock of biometric data in 2017 and 2018.  
H1: There is a significant relationship between AGB/carbon stock modelled from UAV images in 2017 and 2018 and AGB/carbon stock of biometric data in 2017 and 2018.
4. Ho: There is no significant relationship between carbon sequestration modelled from UAV images of the years 2017 and 2018 and carbon sequestration of the biometric data of 2017 and 2018.  
H1: There is a significant relationship between carbon sequestration modelled from UAV images of the years 2017 and 2018 and carbon sequestration of the biometric data of 2017 and 2018.

### 1.4. Conceptual diagram

Mangrove forest in Mahakam Delta, Indonesia has ecosystem services and play an important role to sequester carbon, where mangrove can store carbon higher than another inland tropical forest. On the other hands, economic and population growth are pushing to convert mangroves to other land use, such as shrimp pond, oil palm plantation, mining area and settlement due to market demands. It means that deforestation and forest degradation in mangroves forest of Delta Mahakam emitted carbon due to land use land cover change.

UNCFF has initiative REDD+ MVR program using remote sensing data to estimate carbon stock and carbon sequestration. In this thesis research, UAV images is used to estimating tree parameters, such as crown diameter, species, diameter breast height and trees height which are validated by ground truth data. Carbon stock data gives information to REDD+ MRV to offer compensation and payment for the Mahakam area. There is also a social responsibility from the local community to replanting shrimp ponds with mangroves in term of conservation and restoration. Figure 1.1 shows a conceptual diagram of this research.

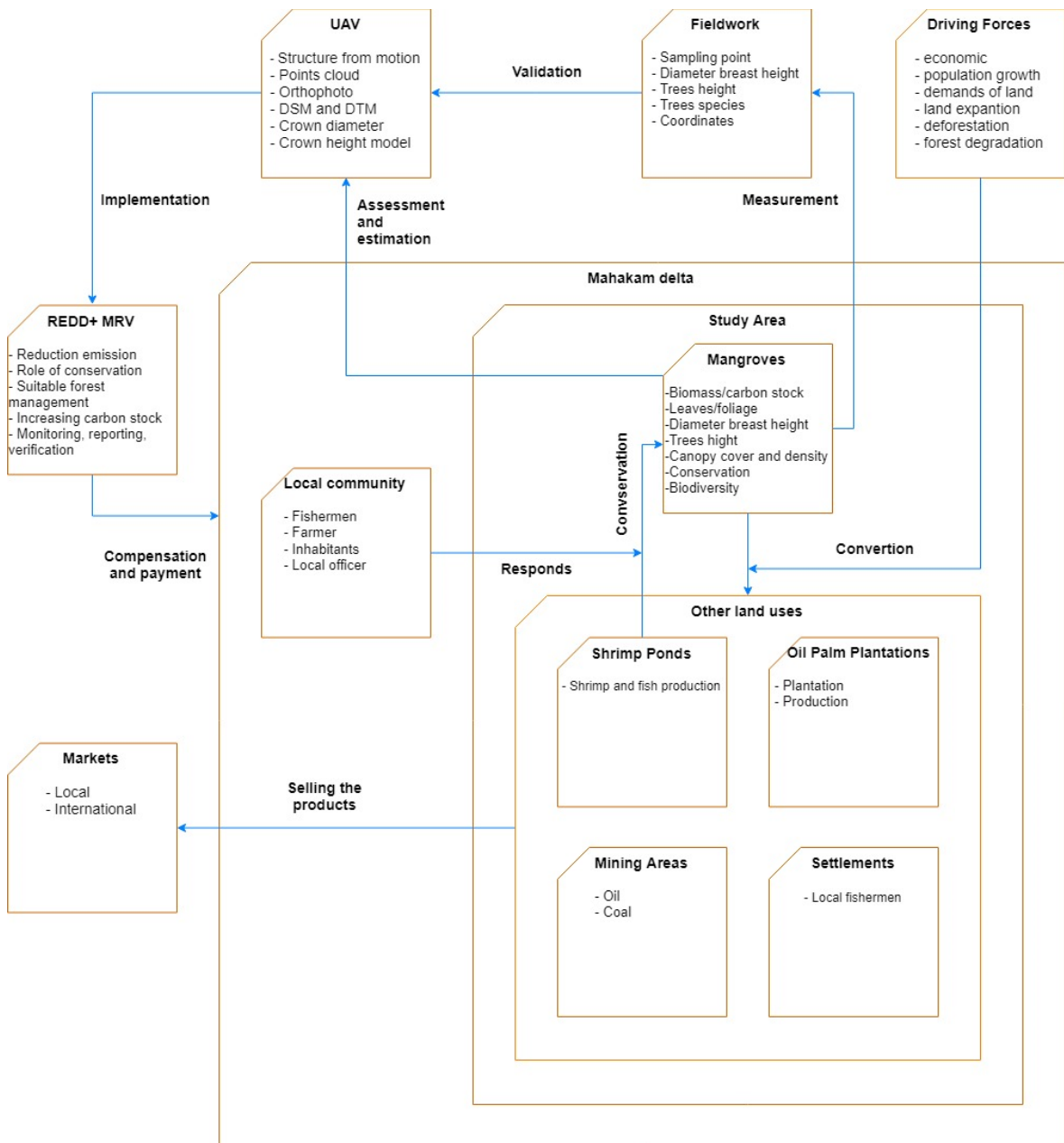


Figure 1.1 Conceptual diagram of the research.

## 1.5. Literature review

### 1.5.1. Biomass and carbon stock in mangroves forest

Mangrove is the type of vegetation grows in the area between land and sea (intertidal zone) which influenced by its environment such as tide, temperature, salinity and sedimentation ((Nagelkerken et al., 2008). There are more than 110 mangroves trees species belong to only 16 families which include 20 genera, and 54 species are recognised as true mangroves which are growing in mangrove habitat (Kuenzer et al., 2011). Regarding environmental adaptation, mangrove has two type of rooting systems comprise of aerial root and below ground root due to salinity and an anoxic factor of its location (Adame et al., 2017).

Mangroves have valuable ecosystem services such as timber and non-timber product, coastal protection, environmental control, water catchment, wildlife habitat, tourism, education and research as well as carbon sequestration (Barbier et al., 2011). In term of carbon stock and carbon sequestration, mangrove act as a potential sink which store and release carbon into the atmosphere (Figure 1.2). Surprisingly, some studies reveal that mangrove store more biomass than other tropical forests in below ground biomass (Soares et al., 2005; Donato et al., 2011). Aboveground biomass is living biomass that contains leaves, trunk, branch and stem while below ground biomass refer to roots, litter, the dead body of the tree, and soil organic matter (Gibbs et al., 2007). Biomass is calculated as the total dry weight of the trees per unit area that usually defined in ton per hectare (Mg/Ha).

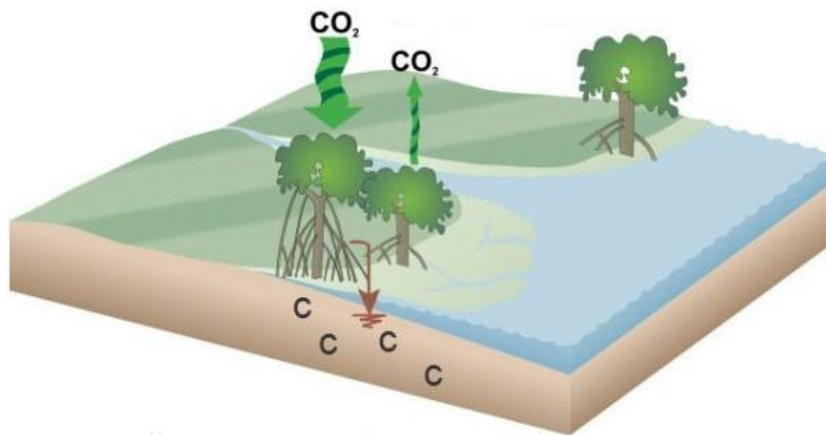


Figure 1.2 Carbon flux in mangrove.

(Modified from: <https://blueocean.net/mangroves-super-forests-must-protect/>).

The destructive method is the direct measurement to quantify biomass by harvesting trees, oven-drying until constant weight and weighing the total mass of the trees. While the non-destructive method is to make the relationship between biometric trees parameters to calculate the weight using the allometric equation (Gonzalez de Tanago et al., 2018; Disney et al., 2018). In term of carbon stock calculation, it is referred to 50% of biomass or approximately 47% which depend on species (Brown, 2002; IPCC, 2006).

### 1.5.2. Unmanned Aerial Vehicle

Unmanned aerial vehicle (UAV) is also recognised as an unmanned aerial system (UAS), the remotely-piloted aerial system (PRAS), or drone which become popular for multi-applications in recent years due to the quality of high spatial resolution aerial images, initially were used for military purposes (Colomina & Molina, 2014). UAV is new platform run by a small fix-wing or rotary-wing aircraft using remotely pilot system which consists of compact and affordable GPS receiver, an inertial measuring unit (IMU) and sensor or camera for capturing the images (Torresan et al., 2016).

UAV offers a fine spatial resolution, cost-effectiveness, reliable data quality, a multi-temporal and consistent outcome which have potential applications for forest management and inventory such as tree segmentation and tree detection (Wallace et al., 2016). Furthermore, the relationship of canopy measurement derived from UAV image and ground truth inventory data has a strong correlation in local scale or species level to generate the robust result of forest inventory (Zhang et al., 2016).

The products of UAV image acquisition are consecutive overlapped images, which are processed using the structure from motion (SfM) method to generate derived results such as 3D point cloud, orthophoto, digital surface model, a digital terrain model and canopy height measurement. SfM method has four stages to reconstruct 3D point clouds that consist of matching point through the whole consecutive overlapped images, recognize the structure and motion recovery of object in the images, refining the existing structure and calculate the camera position for additional images, as well as using bundle block adjustment to refine the structure and motion of the image (Nex, 2018). Figure 1.3 illustrates the SfM between the two adjection image to reconstruct the structure and motion of an object in the images.

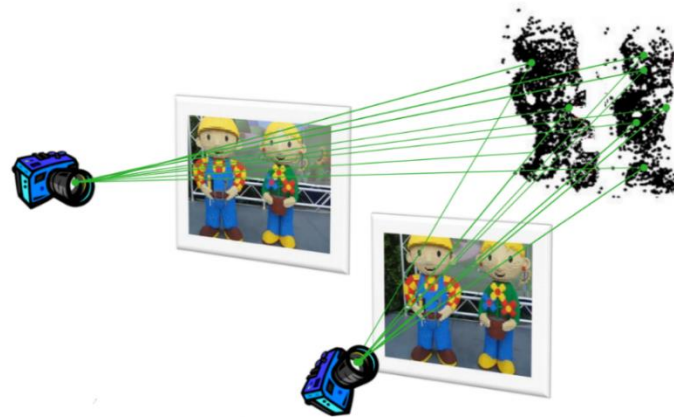


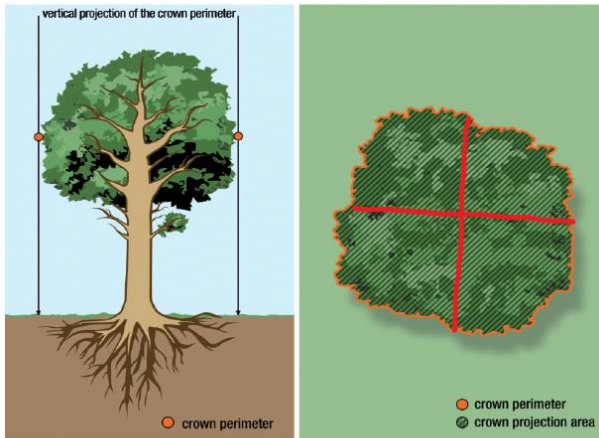
Figure 1.3 Structure from motion.

(Modified from: [https://blackboard.utwente.nl/bbcswebdav/pid-1118314-dt-content-rid-2896431\\_2/courses/M18-EOS-103/04\\_SfM.pdf](https://blackboard.utwente.nl/bbcswebdav/pid-1118314-dt-content-rid-2896431_2/courses/M18-EOS-103/04_SfM.pdf)).

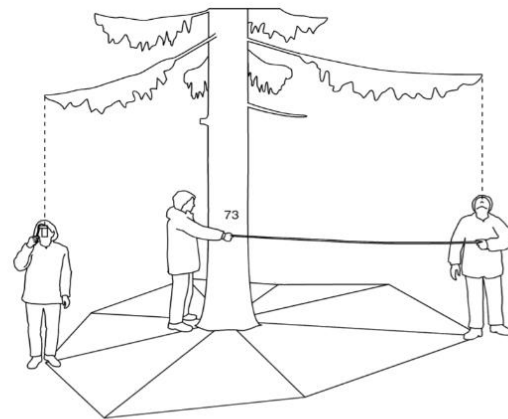
### 1.5.3. The Crown cover of tree

Tree crown diameter and tree projection area represent the canopy cover of trees in two dimensions which measured in meter and meter square respectively. Crown of the tree represents the information of growth of tree, shadow, stream, purify air particles, wind protection as well as biomass and carbon sequestration which affected by species, the age of the tree, resources supply, habitat, location and environment (Pretzsch et al., 2015). The crown diameter is calculated by measuring two perpendicular directions of the crown area and come up with the average of two values while crown projection area was calculated by delineating outermost perimeter of canopy cover in two dimensions horizontal projection (Gschwantner et al., 2009; Pretzsch et al., 2015). Figure 1.4 represents the measurement of the crown projection area and crown diameter.

The crown of trees can be estimated using remote sensing images, some researches have proved that there is high correlation between the area of crown of trees or crown projected area (CPA) and diameter at breast height (DBH). Therefore, CPA can be used to calculate volume or biomass of trees (Pham et al., 2019; Wannasiri et al., 2013; Hirata et al., 2014). Popescu et al., (2003) have explained that using crown diameter on remote sensing image and point cloud of Lidar could improve significantly the estimation of volume and biomass, while Galvencio & Popescu, (2016) were employed Lidar to estimate quantitative biophysical parameters such as tree height, CPA and crown diameter and revealed that this method can improve the estimation in local-individual tree level.



a. Crown projection area



b. Crown diameter

Figure 1.4 Measuring crown projection area and crown diameter.

(Modified from: Gschwantner et al., 2009 and Pretzsch et al., 2015).

#### 1.5.4. Canopy height model

Tree height is one indicator of the growth system of vegetation that can be calculated using direct measurement or estimation using 3D point cloud. As shown in Figure 1.5, the digital surface model (DSM) is a 3D surface model that include vegetation, building, and an artificial object, while the digital terrain model (DTM) represent the 3D ground surface. Thus, CHM of tree height is generated by subtracting DTM from DSM.

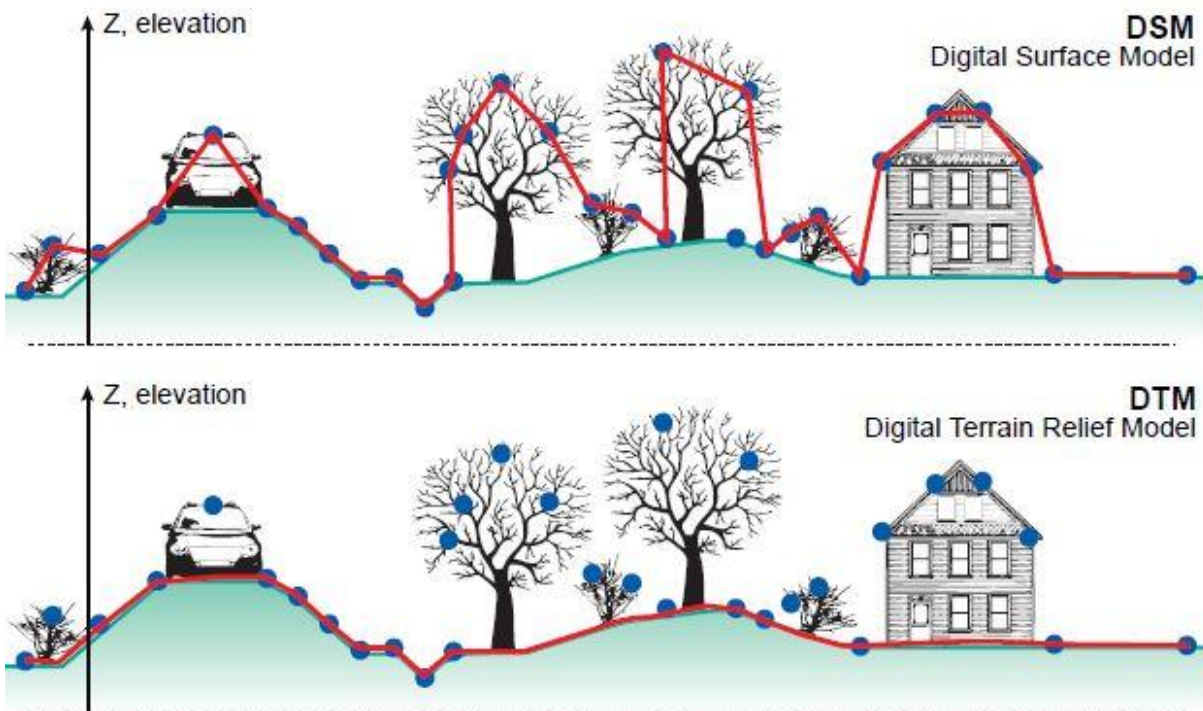


Figure 1.5 DSM and DTM.

Source <http://www.charim.net/datamanagement/32>

Growing system and environmental characteristic of trees can be obtained using a method to estimate biophysical parameters such as tree height applying the crown height model (Díaz-Varela, 2015). Conventional survey method cannot produce data with sufficient and reliable accuracy, especially high spatial resolution in a landscape level in order to quantify the structure while using UAV through SfM method we can obtain accurate data related to vegetation characteristic (Cunliffe et al., 2016). Moreover, CHM is needed to obtain a spatial representation of trees for modelling, inventory, monitoring and sustainable management of forest (Selkowitz et al., 2012).

In term of quantity and accuracy assessment of DSM and DTM, Zarco-Tejada et al., (2014) acknowledge that in agriculture and environment sector UAV which is cost-effectiveness and compact camera platform offer similar accuracy compared to the expensive and complex system of Lidar platform.

### 1.5.5. Error measurement of tree height using handheld laser instrument

The complexity of tree structure leads to generate error using handheld laser height measuring instrument such as Disto Leica due to the distance between sensed object and observer, while hand movement also creates an inaccurate estimation of true height (Bazewew, 2017). As can be noticed in Figure 1.6, the observer has to have a clear view to see and measure the top of the trees and must consider the distance between the observer and trees, for example, 20 – 30 m. In fact, it is difficult to have appropriate space to observe tree height in the forest as a result of tree structure complexity, leaves and branch occlusion as well as density. Moreover, measuring large and high trees in close distance using a handheld laser scanner tends to produce underestimate measurement and create an error (Larjavaara & Muller-Landau, 2013).

Terrestrial laser scanner offers the accuracy in millimetre detail of the object observed height which also allows fast acquisition, automatically measurement and multitemporal for forest application (Liang et al., 2016). TLS is also used to measure the biophysical parameters such as tree height and DBH to calculate aboveground biomass/carbon stock which provides high accuracy estimation (Wilkes et al., 2017; Bazewew, 2017).

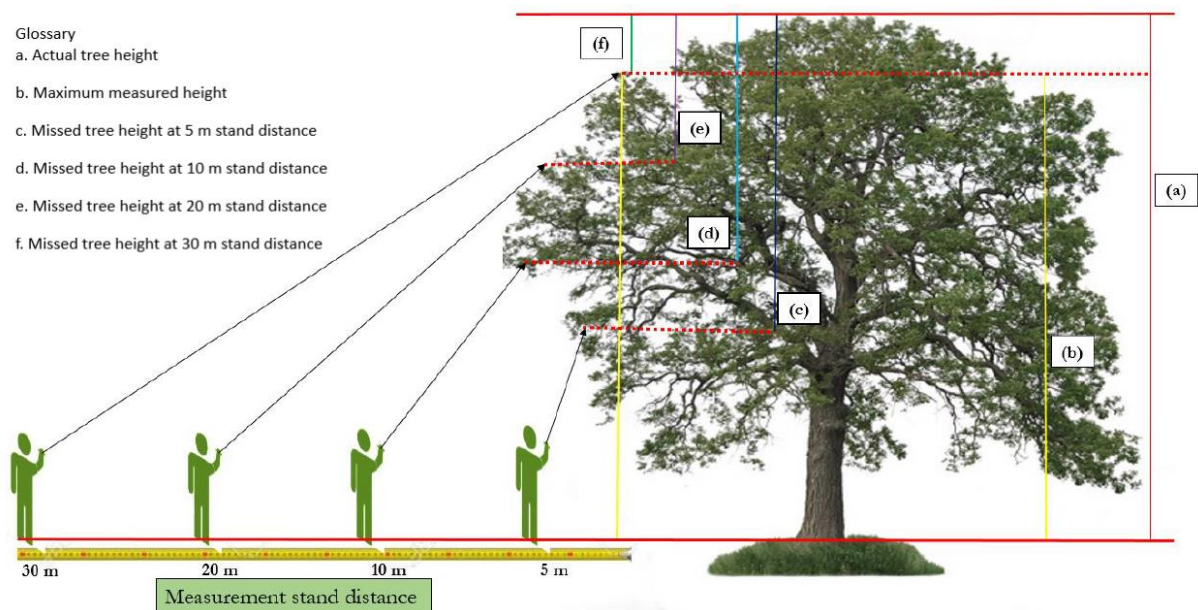


Figure 1.6 Tree height error due to the stand distance position using handheld laser height measuring instrument.

(Modified from: Bazewew, 2017).

## 2. MATERIALS AND METHODOLOGY

### 2.1 Study area

Study area is located in Tani Baru Village, Anggana District, Kutai Kartanegara Region, East Kalimantan Province, Indonesia, which is situated on latitude  $0^{\circ}32'20.95''\text{S}$  and longitude  $117^{\circ}34'8.19''\text{E}$ . It is a conservation area of mangrove forest, where some of the areas were replanted after were converted into shrimp ponds. The study area is remnant mangroves forest which consists of old (natural) and planted mangroves. The study area location can be seen in Figure 2.1

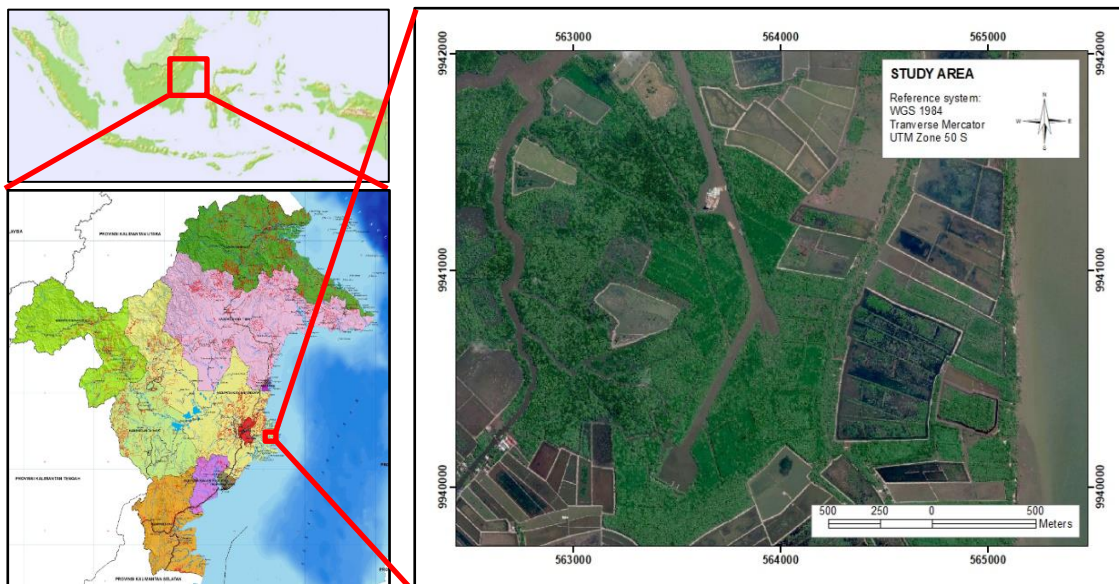


Figure 2.1 Location of the study area.

The study area is located in the equator zone; thus, the climate is humid, and rainfall happens during the year. The average temperature of the study area is approximately in the range of  $23 - 32^{\circ}\text{C}$ , while the average rainfall in the dry season (July-September) is  $35-40$  cm/month and in the wet season (October – June) is  $67-70$  cm/month (Rahman et al., 2017). The annual precipitation in the study area is more than  $2500\text{mm}$ .

Sidik, (2009) divides vegetation zone based on the distance from the sea into Pedada, Bakau, Transition, Nypa and Nibung. Padada is situated close to the delta front and dominated by *Sonneratia alba* and *Avicennia spp.*, while Bakau zone is dominated by *Rhizophora spp.*. The transition zones are with many species such as *Avicennia spp.*, *Sonneratia caseolaris*, *Rhizophora spp.*, *Bruguiera spp.*, *Xylocarpus granatum* and nipa. Meanwhile, Nipa and Nibung zone are located in the central and upper area of Mahakam Delta.

The study area is part of Tani Baru Village which covers an area of  $71\text{ km}^2$ . Tani Baru is located in Anggana District which has  $43,990$  inhabitants in 2017 consist of  $23,341$  male and  $20,469$  female. While the growth rate in Anggana District is  $3.96\%$  and population density is  $24$  per square km in 2017 (BPS, 2018). The majority of inhabitants is Bajau and Bugisness, where the fisherman is the main source of livelihood (Persoon & Simarmata, 2014).

### 2.2 Materials

During the research work of this thesis, materials were used, namely data, equipment and software, which used for fieldwork planning, data acquisition, data pre-processing, data processing and analysis, data and result presentation as well as thesis writing. These materials are described in the following subsections.

### 2.2.1 Data

The list of data and sources of the data used in this research consists of two types, primary and secondary data. Primary data were collected during fieldwork, while secondary data were obtained from other sources, such as institution, internet, and literature review. Collected data in fieldwork comprises ground truth data (biometric) of DBH, tree height and species, while coordinate of sample plot and tree were retrieve by GPS handheld. Moreover, GPC were collected using GNSS RTK, and UAV image 2018 were collected using DJI Phantom 4.

On the other hand, secondary data of Google Earth image were employed to recognise the study area to determine the sample plot and UAV flight plan. TLS and UAV image 2017 were used to retrieve trees parameters such as tree height, CPA, crown diameter and canopy cover. In term of literature review, it was done to search for the mean annual increment of the mangrove growth rate of DBH and height as well as woody density for tree-specific mangrove species, namely *Avicennia spp*, *Rhizophora spp*, and *Xylocarpus granatum*. While other literature review performed to find an allometric equation for mangrove to calculate biomass and conversion factor to calculate carbon stock. Data, the source of data and type of data are illustrated in Table 2.1.

Table 2.1 Data and source of data used in this research.

Data	Sources of data	Type of data
Sample plot plan, flight plan	Google Earth image	Secondary
DBH, tree height, species	Ground truth	Primary
Tree height of TLS	Terrestrial laser scanner (TLS)	Secondary
Coordinate of sample plot and tree	Global satellite system (GPS) handheld	Primary
Ground control points (GCPs)	Global navigation satellite system real-time kinematic (GNSS RTK)	Primary
UAV image 2017	University of Mulawarman	Secondary
UAV image 2018	Unmanned aerial vehicle (UAV)	Primary
Growth rate of mangrove	Literature review	Secondary
Wood density	Word Agroforestry	Secondary
Allometric equation	Literature review	Secondary
Conversion factor	Literature review	Secondary

### 2.2.2 Software

There are several software packages that were used to pre-process, process, analyze and interpret data in this research during planning, fieldwork data collection, pre-processing, processing, analysis, and writing report. Here, Google Earth Pro was used to download fine resolution image of the study area in order to make flight planning and sample plot design. PIX4D Capture, PIX4D Ctr+DJI and PIX4D Mapper were used to make a flight plan, capture image using DJI Phantom 4 and image processing through Structure from Motion (SfM). Coordinate data of sample plot and trees that collected using GPS were processed via Garmin Map Source.

Arc GIS was used for the segmentation of crown canopy, resampling image of DTM, generating CHM and map layout. While Microsoft Excel and R-Studio were used to calculate and analyse statistical data, as well as making tables and diagrams. In term of the research thesis, Microsoft Word and Mendeley were used during thesis writing and retrieving citation. Moreover, Microsoft PowerPoint was used during presentations. Table 2.2 shows the list of software used in this research.

Table 2.2 Software used in this research.

Software	Purpose
Pix4D Capture	UAV flight planning
Pix4D Ctrl+DJI	UAV drone imagery captured
Pix4D Mapper	UAV image processing
Google Earth Pro	Download image, plotting coordinate
Garmin Map Source	GPS handheld data retrieving
ArcGIS	Manual on-screen segmentation of CPA, resampling image, generating CHM, layout
R-studio	Statistical data analysis
Microsoft Excel	Calculation, statistic data, table and diagram
Microsoft Word	Writing report
Microsoft PowerPoint	Presentation
Mendeley	Citation and reference

### 2.2.3 Equipment

Implementation of fieldwork required equipment to collect ground truth or measure trees parameters, e.g., DBH, trees height, setting sample plots. In the same time, they were used for GCP(s) and UAV imaging campaign. Compass was used for navigation. For tree height measurement two instruments were used: Leica DISTO D510 laser ranger and TLS RIEGL VZ 400. Diameter Tape 5 m were used to measure DBH of the individual tree inside the sample plot, while 30m measuring tape was used to measure the radius of the plot from the centre of the circular 500m<sup>2</sup> plot, i.e.,12.6m.

Tree tags were used for numbering the trees in order to easily identify them during the data collection inside the sample plot. Handheld Garmin GPS E-Trax 30x was used to mark the coordinates of the plot centre and tree coordinates. Moreover, the digital camera was used to capture images of the plot in order to reconstruct the trees setup inside the plot and capture images for documentation. Table sheets were used to record fieldwork measurements of DBH and tree height, while some other stationaries were also used during fieldwork. TLS RIEGL VZ 400 was used to collect three-dimension point clouds to derived tree parameters. For UAV image rectification, ground control point was used inside the study area. Before UAV image acquisition and GCP measurement, tie mark was placed on the ground which was used as GCP location, then the X, Y, Z coordinates of the centre of tie marks were measured using GNSS RTK Leica GS 18 T. In terms of UAV image acquisition of 2018, DJI Phantom 4 was used to capture the images of the study area. The equipment is shown in Table 2.3.

Table 2.3 Fieldwork equipment.

Equipment	Purpose
Compass	Navigation
Leica DISTO D510 laser ranger	Tree height measurement
Diameter tape 5 m	DBH measurement
Tape 30 m	Diameter sample plot
Tree tag	Numbering trees
Garmin GPS E-Trax 30x	Navigation, marking coordinates
Digital camera	Capturing pictures
Table sheet	Recoding tree height, DBH, coordinate, trees species
TLS RIEGL VZ 400	Tree height measurement derived from laser point cloud data
GNSS RTK Leica GS 18 T	Measuring the GCPs
DJI Phantom 4	Collecting UAV imagery data
Ties mark paper	GCP ties mark

## 2.3 Research method

Figure 2.2 shows the research methods flowchart.

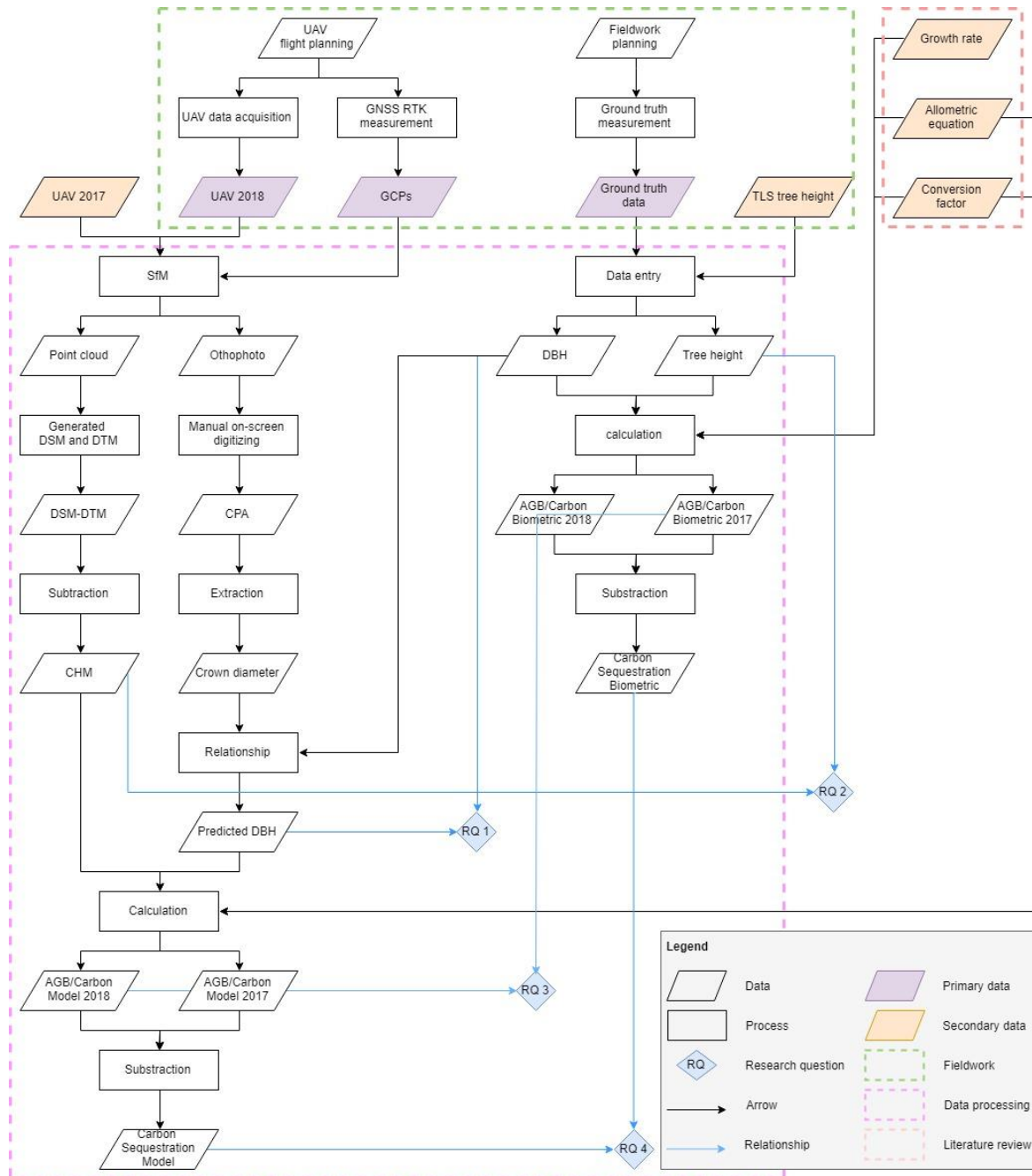


Figure 2.2 Flowchart of research method.

### Abbreviation

AGB : Aboveground biomass  
 CHM : Canopy height model  
 CPA : Crown projection area  
 DBH : Diameter breast height  
 DSM : Digital surface model  
 DTM : Digital terrain model

GCP(s) : Ground control point(s)  
 GNSS : Global navigation satellite system  
 RTK : Real-time kinematic  
 SfM : Structure from motion  
 TLS : Terrestrial laser scanner  
 UAV : Unmanned aerial vehicle

The methods used in this research are explained in the following steps:

1. Fieldwork Planning.

This step has included recognising the study area using Google Earth image to identify coverage area, design sample plot and UAV flight plane. Furthermore, fieldwork planning was included in the preparation of fieldwork equipment to collect data and calculating the budget. On the flowchart, this step refers to UAV flight planning and field work planning.

2. Data Acquisition.

Fieldwork data acquisition was done to collect biometric tree data (e.g., DBH, tree height, species), coordinate of sample plot, coordinate of the tree, TLS trees height measurement, GCPs coordinate and UAV images which were held from 13 – 24 October 2018. This step refers to UAV images 2018 data acquisition, GCP(s) measurement, ground truth data measurement and tree height measurement using TLS.

3. Biometric data processing.

This step included the processing of biometric data e.g., DBH and tree height measured by Diameter Tape, Leica DISTO D510 laser ranger; tree height derived from TLS point cloud, growth rate increment and woody density to calculate aboveground biomass and carbon stock of biometric in 2018 and 2017 as well as biomass/carbon sequestration using allometric equation and the conversion factor. These processes refer from the step of data entry to step of carbon sequestration biometric and step of the literature review.

4. UAV image processing.

PIX4D mapper was used to processing UAV images of 2018 and 2017 in order to generate 3D point clouds, orthophoto, DSM, DTM. In addition, GCPs were used for image geo-referencing using datum WGS 1984, UTM zone 50 S. Meanwhile, DTM image resampling and generating CHM were done in ArcGIS software. On flowchart, this step refers to the process of SfM to produce orthomosaic, DSM and DTM.

5. Derived UAV data.

Crown projection area segmentation was done manually using on-screen digitising on the orthophoto mosaic image of the UAV of 2018 and 2017. This was done using ArcGIS software for each tree throughout the whole plots collected in this research. Afterwards, those CPAs were used to generate CHM of 2018 and 2017 using Spatial Analysis tool in ArcGIS. Then, CPA was also used to generate a crown diameter of trees for the two years of data. On the flowchart, these processes refer to the step of DSM-DTM to generate CHM and step of CPA to produce crown diameter. The results of the relationship between tree height derived from CHM and tree height derived from TLS point clouds in 2017 and 2018 are to answer research question 2.

6. Analysis of UAV data.

This part involved in analysing UAV data. First, all the trees observed in the fieldwork were selected to obtain a significant relationship between biometric data and UAV images data which include crown diameter – DBH relationship and tree height – CHM relationship for 2018 and 2017 data. Next, based on the relationship between crown diameter and biometric DBH, predicted or modelled DBH was calculated. Finally, AGB and carbon stock model in 2018 and 2017, as well as biomass/carbon sequestration, were calculated using predicted DBH model, CHM, wood density and applying allometric equation. On flowchart, these processes start from the step of CHM and crown diameter to step of calculate aboveground biomass/carbon stock in 2017 and 2018 as well as carbon sequestration. The results of the relationship of predicted DBH using crown diameter derived from CPA of UAV images and DBH ground truth data in 2017 and 2018 are to answer research question 1.

7. The relationship between ABG/carbon stock and carbon sequestration model and biometric.

The last part was the comparison of modelled aboveground biomass/carbon stock of 2018 and 2017 with the biometric ground truth data. It includes the calculation of carbon sequestration by subtracting the carbon of 2017 from 2018 and the accuracy assessment. On flowchart, these steps refer to the result of the relationship between ABG/carbon stock model and ABG/carbon stock biometric in 2017 and 2018 as well as comparison between carbon sequestration model and biometric to answer research question 3 and 4.

## 2.4 Fieldwork planning

### 2.4.1 Sampling plot design

Defining sampling plot design, plot shape, and plot size are important steps to be taken before data collection (Laar & Akca, 2007). A circular shape plot with radii 12.62m was chosen to minimise borderline and perimeter of plot shape, to make the boundary of the plot easy to established and seen, to make the simple correction and to represent 500m<sup>2</sup> coverage area (Kershaw et al., 2017)

Purposive sampling was used in this research due to several consideration and difficulties when working in mangrove forest such as time, cost, accessibility, efficiency and plot size (Schreuder et al., 2001). It was too difficult to use any other sampling design than purposive, since the weight of TLS is 28 kg and it needed extra time to set up TLS as well as retro-reflectors in the field. Here, TLS was used to assess trees height.

Consequently, 30 sampling plots were used in this research distributed in the study area and equally spread in both old mangroves trees and planted mangrove to represent all variations in the study site. Fieldwork measurement planning also comprises preparing data tale sheets and equipment used for fieldwork (Appendix 1). We also tried to train our self on the use of the equipment before visiting the study area. Biophysical parameters of the mangrove trees were collected such as DBH, trees height, coordinates of trees and trees species by using Leica DISTO Laser Ranger, diameter tape 5 m and handheld GPS.

### 2.4.2 UAV flight planning

UAV flight planning including drone flight mission and global navigation satellite system (GNSS) measurement were used in this research. Some parameters must be defined before drone flight mission start, namely camera setting, ground sampling distance, flight height, image overlap, surveyed area, flight time, and weather condition (Nex & Remondino, 2014).

This thesis research work used UAV RGB images that were acquired by DJI Phantom 4. Flight height of the drone was within a range of 100 – 200m above the ground in order to achieve very high spatial resolution data with GCD less than 10cm. UAV images were collected in a single grid flight fashion to reduce the time and save on battery power as well as using moderate speed to minimise blurring effect on the images. Furthermore, image overlap determined the number of images acquired which used forward overlap of 80% and side overlap of 60%. In addition, the study area was approximately one km<sup>2</sup>, thus the UAV needed high power of minimum six batteries during the flights. The time of the first flights was between 10:00 and 12:00 hr morning to minimize disturbance from sun illumination, wind, and other unreliable weather conditions. However, the time of the final flight was 6:35 AM. Table 2.4 below shows UAV flight plan parameters in the field.

Table 2.4 UAV flight plan parameters used in this research.

Parameters	Information
Flight height	>100 m
Flight mission	Single grid
Flight speed	Moderate
Forward overlap	80%
Side overlap	70%
Sensor and camera	RGB
Focal length	4 mm
Image resolution	4000 x 3000 pixel
Captured area	1 x 1 km
GCP(s)	12
GNSS data observation	Real-time kinematic (RTK)

A special team from the University of Mulawarman was hired to collect GCP in the field using DGPS (Differential Global Positioning System). The measurement of GCP included the use of GNSS RTK which must consider the area of interest, method, number of GCP(s), ties marks, and post-processing data. In this research, the surveyed area is a flat mangrove coastal zone with one km<sup>2</sup> coverage area. Absolute real-time kinematic was chosen as the method to acquire data, which intend to obtain reference point and GCP(s) with the total of 12 points, namely 6 points as GCP(s) and 6 points as checkpoints to assess the geometric accuracy. Moreover, ties marks that were used in the field must be visible during the flight and placed in stable and safe area (Figure 2.3). List of GCP(s) can be seen in appendix 2.



Figure 2.3 Ground Control Points (GCP) used in the study area before UAV flight.

## 2.5 Field data collection

Field data collection was held in the period 13 - 24 October 2018 in mangroves area of Tani Baru, Mahakam Delta, East Kalimantan, Indonesia. Data collection consisted of ground truth data of biophysical trees parameters and UAV image data.

### 2.5.1 Ground truth data acquisition

Data which are collected in the field were DBH, tree height, tree species, coordinate of the central plot, and individual tree coordinate and field photos. These data were collected in 30 sample plots in two different types of mangroves, namely natural and planted. Moreover, ground truth data collection was recorded by manually in tale sheets and later were input digitally in Excel sheets. While some other data collected in the field were recorded digitally using devices such as handheld GPS Garmin E-Trax 30 x, Leica DISTO D510 laser ranger and TLS RIEGL VZ 400.

Biometric tree properties were collected following the method of Kauffman & Donato, 2012. Diameter at breast height (DBH) was measured approximately 130 cm above ground for *Avicenia spp.* and *Xylocarpus granatum*, while DBH of *Rhizophora spp.* was measured about 30 cm above the highest aerial root. Here, diameter tape 5 m was employed to measure DBH in the field. An example of DBH measurement in the field can be seen in Figure 2.4. Only trees with  $\geq 10$ cm DBH were measured because trees with DBH less than 10cm would have no significant contribution to the amount of biomass/carbon stock of the plot (Brown 2002).



Figure 2.4 Measuring DBH using diameter type.

In the field, tree height which was measured using Leica Disto D510 laser ranger by taking a distance from tree measured approximately 10 to 20 m and depended on the density of trees (Figure 2.5). While TLS RIEGL VZ 400 was also utilized to measure every single tree height in the plot by placing it in four locations: in the centre of the plot and three locations on the border of the plot.



Figure 2.5 Measuring tree height using Leica Disto D510 laser ranger(a) and using TLS RIEGL VZ400 (b).

Each individual tree was observed, and the measurements were recorded in a table sheet which comprised number of trees inside plot, species, DBH, and trees height. It also recorded the number of plots, date measurements, coordinates of plot centre and coordinates of trees

### 2.5.2 UAV image data acquisition

UAV images 2017 and 2018 were collected by a special team from the Faculty of Forestry, University of Mulawarman. These images were collected on 25 October 2017 and 18 December 2018. It was by chance that the University of Mulawarman had done the imaging survey in 2017 for PT PERTAMINA Oil company of Indonesia and we have used these images to assess carbon sequestration.

In 2017, DJI Phantom 4 camera model 3610 was employed using 375 m altitude above ground and 9 mm of focal length to collect 54 images. While in 2018, DJI Phantom 4 FC330 using 4 mm of focal length was used to collect 369 images from an altitude of 165 m above the ground floor. Table 2.5 shows UAV data collection parameters of 2017 and 2018.

Table 2.5 UAV data collection of 2017 and 2018.

Information	UAV 2017	UAV 2018
Date	25 October 2017	18 December 2018
Time	15.30	12.30
Pixel	4864 x 3648	4000 x 3000
Camera model	DJI FC3610	DJI FC330
Focal length (mm)	9	4
Altitude (m)	375	165
Number of images	54	369
Forward overlap	80%	70%
Side overlap	70%	60%

PIX4D Capture was used to make UAV mission planning, which comprised parameters such as flight speed, angle, forward and side overlap, flight height, number of flight lines etc. The number of captured images was determined by area captured, flight height, focal length and forward and side overlap (Nex, 2017). Figure 2.6 shows some of the steps in collecting UAV images using DJI Phantom 4. Before UAV images were acquired, GCPs had collected using GNSS RTK Leica GS 18 T which consisted of base and rover receiver, while tie marks were placed in GCP point locations in the field.

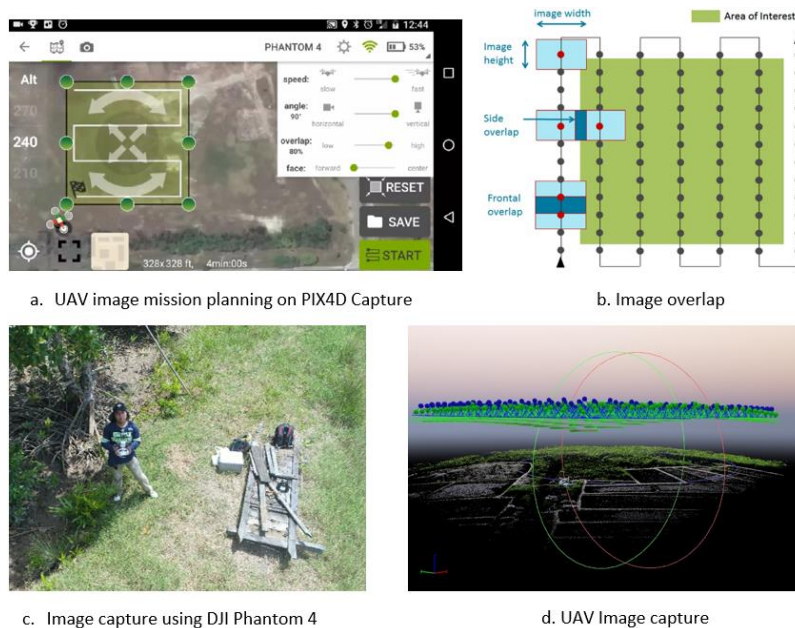


Figure 2.6 Some steps in collecting UAV images using DJI Phantom 4

(Modify from: [www.pix4d.com](http://www.pix4d.com) and [www.questuav.com](http://www.questuav.com))

## 2.6 Ground truth data processing

### 2.6.1 Ground truth data

Field data collection which was recorder first manually and then transferred to Microsoft Excel in a digital format. Microsoft Excel, R-Studio were used to record, calculate, store, present, analyse, interpret and save the data in different types and format. DBH and trees height data were analysed using a statistical method to obtain statistical parameter such as sum, mean, standard deviation, variance, maximum and minimum.

### 2.6.2 Backward prediction

The backward prediction was done to predict DBH and trees height in 2017 by subtracting the value of 2018 data using the annual increment in each mangrove tree species. Backward prediction uses biometric DBH, and TLS tree height of 2018 was performed to calculate above ground biomass/carbon stock and carbon sequestration from 2017 to 2018. We had no choice but to do this step because there was no data collected in the field in 2017, e.g., DBH and trees height.

Based on Saenger & Siddiqi (1993), a mean annual increment of 0.74 cm DBH and 0.40 m in the height of *Avicennia alba* was used to predict the DBH and trees height in 2017 starting from the 2018 data. While for *Xylocarpus mekongensis*, the mean annual increment of DBH was 0.34 cm and 0.30 m of was the mean annual increment trees height. Moreover, Srivastava et al. (1988), stated that mean annual increment of the diameter of *Rhizophora spp.* was 0.47 cm, while the annual increment of height was 0.55 m a year. These literatures were used to backwards predicting DBH and tree height of *Avicennia spp.*, *Rhizophora spp.*, and *Xylocarpus granatum* in 2017 using biometric field measurement of 2018 (Table 2.6).

Table 2.6 The mean annual increment of DBH and tree height.

Mangrove species	MAI of DBH	MAI of tree height
<i>Avicennia spp.</i>	0.74	0.40
<i>Rhizophora spp.</i>	0.47	0.55
<i>Xylocarpus granatum</i>	0.30	0.34

### 2.6.3 Wood density

Wood density can be measured and retrieved easily in sample site, which usually developed by local forest institute (Kauffman & Donato, 2012). Here, wood density was needed as a parameter to calculate biomass/carbon stock using the allometric equation both for the biometric and modelled data of 2018 and 2017. Based on Word Agroforestry Center, 2018, the wood density of *Avicennia spp.*, *Rhizophora spp.*, and *Xylocarpus granatum* are 0.6987, 0.8814 and 0.6721 g/cm<sup>3</sup>, respectively. Table 2.7 shows the wood density of mangrove tree species which used to calculate aboveground biomass.

Table 2.7 Wood density of mangrove tree species.

Mangrove species	Wood density
<i>Avicennia spp.</i>	0.6987
<i>Rhizophora spp.</i>	0.8814
<i>Xylocarpus granatum</i>	0.6721

## 2.7 UAV Image processing

Structure from motion (SfM) is the process for analysing consecutive images to retrieve three-dimensional information of the scene structure and the motion of camera which comprises basic photogrammetry and computer vision (Nex, 2017). In this step, PIX4D Mapper and ArcGIS were used to process UAV images data. PIX4D Mapper was used to process raw image data to generate 3D point clouds, orthophoto, DSM and DTM. Ground control points were stored in text file format, which were used as GCPs and checkpoints in image registration. GCPs were used as input parameters in the absolute orientation of the UAV images, while checkpoints were used to assess the accuracy of GCPs. GCPs that appeared on the images should be marked in order to be used in the image rectification. Figure 2.7 shows marking GCP on the image in PIX4D Mapper.

Structure from motion (SfM) using PIX4D were divided into four stages, namely initial image processing; generating point cloud and mesh; generating DSM, DTM, orthophoto and index; as well as resources information and notification (Pix4d, 2019). Some parameters must be fulfilled or checked such as the minimum number of points matched and additional output of raster DTM to produce digital terrain model.

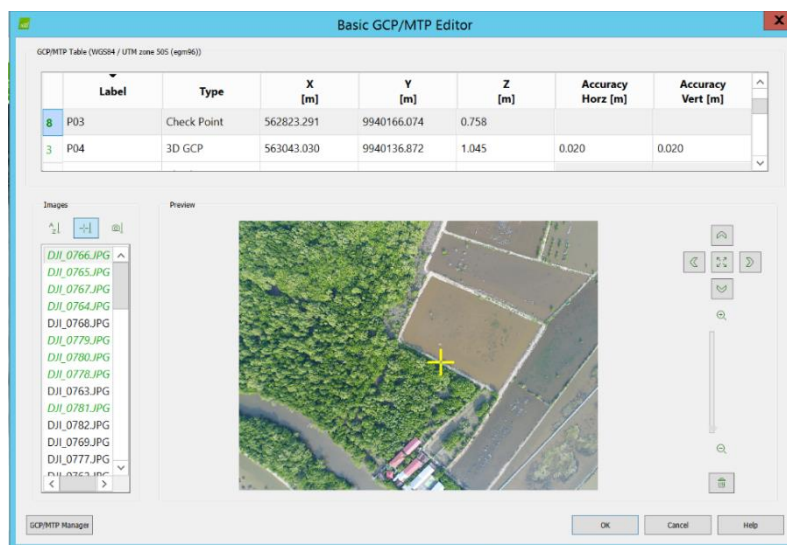


Figure 2.7 Marking appeared GCP on image in PIX4D Mapper.

### 2.7.1 Tree Reconstruction

Tree reconstruction was performed using coordinate of centre plot, the coordinate of trees, photos of each plot, TLS capture image, documentation, fieldwork note and UAV image. It was a bit tricky because some of the plot centres and tree coordinates were shifted. The images of each plot and TLS captured images gave an overview to reconstruct each individual tree inside the plot since in the field tree tag was placed on the tree stem as a proxy of the tree. Plot area (radii 12.6 m) was used to identify the border of the plot on orthomosaic UAV images. Afterwards, the trees could be reconstructed in the UAV 2018 image to identify the location of each individual trees.

On the other hands, the issue of shifted images due to geo-referencing process occurred in both UAV images of 2017 and 2018. In some cases when toggling between UAV image of 2018 and 2017 the trees position was a bit shifted. Therefore, when we do any measurement on the canopy of the trees we must be careful in identifying the tree. Dealing with this issue when reconstructing tree position in the UAV image 2017, all of crown canopy delineation in each plot on UAV image 2018 were relocated in the right position on UAV image of 2017. Then, fitting the position of the crown canopy of the trees in the UAV image of 2017 could be identified in order to generate crown diameter derived CPA and tree height derive CHM.

### 2.7.2 Manual digitising of CPA

Manual digitising of CPA in each recorded individual tree was done on the ortho-mosaic image of UAV 2017 and 2018 using ArcGIS. The issue of identifying and matching every single tree in each plot, which was measured in the field in both ortho-mosaics of UAV images was very crucial. This was because we needed to match between the DBH measured in the field and the CPA and crown diameter (CD) on the image. Manual on-screen digitization of CPA was done by delineating the crown area of each individual tree. After that, we calculated its area to represent CPA and then CPA was used to generate CD. In this case, we had to make sure that we were using the same canopy the same corresponding trees on both ortho-mosaic images of UAV 2017 and UAV 2018. As mentioned before, this step was very critical because there was a little shift related to the geo-referencing and difference in spatial resolution of the UAV images in the two years of 2017 and 2018. It was by chance that the University of Mulawarman had done the imaging survey in 2017 for PT PERTAMINA Oil company of Indonesia and we have used these images to assess carbon sequestration.

Identification number of trees (ID number) was crucial to distinguish every individual tree. This number could be used to identify the trees in other data processing steps. The ID number of trees had four digits, the first two figures presented the number of the plot, while the second two-digits represented the number of trees in each plot. For example, tree 1208, meant that tree located in plot 12 and it was tree number 08. This ID number of trees was applied in the manual on-screen digitising to generate CPA, assessed the CHM and derived CD. Figure 2.8 shows the difference between canopy projection area on othomosaic of UAV 2017 and 2018. CPA of UAV images 2018 was larger than 2017 because tree grew and expanded its canopy. The growth of trees could detect by comparing CPA of UAV images 2018 and 2017. Moreover, 2018 image was sharper and focus because of the differences in the quality of the images and the spatial resolution.



a. CPA 2017

b. CPA 2018

Figure 2.8 Manual digitising of CPA 2017 and CPA 2018.

CPA segmentation was done manually on UAV ortho-photo. Afterwards, CPA was used to generate a crown diameter (CD). The CPA is the size or area of the crown. It is measured in square meters. The crown diameter was derived from the CPA (crown shape was a circle or near circle) using the following equation.

$$CPA = (\text{radius})^2 * \pi$$

$$\text{Radius} = \text{Square} (CPA / \pi)$$

$$CD = \text{Radius} * 2$$

Where, CPA= Crown projection area (m<sup>2</sup>), CD= Crown diameter (m), and  $\pi = 3.142$

The relationship between crown diameter and DBH was used to predict modelled DBH. Then it was compared to DBH measured in the field for accuracy assessment for calculating biomass/carbon stock in 2018 and 2017 as well as biomass/carbon stock and carbon sequestration.

### 2.7.3 Extracting individual tree height of CHM

Extracting individual tree height derived from CHM was done using CPA area using the Spatial Analyst Tool in ArcGIS software. In this case, CHM was overlaid and masked by the shapefile of CPA. Furthermore, the zonal statistic was run to calculate the maximum value in the CHM, which is the highest point in the canopy. Afterwards, the CPA of the individual tree is converted into a point feature. Then, the maximum value of CHM within CPA for every individual tree was used to retrieve tree height derived from UAV CHM. Then, this tree height was used to assess the relationship between tree height calculated from TLS and tree height derived from CHM-UAV.

Figure 2.9 shows an example of individual tree height derived from CHM of 2017 and 2018. The value of tree height is retrieved from the maximum number within the crown area. It is clear that CHM 2018 is brighter than CHM 2017. It means the more vivid the colour is, the higher the trees are.

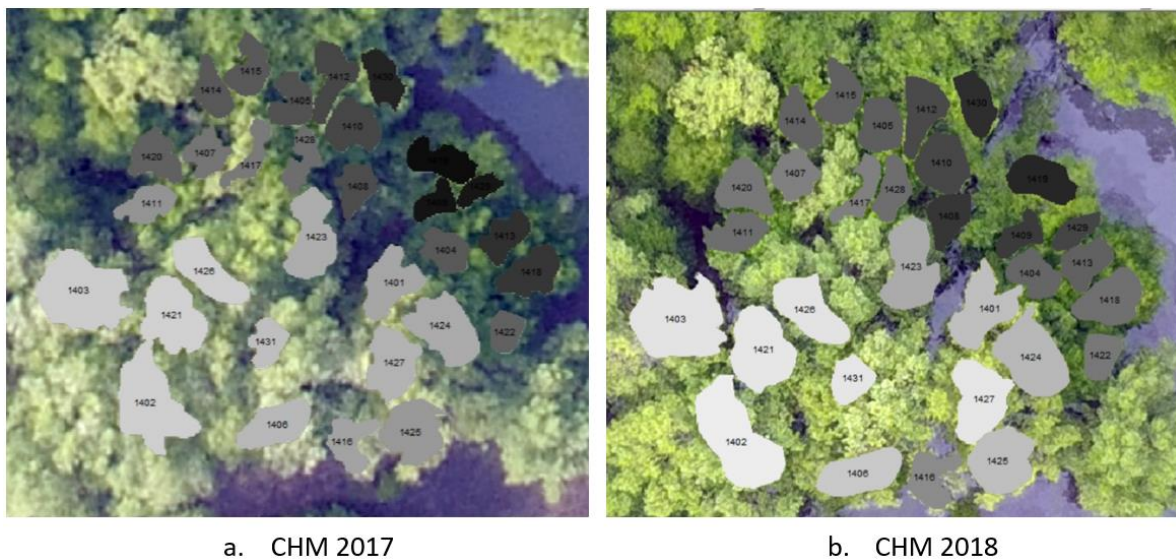


Figure 2.9 Example of individual tree height derived CHM 2017 and CHM 2018.

## 2.8 Data analysis

In this research, data analysing comprised the relationship between DBH and crown diameter, the relationship between tree height and CHM, aboveground biomass and carbon stock calculation which explained in the following section.

### 2.8.1 Relationship between DBH and crown diameter

The relationship between the diameter breast height and crown diameter to calculate aboveground biomass/carbon stock was done by a number of researches (Clough et al., 1999; Pouliot et al., 2002; Hemery et al., 2005; Fu & Wu, 2011), while some of them used remote sensing data and very high spatial resolution images (Brown et al., 2000; Feng, Li, & Tokola, 2010; Song et al., 2010; Panagiotidis et al., 2017). The relationship between DBH and crown diameter was powerful to assess biomass/carbon stock in multi-stem of mangroves trees such as *Avicennia spp.*, *Rhizophora spp.*, and *Xylocarpus granatum* (Suhardiman et al., 2013).

A number of ITC MSc theses also assessed the relationship between DBH and trees parameters derived from remote sensing data in a tropical forest where the majority of the trees has a single stem (Berhe, 2018; Odia, 2018). Instead of using the crown projection area, this study assessed the relationship between DBH, and crown diameter derived from the CPA of UAV. Selected trees were used to build the relationship between DBH and crown diameter in 2018 and 2017. The number of selected trees then were used to create a model and validation of predicted DBH based on crown diameter.

### **2.8.2 Predicted DBH model and validation**

Predicted or modelled DBH using remotely sensed data are reported by some researchers. These researchers have found that there was a strong relationship between DBH field measurement and predicted DBH derived from Lidar data (Prieditis et al., 2012; Wu et al., 2015; Shen et al., 2018). Thus, remotely sensed data, particularly very high spatial resolution images such as UAV is used to predict tree biophysical parameters.

Predicted or modelled DBH and its validation were done using selected trees that used to make the relationship between DBH and crown diameter. The number of selected trees were divided into 70% for model data and 30% for validation. The equation of predicted modelled DBH was applied on the model and validation data to predict DBH base on crown diameter. The R-square and RMSE then were calculated to see the validation results.

### **2.8.3 Relationship between trees height and CHM**

Structure from motion (SfM) technique using basic photogrammetry and computer vision offers capabilities to retrieve three-dimensional information of trees structure using point cloud of very high spatial resolution and by assessing trees height (Mohan et al., 2017; Panagiotidis et al., 2017). Crown height model (CHM) is an SfM product which is calculated as a relative height using DSM and DTM (Mohan et al., 2017). Then assessing the relationship with ground truth data is essential (Iizuka et al., 2018). The accuracy of CHM derived UAV as a proxy of tree height was assessed by using its relationship with trees height derived from TLS in 2018 and 2017 using selected trees. This step was aiming to answer the research question regarding the relationship between trees height and crown height model of UAV in 2017 and 2018.

### **2.8.4 Calculation of aboveground biomass**

Aboveground biomass is estimated using an allometric equation which is a mathematic equation to calculate biomass using DBH, tree height and woody density (Chave et al., 2014a). This research has used DBH, trees height and wood density as explanatory variables in the allometric equation to calculate biomass. Aboveground biomass model was calculated and reconstructed based on selected trees and assessed its accuracy using aboveground biomass/carbon stock biometric. The allometric equation which was used to calculate biomass is based on Chave et al., (2014).

$$AGB = 0.0509 * WD * DBH^2 * H$$

Where, AGB= above ground biomass (kg/tree), WD= wood density DBH= diameter breast height (cm), and H= trees height (meter)

### **2.8.5 Calculation of carbon stock and carbon sequestration**

Generally, the calculation of carbon stock based on spatial extrapolation of remote sensing data and temporal analyse of fieldwork carbon stock measurement (Hairiah et al., 2011). Carbon stock was estimated using the above ground biomass (ABG) and the conversion factor (CF). Conversion factor that was used to calculate carbon stock both on biometric and model data was in the amount of 0.5 (Brown, 2002; IPCC, 2006).

$$C = ABG * CF$$

Where, C=carbon stock, ABG= above ground biomass, CF= conversion factor (0.5)

## 3. RESULTS

### 3.1 Statistics of field data collection

This following section explains the statistic fieldwork data collection which comprises biometric DBH of field data collection; biometric trees height measured using Leica DISTO D510 laser ranger, trees height derived from TLS point clouds data and comparison trees height between biometric and TLS.

#### 3.1.1 Biometric DBH field data collection

Fieldwork data collection was done in 30 circular 500m<sup>2</sup> plots. The mangrove forest parameters which were collected in the mentioned plots were DBH and tree height, which contained 873 trees in total. Each plot had a different number of trees, and the average number of trees was 29 per plot. While the maximum and the minimum number of trees were 42 and 17 which were located in plot 7 and plot 18 respectively. Summary statistics and the number of trees in each plot are shown in Table 3.1 and Figure 3.1. While the location of the sample plot is depicted in Appendix 3.

Table 3.1 Descriptive statistics of fieldwork data collection in all 30 plots.

Statistics	Number of trees
Total	873
Average	29
St. Dev	7.4
Max	42
Min	17

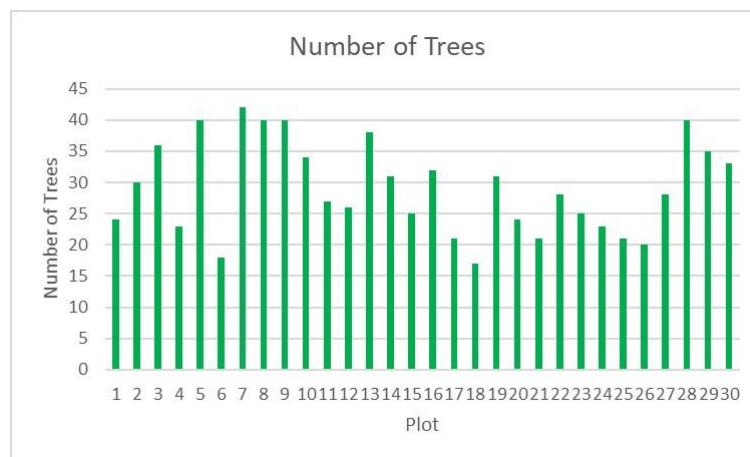


Figure 3.1 Distribution of the number of trees in each plot.

Three species of mangroves grew and spread in the study area, which comprised 455 trees of *Avicennia spp* (52%), 407 trees of *Rhizophora spp* (47%), and 11 trees of *Xylocarpus granatum* (1%). The percentage of tree species in the study area is illustrated in Table 3.2

Table 3.2 The number of trees according to different species.

Species	Number of Trees	The percentage of tree species (%)
<i>Avicennia spp.</i>	455	52
<i>Rhizophora spp.</i>	407	47
<i>Xylocarpus granatum</i>	11	1
Total	873	100

Figure 3.2 shows that the majority of the trees had DBH in the range 10 cm-15 cm (524 trees). Less than 200 trees had DBH in the range 15 cm to 20 cm. The DBH between 20 cm and 25 cm were nearly 100 trees. The total number of DBH more than 25 cm were 79 trees.

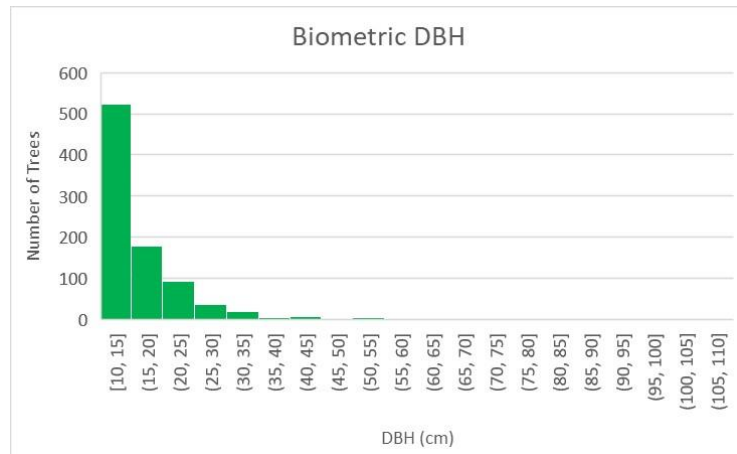


Figure 3.2 Histogram distribution of biometric DBH measured in the field.

The boxplot of the 873 trees found in 30 sample plot shows that the DBH which higher than its median of each plot indicated the outlier, for example in plot 18, the median of DBH was 12.9 cm, while there were two outlier trees had DBH less than 40 cm. The boxplot of DBH also depicted that 52 outliers spread in 20 plots (Appendix 4 Figure 1)

### 3.1.2 Biometric tree height measured Leica DISTO D510 laser ranger

Table 3.3 shows the summary statistics of trees height measured in the field using Leica DISTO D510 laser ranger. The average biometric tree height in the study area was 13.3 m and 2.9 m of the standard deviation. Meanwhile, the maximum and the minimum measure of trees height were 22.6 m and 6.9 m respectively.

Table 3.3 Summary statistics of biometric trees height measured in the field.

Statistics	Biometric Tree Height
Total	11602.3
Average	13.3
St. Dev	2.9
Max	22.6
Min	6.9

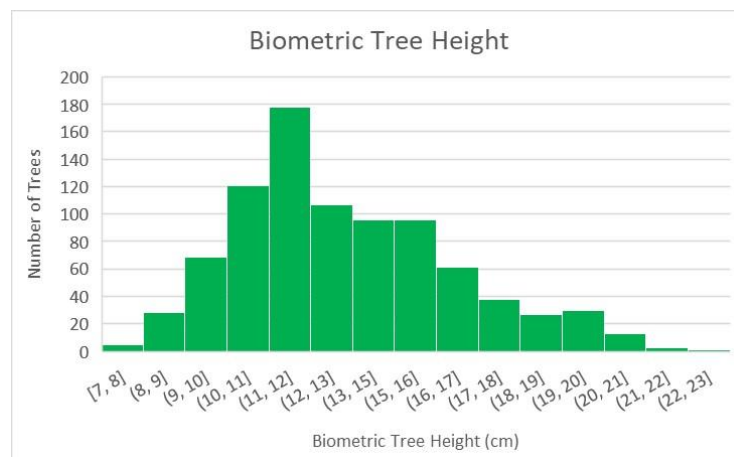


Figure 3.3 Histogram distribution of biometric trees height measured in the field.

Furthermore, the histogram of biometric trees height shows that it was right skewed. Nearly 180 of trees had a height in the range of 11 m to 12 m. When it was classified into three classes, there were 102 trees of low height (<10m). The dominant tree height was in the range of 10-20 m which consisted of 705 trees, while 17 other trees had more than 20 m height (Figure 3.3). The boxplot of biometric trees height measured in the field using Leica DISTO D510 laser Ranger depicts that there were 25 outliers of trees height which were spread in 13 plots. For instance, plot 1 had five outliers with 10.3m of the median tree height. The boxplot of biometric trees height measured is shown in Appendix 4 Figure 2.

### 3.1.3 Tree height derived from TLS point clouds data

This research work also used secondary data of trees height that derived from terrestrial laser scanner (TLS) point clouds data. The summary statistics of TLS trees height are presented in Table 3.4 Summary statistics of trees height measured using TLS point clouds data. Table 3.4. It shows that the average of TLS trees height was 14.4 m and the standard deviation of 2.8 m. Moreover, the minimum measured trees height was 7.2 m, while 22.9 m was the highest tree height measured by TLS.

Table 3.4 Summary statistics of trees height measured using TLS point clouds data.

Statistics	TLS Tree Height
Total	12537.5
Average	14.4
St. Dev	2.8
Max	22.9
Min	7.2

The histogram of TLS tree height (Figure 3.4) depicts that the data was right skewed. Dividing the range of tree height into 1m, there were more than 140 trees belong to 12-13 m height. When TLS tree height data were classified into three classes, the majority of trees height was in the range of 10-20 m (counted 790 trees). Only 51 trees and 32 trees had height less than 10 m and height of more than 20 m respectively. The histogram of trees height derived from TSL point cloud data can be seen in Figure 3.4.

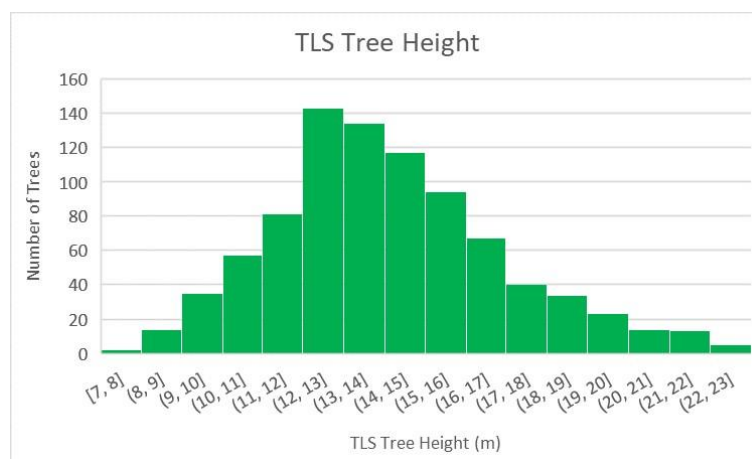


Figure 3.4 Histogram distribution of trees height derived from TLS point cloud data.

As shown in the boxplot of TLS trees height (Appendix 4 Figure 3), 19 trees were counted as outliers, located and spread in 9 plots. Plot 23 had the highest mean of trees height (18.7 m) compared to other plots, while the lowest mean of trees height was 11 m found in plot 18. The boxplot also shows that trees height more than 20 m located in plot 4, 5, 8, 14, 22 and 23, while in plot 8, it is counted as an outlier. Furthermore, the trees that have the height in the range of less than 10 m and counted as outliers which are in plot 1, 2 and 7.

### 3.1.4 Comparison biometric and TLS tree height

The summary statistics of biometric trees height and TLS tree height in Table 3.3 and Table 3.4 exhibit that trees height derived from TLS had a higher value than biometric tree height. The sum of TLS trees height measurements was higher than the sum of trees height measurement in the field using Leica DISTO D510 laser Ranger. The difference between the sum of the two measurement was 935 m. This clearly shows that Leica DISTO D510 laser Ranger had underestimated tree height. Figure 3.5 evidently show the shift in the distribution of the measurements using Leica DISTO and the TLS measurement. According to Bazezew (2017), when the laser beam of TLS can reach the point want to be measured (i.e., top of the tree) then TLS is the most accurate instrument to measure trees. Furthermore, the maximum and the minimum tree height of TSL (22.9 m and 7.2 m) were also higher compared to Leica DISTO data (22.6 m and 6.9 m). On the other hand, the standard deviation of TSL was less 0.1 m compared to Leica DISTO measurements.

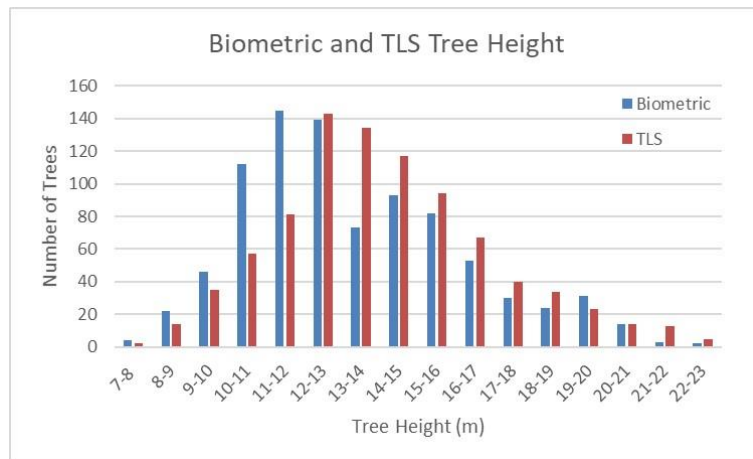


Figure 3.5 Trees height measured using Leica DISTO D510 laser Ranger and TLS trees height.

Figure 3.5 shows the comparison of tree height derived TLS and biometric, classified by 1 m in the range of trees height, starting from 7 m to 23m in both data. There were large gaps in the measured trees between 10-11 m, 11-12 m and 13-14 m. In these classes, the difference between two data were more than 20 trees. Leica DISTO had nearly double compared to TLS in the range of 10-11 m and 11-12 m when TLS had almost twice number of trees in the range of 13-14 m. Moreover, 24 measured trees had the same amount in the range of 20-21 m of both data. Both datasets were right-skewed. The Leica DISTO measured tree height data was righter skew than TLS data. From Figure 3.5, it is clear that the majority of measured trees height was in the range of 10 to 17 m.

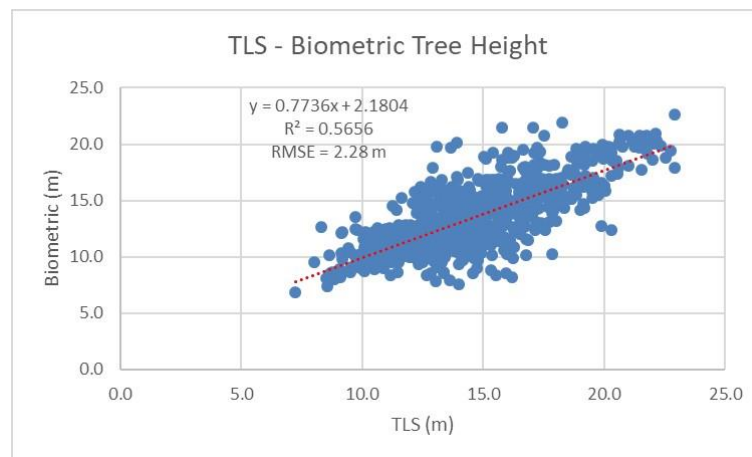


Figure 3.6 Scatterplot of TLS and Leica DISTO measured trees height regression analysis.

The relationship between TLS and Leica DISTO measured trees height depicted that R-square was 0.5656 and RMSE was 2.28 m (Figure 3.6). By using linear regression, the equation had 2.1804 as an intercept and 0.7736 as a slope. Based on data of Leica DISTO and TLS trees height, there were 213 trees of Leica DISTO measurement overestimate, and 660 trees underestimate compared to tree height derived TLS. Consequently, trees height measured by TLS will be used as the reference measured height (i.e., ground truth).

### 3.2 Backward prediction of 2017

The following section explained the result of backward prediction using mean annual increment/growth rate of DBH and tree height for three difference mangrove species. Backward prediction of DBH and tree height 2017 was calculated by subtracting DBH and tree height derived TLS in 2018 with mean annual increment.

#### 3.2.1 The results of backward prediction of DBH 2017

Summary statistics of DBH 2017 presents that the average DBH was 15.5 cm, declining by 0.6 cm compared to DBH 2018. The maximum and the minimum DBH 2017 were 108.2 cm and 9.3 cm when the standard deviation was 8.9 cm (Table 3.5).

Table 3.5 Summary statistics of DBH of 2017 calculated using backward prediction.

Statistics	DBH 2017
Total	13514.0
Average	15.5
St. Dev	8.9
Max	108.2
Min	9.3

Histogram of DBH 2017 depicts that more than 500 trees had DBH in the range of 9 - 14cm and nearly 200 trees had a class of DBH between 14 - 19cm. Almost a hundred trees had 19 - 24cm of DBH range, while 83 trees were more 25cm of DBH (Figure 3.7)

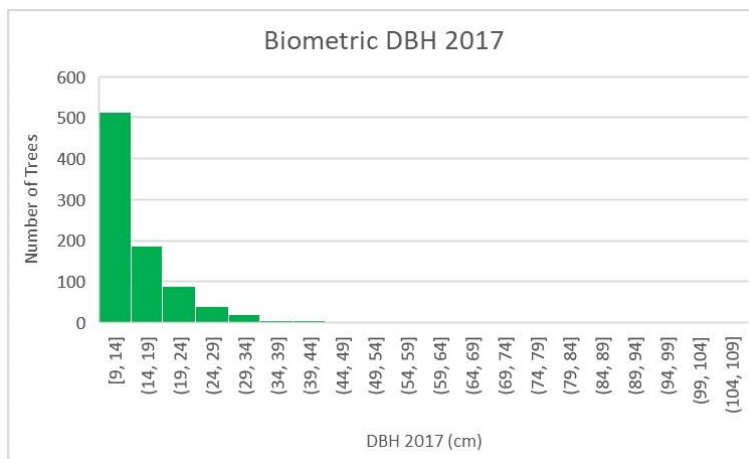


Figure 3.7 Histogram distribution of DBH of 2017 calculated using backward prediction.

As can be seen in the boxplot of DBH 2017, 55 trees were indicated as outliers, located in 21 plots. Six and four outliers were located in plot 19 and plot 7 respectively. While four outliers are in plot 25 and 30. Three outliers were spread in plots 8, 12, 15, 16, 17, 26, 27 and 28. Meanwhile, two outliers of DBH were in plot 5, 10, and 18. Whereas plots 1, 4, 20, 23, 24 and 29 had one outlier. The boxplot of DBH 2017 is presented in Appendix 4 Figure 4.

### 3.2.2 The results of backward prediction of TLS tree height 2017

The results backward prediction of TLS trees height of 2017 is presented as the summary statistics in Table 3.6 which shows that the average tree height in 2017 was 13.9 m, with 2.8 m of the standard deviation. The maximum tree height was 22.5 m, while 6.8 m was the lowest tree height.

Table 3.6 Summary statistics of TLS trees height in 2017 calculated using backward prediction.

Statistics	TLS Tree Height 2017
Total	12129.7
Average	13.9
St. Dev	2.8
Max	22.5
Min	6.8

Histogram of TLS trees height in 2017 illustrates the distribution of trees height of 2017 by 1 m range or class between 7 m to 23 m. The highest number of trees was in the range of 13 -14 m and the range of 7–8 m was the lowest number of trees. By classifying trees height into three classes, 53 trees had a height of less than 10 m, while the majority (795 trees) were in the range class of 10-20 m and 28 trees had a height above 20 m (Figure 3.8).

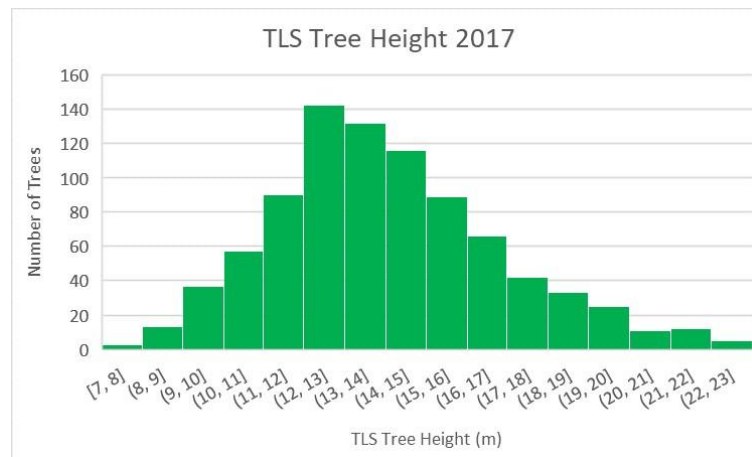


Figure 3.8 Histogram of TLS trees height measurements in 2017 calculated using backward prediction.

Boxplot of TLS trees height measured in 2017 concludes that plot 23 had the highest mean of trees height while the lowest mean of trees height was in plot 18. There were 21 outliers which indicated and spread in 10 plots. Plot number 2, 7, 17, 19, 23, 24 and 29 had one outlier, while plot number 9, 10 and 28 had two outliers. Three outliers were in plot 1, and four outliers were founded in plot 5 and 8. The boxplot (Appendix 4 Figure 5) shows the short range of trees height was in plot 28 and most of the median of trees height was in the range 11- 15m, and it was close to the average tree height of 2017 derived from TLS.

### 3.3 UAV image processing

The consecutive overlapped images of UAV 2018 and 2017 were processed using SfM method to produce orthomosaic, digital surface model (DSM) and digital terrain model (DTM). This process was done by employing software Pix4D MapperPro version 4.0.24. Moreover, GPCs and checkpoints were utilised as geo-references in the image rectification process. While generating canopy height model (CHM) was executed by subtraction between DTM from DSM using ArcGIS version 10.6.1. These UAV image processing of 2018 and 2017 are explained in the following sub-sections.

### 3.3.1 UAV 2018 image processing

UAV 2018 images were acquired on 18 December 2018 using Phantom 4 DJI with camera model FC 3610 was covered nearly one km<sup>2</sup> in the study area. It measured approximately 165m of flight height and using 4mm of focal length camera and captured 369 single overlapped consecutive photos. Pixel dimension of UAV 2018 was 4000 x 3000, while exposure time was every 1/60 second and had f/2.8 for F-stop. The UAV 2018 parameters can be seen in Table 3.7.

Table 3.7 UAV 2018 imaging parameters.

Parameters	UAV 2018
Acquisition	18 December 2018
No. of Photos	369
Flight height (m)	165
Focal length (mm)	4
Dimension (pixels)	4000 x 3000
F-stop	f/2.8
Exposure time (second)	1/60
Camera model	DJI FC6310

Figure 3.9 represents the UAV 2018 consecutive overlap image location which illustrates the flight route of UAV images, coordinates and reference system and the GCPs location in the study area. The red dots were single images, the blue crosses were GCP while the green lines were flight route.



Figure 3.9 UAV 2018 image processing.

### 3.3.2 Orthomosaic, DSM and DTM of UAV 2018

The result of UAV 2018 image processing is shown in Table 3.8 which captured 98 ha of covered area, had 6.21 cm of ground sampling distance. Root mean square errors (RMSE) of UAV 2018 was 47 cm, and the number of generated tiles was 7. More than 100 million 3D densified points generated 30.27 average density per m<sup>3</sup>. Orthomosaic had the same as image resolution as DSM, namely 6.21 cm when DTM has five times image resolution (30.05 cm) compared to the image resolution of orthomosaic/DSM.

In term of GCPs of UAV 2018, it shows that the RMS Error was 0.047 m. Four GCPs were used to rectify the images of 2018. Table 3.9 shows that GPC P07 had the highest error, which comprises -0.105 in X coordinate and 0.057 in Z coordinate, while GCP P05 contributes the higher error on Y coordinate (-0.069). RMS error consisted 7cm on X-axis, 48cm on Y-axis and 24 on Z-axis.

Table 3.8 UAV 2018 images result.

Parameters	UAV 2018
Ground sampling distance (cm)	6.21
Covered area (km <sup>2</sup> )	0.98
Georeferencing RMSE (m)	0.047
Number of generated tiles	7
Number of 3D densified points	107775485
Average density (m <sup>3</sup> )	30.29
DSM and orthomosaic resolution (cm)	6.21
DTM resolution (cm)	30.05

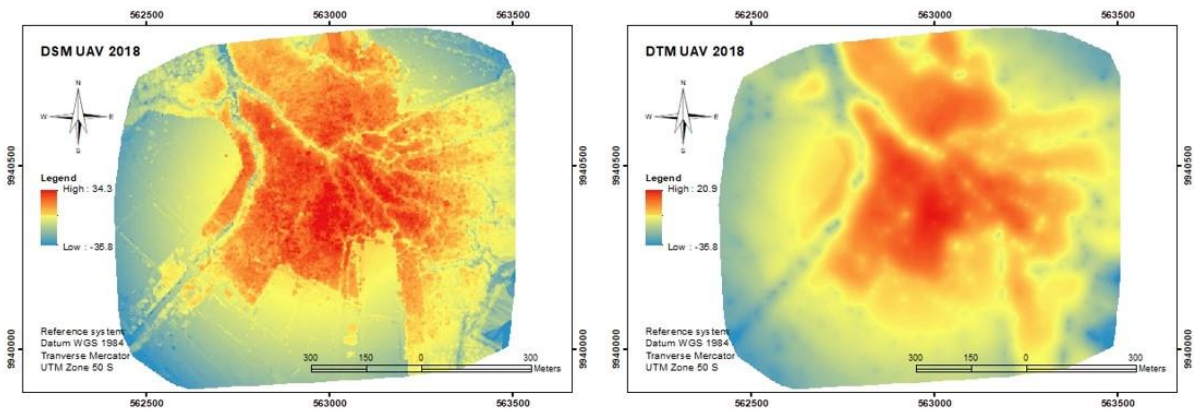
Table 3.9 GCPs of UAV 2018.

GCP	X	Y	Z
P02	0.080	0.046	0.008
P05	0.020	-0.069	-0.006
P07	-0.105	-0.045	0.057
P11	0.043	-0.015	0.002
Mean (m)	-0.012	0.001	0.015
Sigma (m)	0.069	0.047	0.024
RMS Error (m)	0.070	0.048	0.029

Orthomosaic image of the UAV 2018 is presented in Figure 3.10. The reference system used datum WGS 1984 when the projection employed Transverse Mercator (TM). UAV 2018 which had 369 images, covered 98 ha and located in UTM zone 50 S.



Figure 3.10 Orthomosaic image of UAV 2018.



a. DSM 2018

b. DTM 2018

Figure 3.11 DSM and DTM UAV 2017.

Beside to generate orthomosaic, UAV image processing using Pix4D Mapper Pro also produced point clouds, DSM and DTM. There was a different pixel resolution between DSM and DTM. Thus, the resampling process was applied to the DTM so that DSM and DTM had the same pixel size, then CHM could have been generated by subtracting DTM from DSM. DSM, DTM of UAV 2018 are shown in Figure 3.11

### 3.3.3 Generating CHM 2018

The result of CHM UAV 2018 had the range value from -6.9 m to 29.3 m, which is represented by a colour ramp from blue to red. It meant the redder the colour, the higher the trees were. Figure 3.12 shows that the majority of the high trees mangrove in the UAV 2018 had a yellow colour, while red colour spread randomly. Thus, most of the trees have a height range between 10 m-20 m. In term of the red colour of CHM, this colour of trees also had a pattern along the river. This pattern related to the issues that fisherman preserve the mangroves near the river to deceive the forest ranger or local government. While low trees height area and shrimp ponds were represented by the blue-yellowish colour.

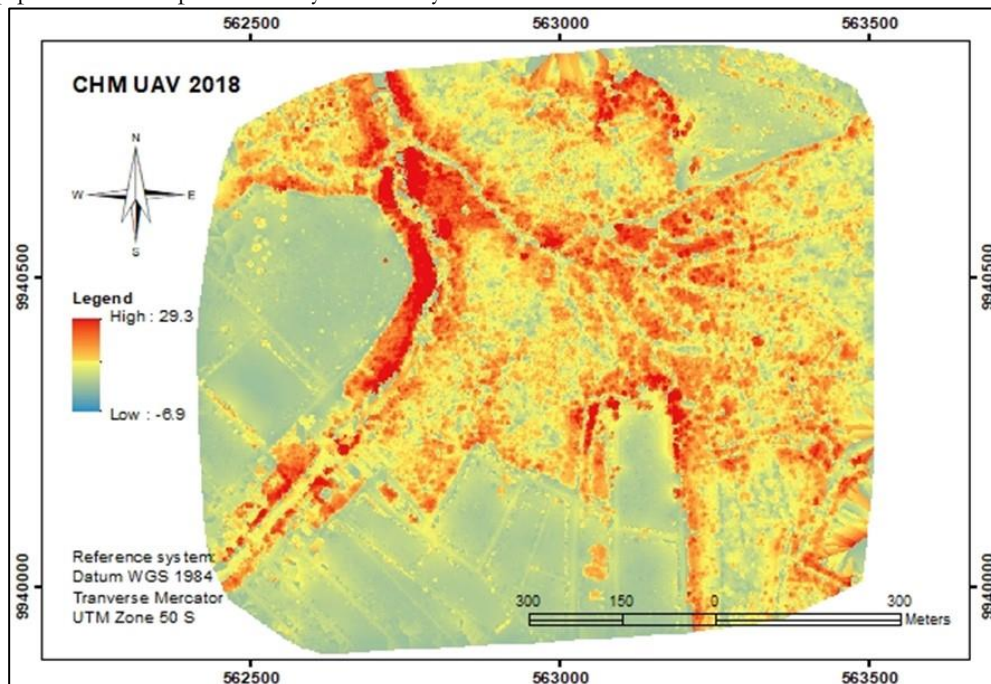


Figure 3.12 CHM of UAV 2018.

### 3.3.4 UAV 2017 image processing

UAV 2017 images were collected on 25 October 2017 which contained 54 images in 5 flight lines. It employed Phantom 4 DJI with camera model FC330, while the flight height was approximately 372 m. The camera used 9mm of focal length, and the pixel dimension was 4864 x 3648. It captured by 1/20second (exposure time) which had f/4.5 for F-stop (Table 3.10).

Table 3.10 UAV 2017 imaging parameters.

Parameters	UAV 2017
Acquisition	25 October 2017
No. of Photos	54
Flight height (m)	372
Focal length (mm)	9
Dimension (pixels)	4864 x 3648
F-stop	f/4.5
Exposure time (second)	1/20
Camera model	DJI FC330

Figure 3.13 shows UAV 2017 by the number of photos, flight line, GCPs location which was represented by red dots, blue crosses and green lines as well as a reference system, using WGS 1984 UTM zone 50 S.

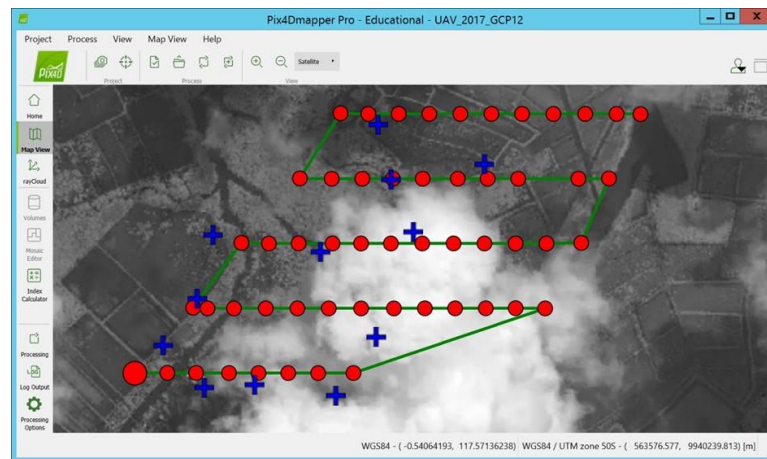


Figure 3.13 UAV 2017 image processing

### 3.3.5 Orthomosaic, DSM and DTM of UAV 2017

The results of UAV 2017 image processing which produced orthomosaic, DSM, DTM and points cloud, also provided information related to the derived products. UAV 2017 which captured 130 ha of study area having 9.3 cm of ground sampling distance (GSD) with 30.2 cm of RMSE. The number of generated tiles was 10, while the number of 3D densified points were more than 134 million and the average density of 3D points were 29.6 m<sup>3</sup>. Moreover, DTM image resolution had five times larger than orthomosaic and DSM. Base on that case, resampling was done to the DTM in order to get the same image resolution with the DSM. The imaging parameters of the UAV 2017 are presented in Table 3.11

The result report of mosaicking the images of UAV 2017 is shown in Table 3.12. The report provides information related to GCPs. UAV 2017 used 6 GCPs to geo-referencing the images, which spread in the whole study area and can be seen in Figure 3.17 (in blue crosses). Regarding GCPs UAV 2017, the average RMS error was 30 cm, while it was higher in X-axis and Y-axis contribute twice compared to Z-axis. GCP P07 had the highest error in X-axis while in the Y-axis and Z-axis were much less. GCP P10 had 0.599 m and -0.473 m of Y and Z-axis respectively (Table 3.12)

Table 3.11 UAV 2017 imaging parameters.

Parameters	UAV 2017
Ground sampling distance (cm)	9.29
Covered area (km <sup>2</sup> )	1.28
Georeferencing RMSE (m)	0.302
Number of generated tiles	10
Number of 3D densified points	134704464
Average density (m <sup>3</sup> )	29.63
DSM and orthomosaic resolution (cm)	9.29
DTM resolution (cm)	46.45

Table 3.12 GCPs of UAV 2018.

GCP	X	Y	Z
P02	0.181	0.187	-0.105
P03	0.340	-0.359	-0.188
P06	-0.483	-0.385	-0.001
P07	0.435	-0.156	-0.003
P10	-0.228	0.599	-0.473
P11	-0.045	0.020	0.163
Mean (m)	0.003	-0.016	-0.101
Sigma (m)	0.370	0.339	0.198
RMS Error (m)	0.371	0.340	0.222

The result of the orthomosaic UAV 2017 image is presented in Figure 3.14. This UAV product employed the same reference coordinate system as UAV 2018 products. WGS 1984 was applied as a global datum, and Universal Transverse Mercator was employed as a projection system, while UTM zone 50 S was used in the study area to calculate in the metric unit (meter).

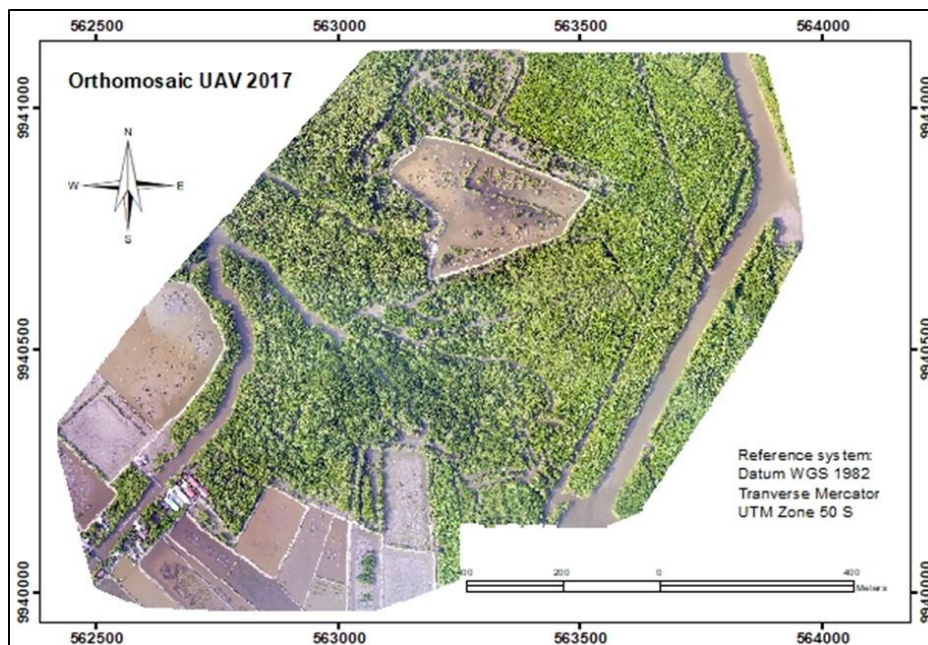


Figure 3.14 Orthomosaic UAV image of 2017.

After resampling DTM, it had the same image resolution as DSM (i.e., 9.29cm), thus generating CHM was possible. Figure 3.15 shows both DSM and DTM of 2017 had the same low value of height (-19.9 m), while in the highest value in DSM reaches up to 23.8 m and in the DTM was 17.3 m. It is logic that DSM is higher than DTM because DSM represents the surface while the terrain is illustrated by DTM.

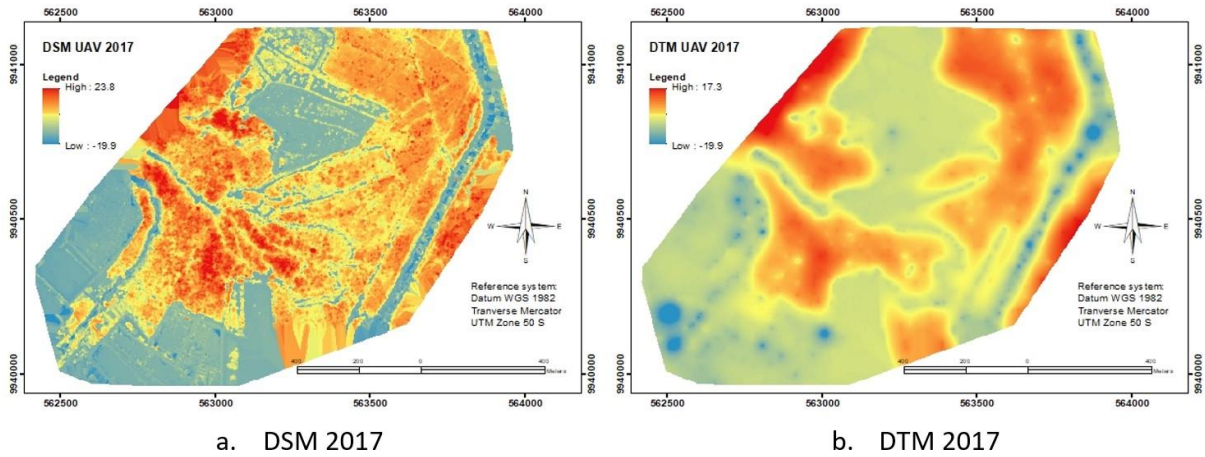


Figure 3.15 DSM and DTM images of UAV 2017.

### 3.3.3 Generating CHM 2017

Canopy height model (CHM) was derived by subtracting DTM from DSM. In this case, we have used the Raster Calculator-Spatial Analyse Tool in ArcGIS software. The result shows that DSM had a range between -19.9 m to 23.4 m, while the range of DTM was -19.9 m to 17.3m. CHM is relative height between DSM and DTM. CHM image showed a range of -4.9 m to 27.3 m. In term of colour in the legend, the blue colour was represented low value, and a high value was a red colour. Figure 3.16 shows the generated result of the CHM image of UAV 2017.

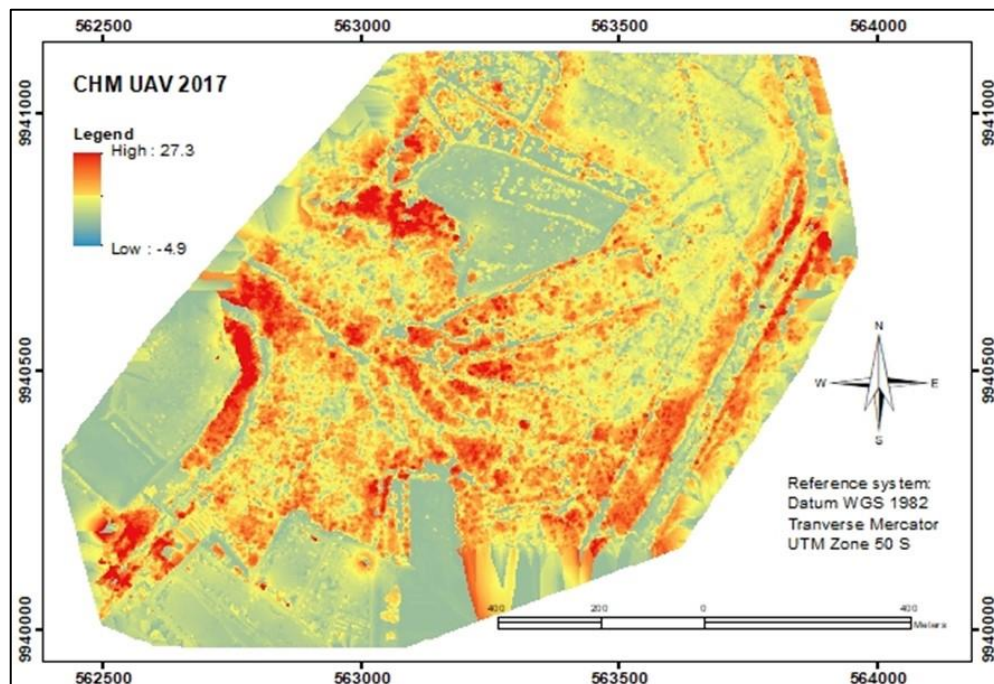


Figure 3.16 CHM image of UAV 2017.

### 3.4 Crown Projection Area

Crown projection area was produced by manual digitising the two dimensions of the crown area of the trees in every plot using orthomosaic of UAV 2018 and UAV 2017. Afterwards, CPA was employed to derive crown diameter.

#### 3.4.1 The crown projection area of 2018

The average of the crown projection area of 2017 was 7.7 m<sup>2</sup>, and 5.5 m<sup>2</sup> was the standard deviation of the data. While the maximum and the minimum of CPA were 67.9 m<sup>2</sup> and 1.5 m<sup>2</sup> respectively. The summary statistic of CPA 2018 can be seen in Table 3.13

Table 3.13 Statistics summary of crown projection area measured from UAV images of 2018.

Statistics	CPA 2018
Total	6729.8
Average	7.7
St. Dev	5.5
Max	67.9
Min	1.5

The histogram Figure 3.17 of the crown projection area of 2018 reveals that the data which was right-skewed had a range of CPA from 1.5m<sup>2</sup> to 67.9m<sup>2</sup>. Majority of trees had CPA in the extent of 1m<sup>2</sup> to 19m<sup>2</sup> that comprised more than 800 trees. The most frequent class was the range of 3m<sup>2</sup> to 5m<sup>2</sup> of CPA which was almost 250 trees. Only three frequency classes of CPA reached more than a hundred trees, while CPA between 1m<sup>2</sup> and three m<sup>2</sup> was nearly hundred trees.

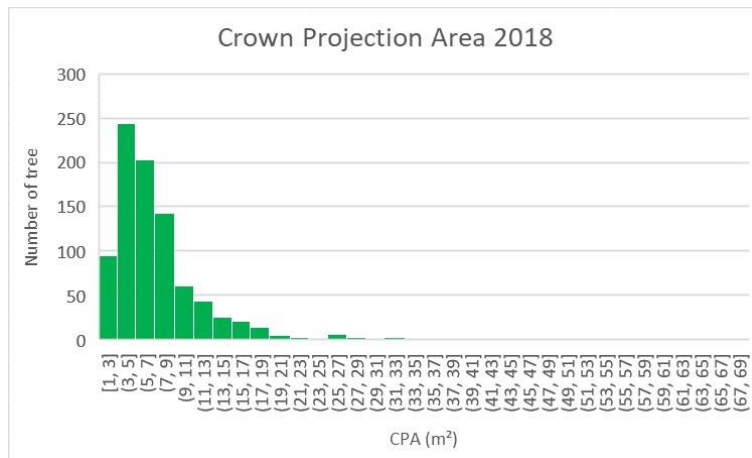


Figure 3.17 Histogram distribution of the crown projection area in 2018.

Based on the boxplot of CPA 2018 (Appendix 4 Figure 6), 53 outliers were in 21 plots. Seven outliers had the highest values which were located in plot 9 and a total of five outliers in Plot 7. Trees with large CPA (e.g., more than 30 m<sup>2</sup>) became an outlier in plot 4, 5, 17, 20, 27 and 30. Moreover, less than ten trees had CPA above 30 m<sup>2</sup>, and the largest CPA had reached almost 70m<sup>2</sup>.

#### 3.4.2 The crown projection area of 2017

In terms of CPA 2017, the average CPA was 6.7 m<sup>2</sup> compared to 7.7 m<sup>2</sup> of 2018. The maximum and minimum CPA of 2017 was 62.5 m<sup>2</sup> and 1.4 m<sup>2</sup>, while 5m<sup>2</sup> was the standard deviation of this dataset. Contrasted to 2018, all the figure of statistic summary of CPA 2018 was lower (Table 3.14).

Histogram of the crown projection area of 2017 which had a range of CPA from 1 m<sup>2</sup> to 63 m<sup>2</sup> was right-skewed like 2018. More than 800 trees had CPA less than 20 m<sup>2</sup>, while CPA values more than 20 m<sup>2</sup> comprised of 19 trees. Only four classes exceeded a hundred trees in total, which located in the range of 1

m<sup>2</sup> to 9 m<sup>2</sup>. The total number of CPA more than 10 m<sup>2</sup> did not exceed the number of trees in the frequency class of 3 – 5 m<sup>2</sup>. This frequency class had the highest number of the tree in CPA 2017, which contained more than 250 trees. Figure 3.18 illustrates the histogram of CPA 2017.

Table 3.14 Statistics summary of crown projection area in 2017.

Statistics	CPA 2017
Total	5872.0
Average	6.7
St. Dev	5.0
Max	62.5
Min	1.4

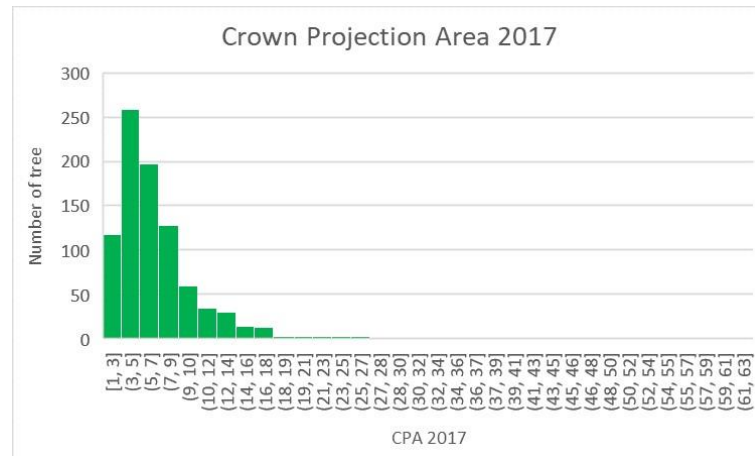


Figure 3.18 Histogram distribution of the trees crown projection area in 2017.

Boxplot of CPA 2017 depicts that there were 54 outliers spread in 22 plots. The highest number of outliers were located in Plot 19 which consisted of 6 outliers, followed by Plot 7 with five outliers. Meanwhile, only eight plots did not have outliers, namely plots 2, 10, 11, 12, 21, 22, 23 and 29. There was an increase in the number of outliers in plot 1, 6, 16, and 26, while the number of outliers in plot 17 and 19 was less compared to CPA 2018. Boxplot of CPA 2018 is shown in Appendix 4 Figure 7.

### 3.5 Crown Diameter

Crown diameter could be observed in the field, which was measured by averaging the of two perpendicular measurements of the crown diameter which was shown in Figure 1.4 (b) in Chapter 1. To avoid subjective measurements due to human error, the crown projection area was used to generate crown diameter.

#### 3.5.1 The crown diameter of 2018

The statistical summary of crown diameter of 2018 is shown in Table 3.15. It shows that the average crown diameter was 3 m with 0.9 m of standard deviation. The maximum and minimum crown diameter of the trees were 9.3 m and 1.4 m, respectively.

As shown in Figure 3.19, the histogram distribution of the crown diameter in 2018 was right-skewed. The highest number of trees were in the frequency class of 2.4-2.7 m, while most of the data located in the range of 1.7m to 4.0m of crown diameter. There were four classes in the range of 2.0 m to 3.4 m of the crown diameter which had the number of trees more of than 100. Moreover, the maximum crown diameter of 2018 was in the range 9.0 m to 9.3 m which had the lowest number of trees.

Table 3.15 Statistics summary of crown diameter 2018.

Statistics	Crown Diameter of 2018
Total	2621.5
Average	3.0
St. Dev	0.9
Max	9.3
Min	1.4

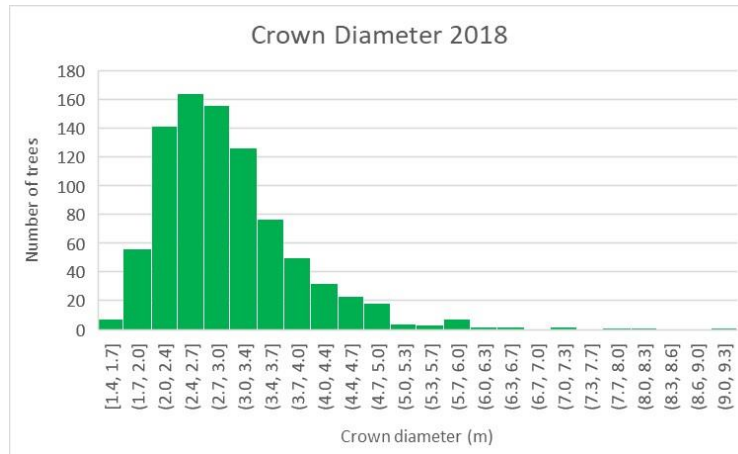


Figure 3.19 Histogram distribution of crown diameter of trees in 2018.

The boxplot of crown diameter 2018 (Appendix Figure 8) shows that most of the plots had the mean in the range 2.5 m to 3.5 m. There were 27 outliers, located in 16 plots. Plots 19 has the most outliers, followed by Plot 27 with three outliers. There were two outliers in plots 5, 8, 16, 25 and 30, while plots 3, 4, 9, 17, 20, 24 and 29 had one outlier.

### 3.5.2 The crown diameter of 2017

Compared to the crown diameter of 2018, the crown diameter of 2017 was lower. The average crown diameter of 2017 was 2.8 m with 0.8 m of standard deviation. Also, the maximum crown diameter was 8.9m while the minimum was 1.3 m. The summary statistics of crown diameter of 2017 is presented in Table 3.17.

Table 3.16 Statistics summary of crown diameter 2017.

Statistics	Crown Diameter of 2017
Total	2445.9
Average	2.8
St. Dev	0.8
Max	8.9
Min	1.3

Histogram of the crown diameter of 2017 (Figure 3.20) has the same pattern of right-skewed like in 2018. The highest number of trees were located in the frequency class of 2.3 - 2.6 m, while the majority of trees with the crown diameter were in the range of 1.6 m to 3.8 m compared to 2018 data (2.0 m to 3.4 m). It also consists of 4 classes of the crown diameter frequency classes that had the number of the trees which were more than hundreds namely frequency classes 2.0-2.3 m, 2.3-2.6 m, 2.6-2.9 m, and 2.9-3.2 m.

Regarding boxplot of crown diameter in 2017, most of the plots also had the mean in the range of 2.5 m to 3.5 m. The outlier of crown diameter also increases to 31, where spread in 19 plots. Plot 7 was having the

highest outliers, followed by three outliers in plots 27 and 30. While plots 3, 5, 8, 16, 25 had two outliers. Whereas one outlier was found in plots 1, 4, 9, 13, 14, 17, 18, 19, 20, 24, and 28. Boxplot of the crown diameter of 2017 is presented in Appendix 4 Figure 9.

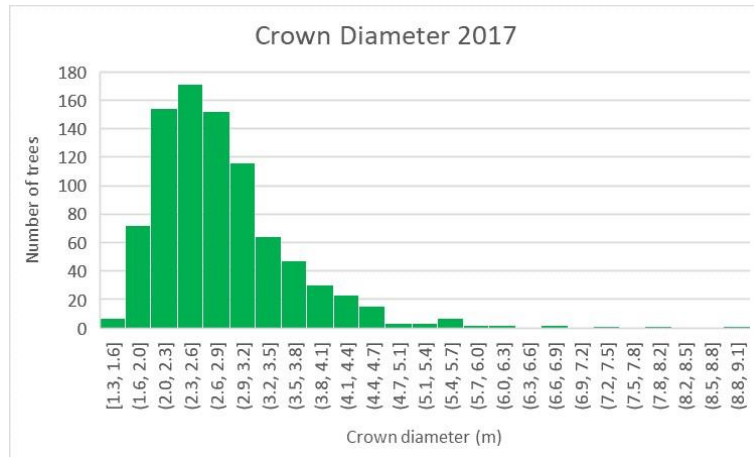


Figure 3.20 Histogram distribution of trees crown diameter in 2017.

### 3.6 Crown Height Measurement

Crown height measurement (CHM) of an individual tree was extracted by generating the maximum value of CHM of 2018 and 2017 using the CPA (i.e., crown) of every single tree. The result of CHM was applied to make a relationship with trees height measurements derived from TLS point cloud data. Then CHM was used to calculate aboveground biomass/carbon stock and compares it to biometric AGB.

#### 3.6.1 The crown height measurement of 2018

Statistic summary of CHM 2018 shows that the average was 14.1 m which had 2.9 m of standard deviation. The maximum and minimum values of tree height derived from CHM of UAV 2018 were 23.4 m and 6.8 m respectively. Table 3.17 Statistics summary of CHM 2018 shows the summary statistics of CHM in 2018.

Table 3.17 Statistics summary of CHM 2018.

Statistics	CHM 2018
Total	12273.4
Average	14.1
St. Dev	2.9
Max	23.4
Min	6.8

Histogram of CHM 2018 Figure 3.21 was right-skewed which dominated by CHM in the range of 10 m – 20 m. CHM 2018 started from 7 m to 24 m, and the highest number of the trees was in the frequency class of 13 - 14m, which included more than 150 trees. Four classes of CHM 2018 exceeded 100 trees, which consisted of the classes of 11 – 12 m, 12 – 13 m, 13 – 14 m and 14 – 16 m. Moreover, CHM 2018 of more than 20m comprises 43 trees only.

Boxplot of CHM 2018 shows that the median plots were in the range 10 to 15 m, while the highest was located in plot 23. Outliers were spread in 11 plots, which consisted of 23 outliers in total. Plot 17 and 28 had four outliers, followed by three outliers were in plot 19. Plot 8 had the highest range of tree height, approximately from 8 m to 23 m, while plot 28 was the smallest range (Appendix 4 Figure 10).

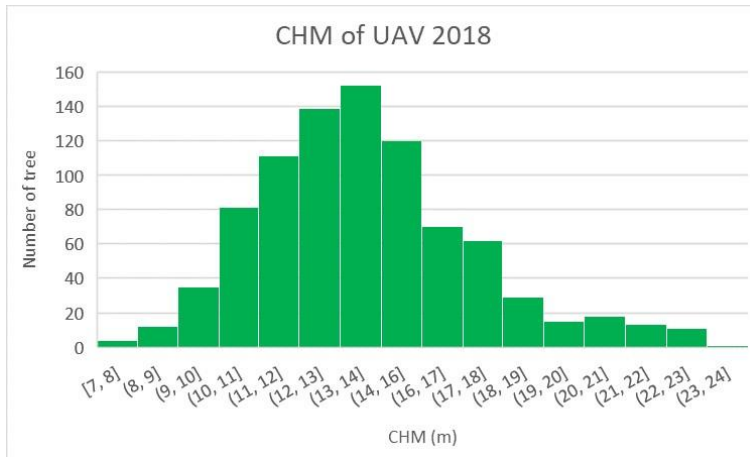


Figure 3.21 Histogram CHM 2018.

### 3.6.2 The crown height measurement of 2017

The maximum and minimum tree height or CHM was 22.3 m and 5.8 m respectively. While the average of CHM derived from UAV 2017 data was 12.4 m and the standard deviation was 2.9 m. Comparing to 2018, CHM of 2017 had low altitude; which was normal because the trees in 2018 were higher than in 2017. Table 3.18 presents the summary statistic of CHM in 2017.

Table 3.18 Statistics summary of CHM 2017.

Statistics	CHM 2017
Total	10792.1
Average	12.4
St. Dev	2.9
Max	22.3
Min	5.8

Histogram of CHM 2018 was right skew. However, it had high value in the range of 11 – 12 m. Four frequency classes of trees height in the range 9 – 13 m exceed 100 trees, while each class of trees height of 11 – 12 m 12 – 13 m and 13 – 14 m have more 125 trees in total. The minimum and maximum trees height classes are started from 6 m to 23 m. The amount of tree having a height of less than 10 m were 89 trees, and 15 trees had a height more than 20 m (Figure 3.22).

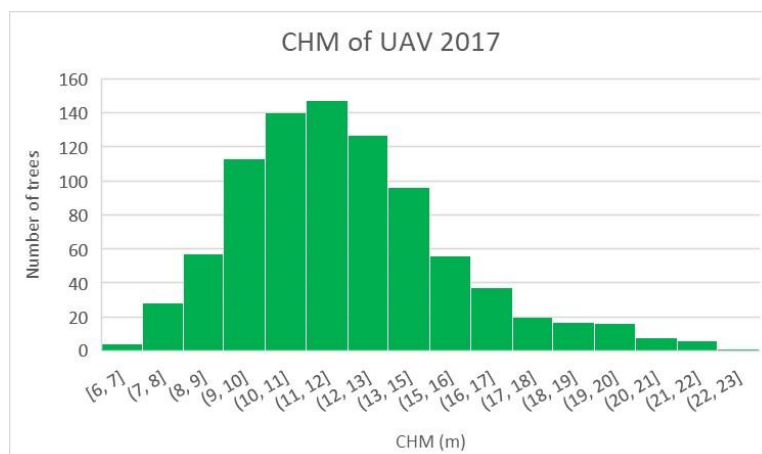


Figure 3.22 Histogram distribution of trees height or CHM in 2017.

Boxplot of CHM 2017 (Appendix Figure 11) shows that there were 19 outliers spread in 12 plots. Plots 28 had the highest number of outliers (counted four outliers), followed by three outliers located in plots 10. Plot 1 and 2 had two outliers, while one outlier was located on plot 5, 7, 8, 9, 17, 19, 20 and 29. Trees height more than 15m were located in plot 8, and plot 9 were identified as outliers when low altitude trees less than 10 m were also recognized as outlier in plot 1, 7, 10, 20, 28 and 29. Most of the median in plots were in the range of 10 m to 15 m, while plot 23 had the highest median value around 19 m.

### 3.7 The relationship between DBH and CPA

The regression model of DBH and CPA was performed to obtain the relationship between DBH of biometric field measurement and CPA derived from UAV in both 2018 and 2017. Four hundred seven trees were selected randomly to assess the relationship between their DBH and CPA. Thus, DBH could be modelled through CPA and used with the CHM to assess AGB/carbon stock.

#### 3.7.1 The relationship between DBH and CPA of 2018

The correlation and regression of DBH and CPA 2018 showed 0.87 in R-square, while the relationship between two variables consisted of intercept and slope, namely -1.6148 and 0.5795x. Figure 3.23 shows the relationship between DBH and CPA in 2018.

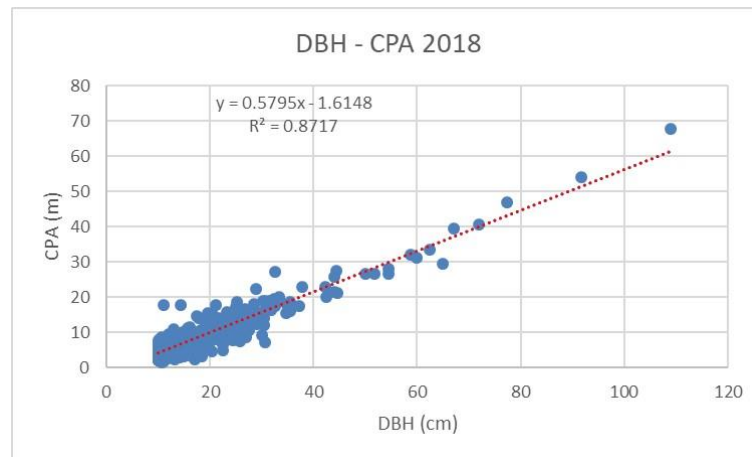


Figure 3.23 Relationship of DBH and CPA of 2018.

#### 3.7.2 The relationship between DBH and CPA of 2017

The relationship between DBH and CPA in 2017 using the elected trees was assessed. The R-square was almost the same as R-square of DBH and CPA 2018. R2 of 2017 data was 0.874. While its intercept was -1.4016 and 0.5251x was its slope (Figure 3.24).

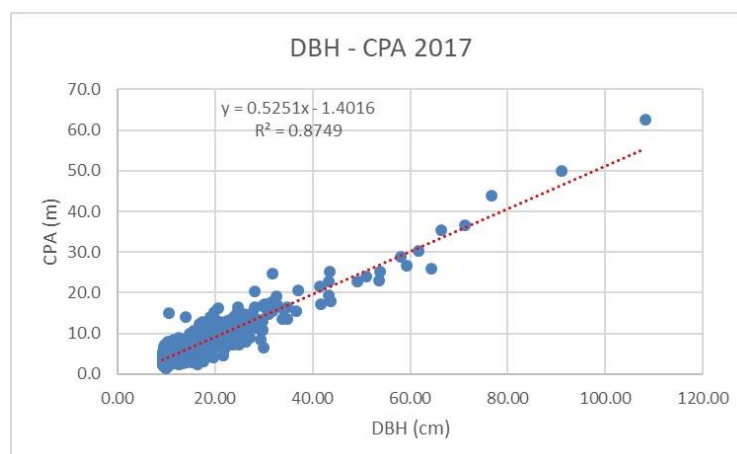


Figure 3.24 Relationship of DBH and CPA of 2017.

### 3.8 The relationship between tree height derived TLS and tree height derived CHM of UAV

The same 301 trees, which were selected randomly to assess the relationship between DBH and CPA, were used to assess the relationship between the TLS trees height and CHM or UAV trees height in both years of 2017 and 2018. Based on those trees, the correlation and regression were performed to observe the relationship between tree height derived from TLS and tree height derived CHM of UAV in 2018 and 2017.

#### 3.8.1 The relationship between tree height TLS and CHM of 2018

The relationship between tree height TLS and CHM 2018 for selected trees showed a high correlation. The figures showed 0.85 of R-square, 0.5367 of intercept and 0.9556x of the slope. The relationship between tree height TLS and CHM 2018 is presented in Figure 3.25.

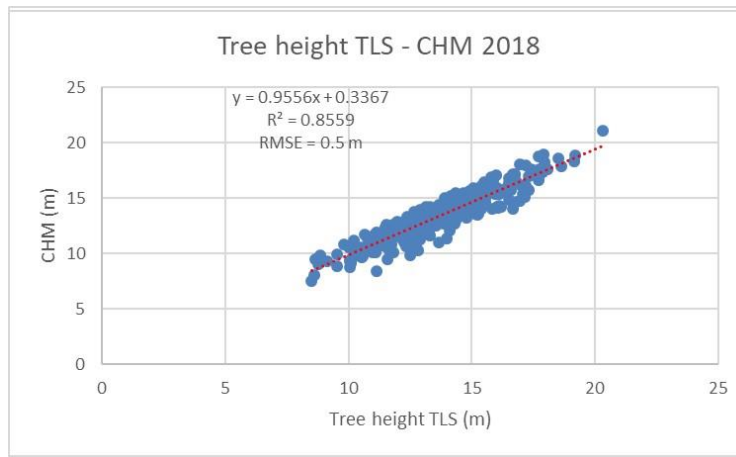


Figure 3.25 Relationship between tree height TLS and CHM of 2018.

#### 3.8.2 The relationship between tree height TLS and CHM of 2017

Compared to the relationship of tree height TLS and CHM 2018, the relationship between tree height TLS and CHM in 2017 was lower. It just performed 0.81 of R-square compared to 0.85. The intercept and slope are -0.5874 and 0.9427x respectively (Figure 3.26).

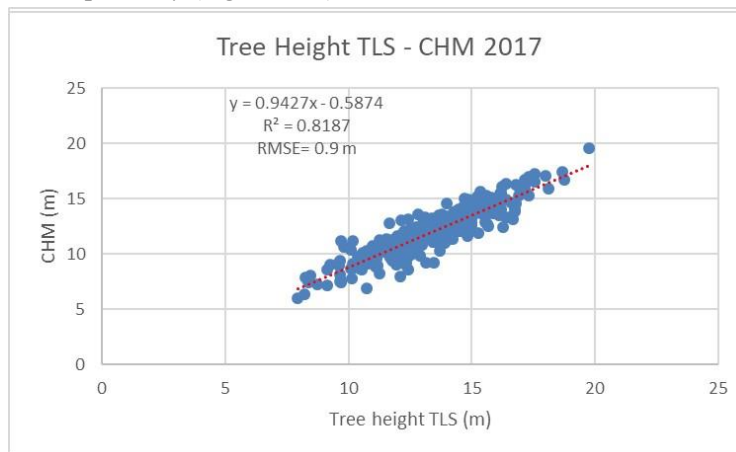


Figure 3.26 Relationship between tree height TLS and CHM of 2017.

### 3.9 The relationship between DBH and CD

In this research, the crown diameter was generated and derived from crown projection area. Related to the objective of the research, crown diameter was used to predict the DBH model from UAV data. The relationship between DBH and CD was assessed because later on when we used the DBH modelled from CPA, the AGB was not accurately estimated. While when CD was used instead of CPA to model the DBH, the modelled DBH did a reasonable job with the CD to accurately estimate AGB.

### 3.9.1 The relationship between DBH and CD of 2018

The relationship between DBH and CD in 2018 for selected trees had a high R-square of 0.80. The intercept and slope showed 1.623 and 0.0828x respectively. Figure 3.27 depicts the relationship between DBH and crown diameter of 2018.

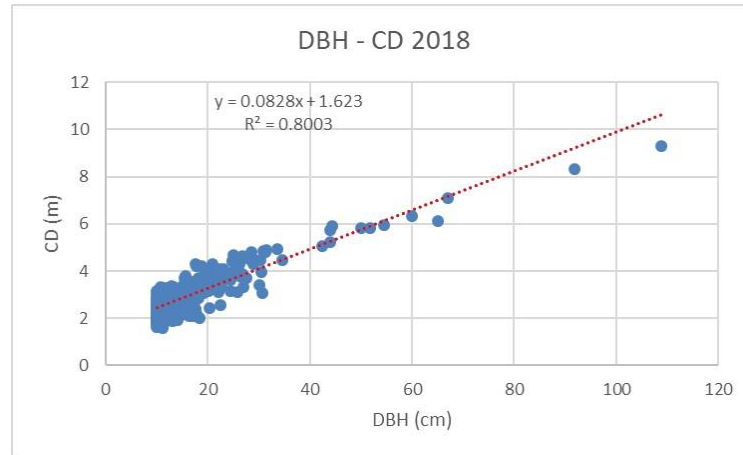


Figure 3.27 Relationship between DBH and CD of 2018.

### 3.9.2 The relationship between DBH and CD of 2017

In terms of the relationship between DBH and CD 2017, it showed a similar pattern as in 2018 data. The R-square show the value of 0.80, which almost the same as in 2018. Moreover, the intercept and slope of this relationship were 1.5375 and 0.0791x respectively (Figure 3.28).

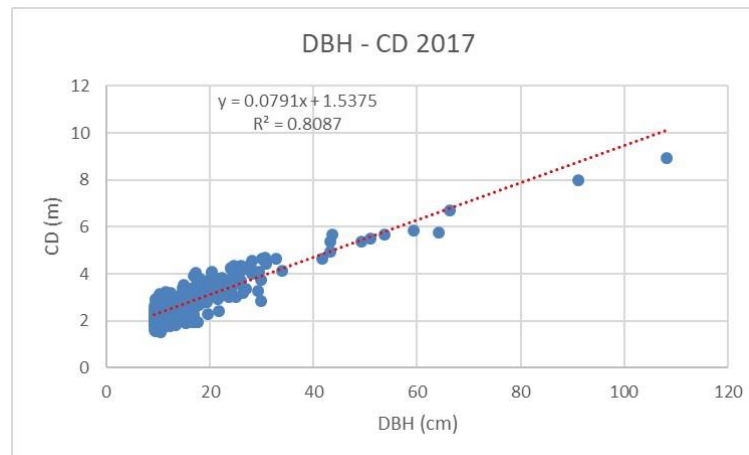


Figure 3.28 Relationship between DBH and CD of 2017.

### 3.10 Model of predicted DBH

Model and validation of predicted DBH were performed base on 407 trees, which divided into 75% for the model and 25% for validation. The number of trees that were used for the model were 301 trees, while the other trees were for validation.

#### 3.10.1 Model of predicted DBH 2018

Figure 3.29 shows the model of predicted DBH base on the relationship of crown diameter and diameter breast height had high R-square (0.80). Using the equation  $y = 10.021x - 13.329$ , DBH of 2018 was predicted. After it was performed, the RMS error of biometric DBH and predicted DBH were calculated. The result showed that the RMSE was 1.46 cm.

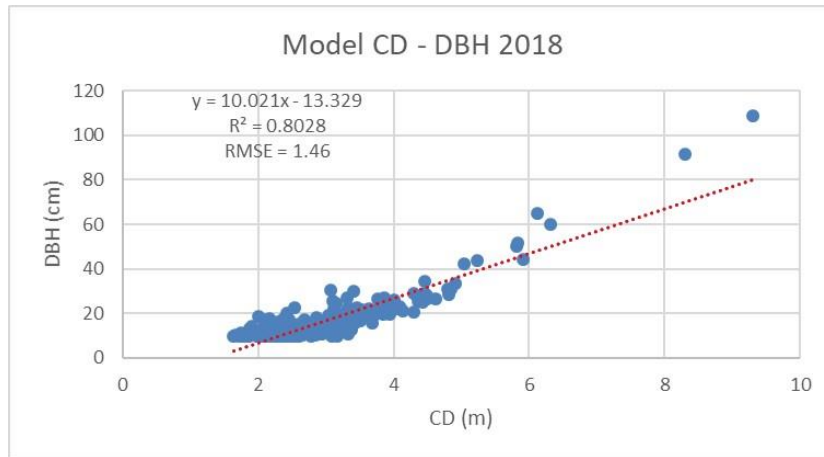


Figure 3.29 Relationship between CD and DBH of the model of predicted DBH 2018.

### 3.10.2 Model of predicted DBH 2017

The relationship between CD and DBH in 2017 was 0.81 for R-square, which was slightly higher compared to the relationship between CD and DBH in 2018. The equation to predict DBH 2017 was  $y=10.591x - 13.578$ . The RMSE was generated by comparing DBH and predicted DBH model. In this case, the RMSE was slightly lower at 1.40 cm than RMSE 2018 (Figure 3.30).

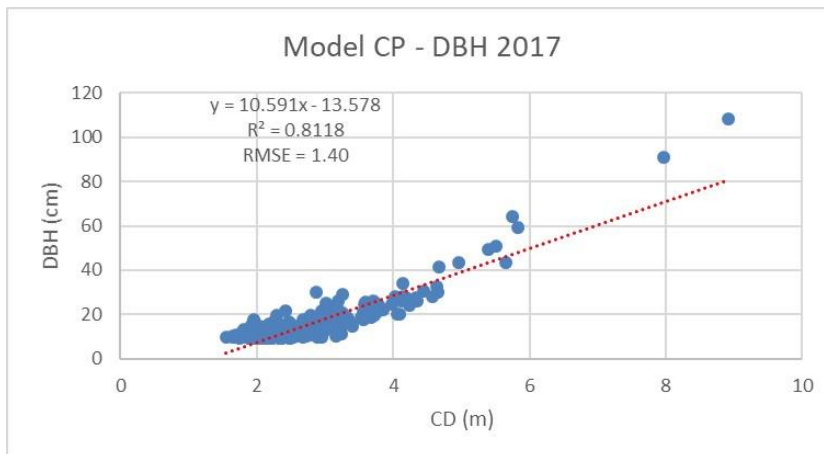


Figure 3.30 Relationship between CD and DBH of the model of predicted DBH 2017.

### 3.11 Validation of predicted DBH

Validation of the model was employed in 105 out of 406 trees (25% of selective trees). This validation was to test the performance of the model to predict DBH based on the relationship of CD and DBH. Validation also covered similar variability of the developed model.

#### 3.11.1 Validation of predicted DBH 2018

Based on the scatterplot of validation model between CD and DBH 2018, the R-square was slightly higher than the model, namely 0.81 compared to 0.80. After running the equation model 2018 to predict DBH, the RMS error of the validation was calculated by subtracting predicted DBH and measured DBH. The result shows that RMSE was the amount of 2.54 cm. Scatterplot validation model is presented in Figure 3.31.

#### 3.11.2 Validation of predicted DBH 2017

Validation model between CD and DBH 2017 had better R-square than 2018. The R-square of validation model 2017 was 0.82, compared to R-square of validation model 2018. While the RMS error of 2017 was higher than in 2018, it was in the amount of 2.47 (Figure 3.32)

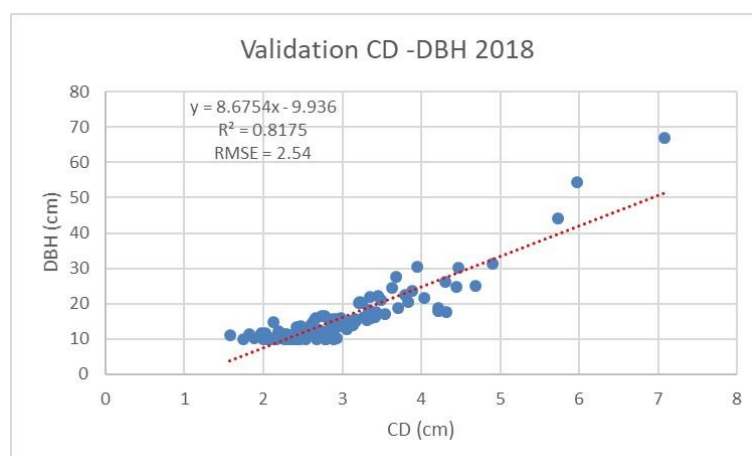


Figure 3.31 Relationship between CD and DBH of the validation of predicted DBH 2018.

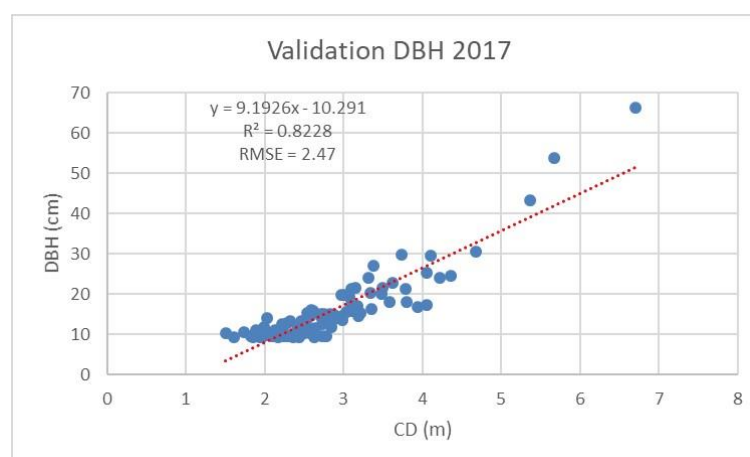


Figure 3.32 Relationship between CD and DBH of the validation of predicted DBH 2017.

### 3.12 Aboveground biomass

Based on the calculation, there were two results of aboveground biomass which consists of aboveground biomass biometric and aboveground biomass model. Both calculations used the allometric equation of Chave et al. (2005). Above ground biomass biometric was calculated based on field measurement DBH and tree height derived from TLS. While aboveground biomass modelled was calculated from DBH modelled using crown diameter and CHM of UAV. The results of both aboveground biomass/carbon stock are presented in Table 3.19 while the calculation of each plot is shown in Appendix 5.

Table 3.19 Statistics summary of aboveground biomass

Statistics	AGB Biometric (Mg/ha)			AGB Model (Mg/ha)		
	2018	2017	Sequestration	2018	2017	Sequestration
Total	3422.8	3131.2	291.6	3374.6	3047.4	327.2
Average	114.1	104.4	9.7	112.5	101.6	10.9
St. Dev	58.4	55.6	3.1	50.3	48.4	2.5
Max	293.3	273.9	19.4	274.4	258.7	15.7
Min	33.2	28.5	4.0	48.5	42.2	5.1

Table 3.19 shows that the average aboveground biomass of biometric in 2018 and 2017 was 114.1 Mg/ha and 104.4 Mg/ha. Thus, the biomass was increased by 9.7 Mg/ha on average. Moreover, the aboveground biomass model had an average of 112.5 Mg/ha in 2018 and 101.6 Mg/ha in 2017. The model showed higher growth or increase in biomass was more than the biometric, in the amount of 10.9 Mg/ha on average. The maximum plot in biometric data stored 19.4 Mg/ha of biomass, while in the AGB model, it sequestered less, in the amount of 15.7 Mg/ha. On the other hand, the minimum plot in biometric has stored 4 Mg/ha while the modelled minimum plot was higher than biometric, which was 5.1 Mg/ha with a difference around 1.1 Mg/ha. Overall, the value of the sum of biomass in 2018, 2017 as well as biomass sequestration of ABG biometric was higher than AGB model.

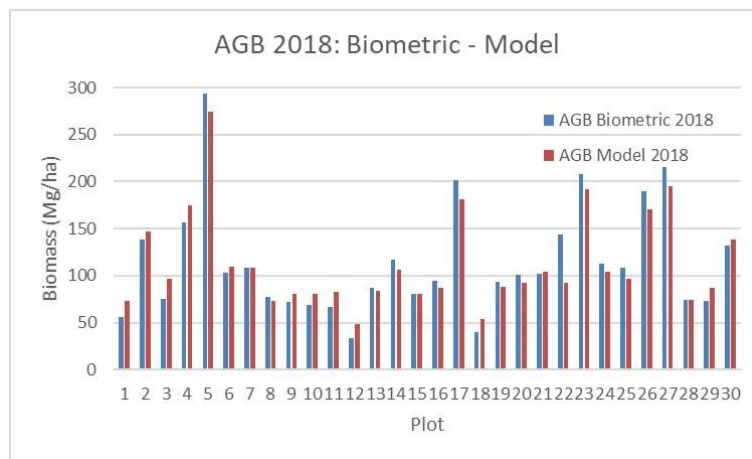


Figure 3.33 Comparison biometric and modelled AGB in 2018.

### 3.12.1 Comparison biometric and modelled of ABG 2018

As shown in Figure 3.45, in 2018 aboveground biomass biometric and model shows close values. There was a steady difference in the amount of biomass on both data in plot 5, 17, 22, 23, 26, and 27. In those plots, aboveground biomass biometric 2018 was around more than 10 Mg/ha higher compared to aboveground biomass model. On the other hand, above ground biomass model 2018 was slightly higher than biometric in plots 1, 2, 3, 4, 11, and 29. Majority of plots had biomass in the extent of 50 to 100 Mg/Ha in 2018.

As shown in the scatter plot of biometric and model of AGB 2018 (Figure 3.34), the correlation was high. The R-square is 0.93, while the RMS error was 15.5 Mg/ha. The intercept and slope of this correlation were 17.242 and 0.8348x. There was high distance across the trend line in 4 plots as illustrated in the green circle.

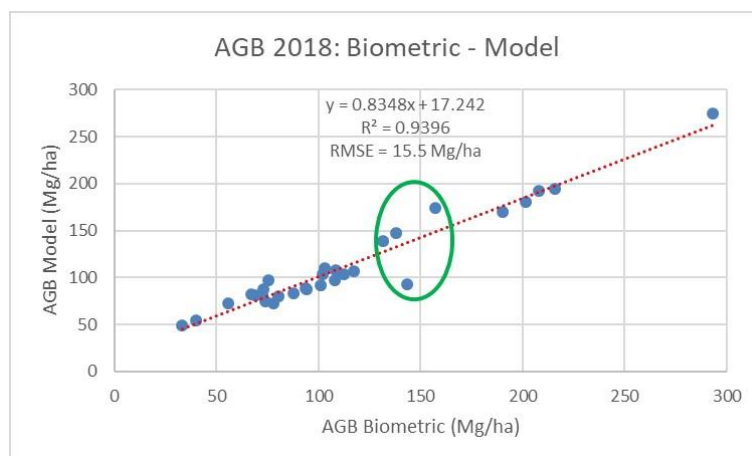


Figure 3.34 Relationship between biometric and modelled of AGB in 2018.

### 3.12.2 Comparison biometric and modelled of AGB 2017

In term of aboveground biomass biometric and model 2017, Figure 3.47 shows a similar pattern as 2018. In general, aboveground biomass biometric 2017 was higher than the model. In plot number 6, 7, 21, and 28, both of aboveground biomass were close to biomass stored in 2017. The comparison between biometric and model of AGB 2017 was presented in Figure 3.35.

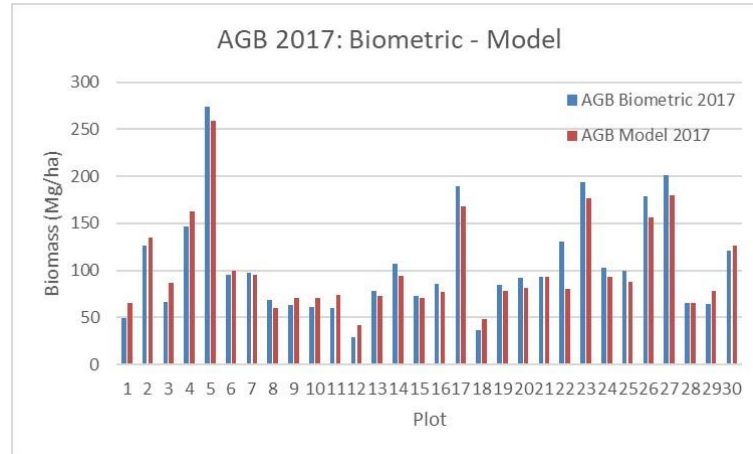


Figure 3.35 Comparison of biometric and modelled AGB in 2017.

Scatterplot of biometric and model of ABG 2017 shows a significant relationship. The R-square which was less than 2018 data, was 0.93, while the RMS error was slightly higher than in 2018 was 15.4 Mg/ha. Moreover, the result show intercept and slope were 13.906 and 0.84x. There was also large distance across the trend line as presented in the green circle (Figure 3.36).

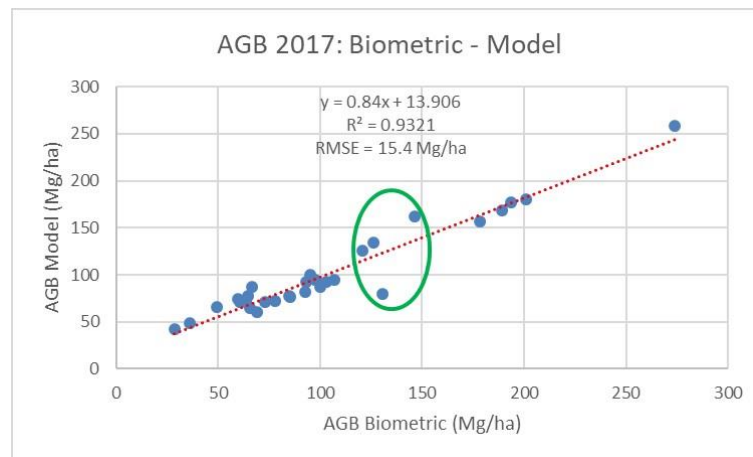


Figure 3.36 Relationship between biometric and modelled of AGB in 2017.

### 3.12.3 Comparison biometric and modelled of AGB sequestration

Figure 3.37 shows biometric and model aboveground biomass sequestration. In general, the AGB modelled in most of the plots were sequestering higher than the biometric. There was a gradual difference in sequestration of biomass both of two data in plot 5, 7, 8, 20, 21, 24 and 26. In those plots except plot 5, the model was more sequester than biometric, while in plot 5, the only plot in which biometric was higher than the model. There was the same amount of sequestration of both data in plot 17 and 22. Majority of the plot in both data sequestered in the range between 5 Mg/ha to 10 Mg/ha a year.

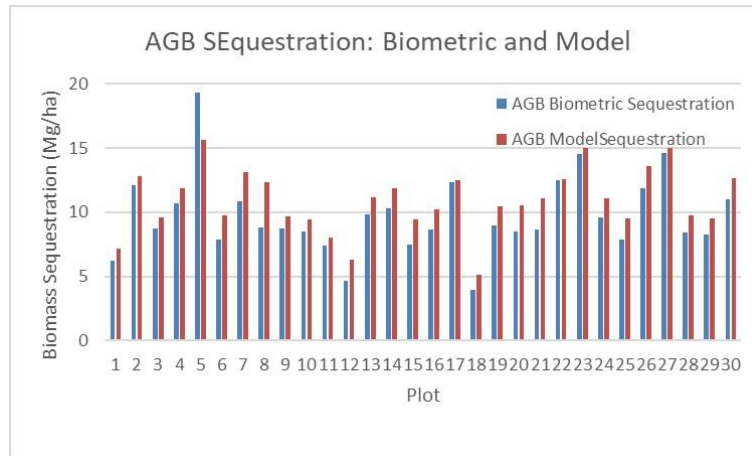


Figure 3.37 Comparison biometric and modelled of AGB sequestration.

The relationship between biometric and model of biomass sequestration shows that there was a significant relationship of biomass sequestration. The intercept and slope are 3.5911 and 0.7526x. The R-square and RMS error are 0.87 and 1.6 Mg/ha respectively (Figure 3.38).

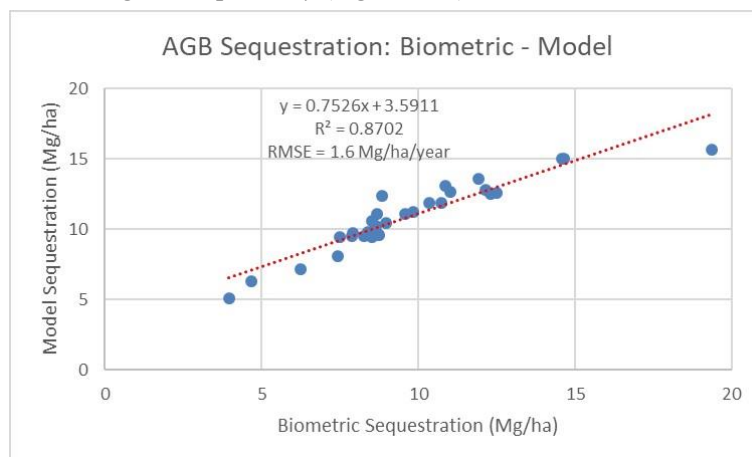


Figure 3.38 Relationship between biometric and modelled AGB sequestration.

### 3.13 Carbon stock

In general, carbon stock was half of the biomass, which was calculated by multiple 0.5 or 0.47. In this case, carbon stock was computed using 0.5 as a multiplier number. Table 3.20 Statistics summary of carbon stock shows the average carbon stock biometric data in 2018 and 2017 were 57 Mg/ha and 52.2 Mg/ha, which sequestered almost 5 Mg/ha/year. Meanwhile, the carbon stock model on average stored 56.2 Mg/ha in 2018 and 50.8 Mg/ha in 2017 and it sequestered carbon in the amount of 5.5 Mg/ha/year. Thus, the maximum sequestration showed 9.7 and 7.8Mg/ha in the biometric and modelled carbon stock with a difference of 1.9 Mg/ha. While the minimum carbon sequestration was 2.0 and 2.6 Mg/ha for the biometric and modelled carbon stock with a difference of 0.6 Mg/ha. The calculation of carbon stock and carbon sequestration each plot is shown in Appendix 6.

#### 3.13.1 Comparison biometric and modelled of carbon stock 2018

As illustrated in Figure 3.39, there were four plots that stored more carbon stock than 100 Mg/ha in the biometric data in 2018 which comprise of plot 5, 17, 23 and 27. Only five plots of the carbon stock model 2018 data exceeded the storage of 75Mg/ha. Most of both biometric and model of carbon stock data sequestered carbon stock in the range of 25 to 75Mg/ha in 2018.

Table 3.20 Statistics summary of carbon stock

Statistics	Carbon Stock Biometric (Mg/ha)			Carbon Stock Model (Mg/ha)		
	2018	2017	Sequestration	2018	2017	Sequestration
Total	1711.4	1565.6	145.8	1687.3	1523.7	163.6
Average	57.0	52.2	4.9	56.2	50.8	5.5
St. Dev	29.2	27.8	1.5	25.2	24.2	1.2
Max	146.6	137.0	9.7	137.2	129.3	7.8
Min	16.6	14.3	2.0	24.3	21.1	2.6

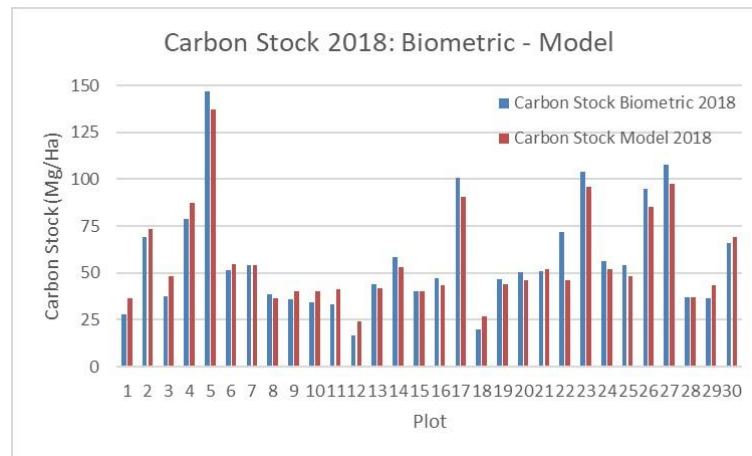


Figure 3.39 Comparison biometric and modelled of carbon stock in 2018.

Correlation between carbon stock 2018 biometric and model shows a significant relationship. The R-square was 0.93, while the RMS error was 7.8 Mg/ha. Furthermore, intercept and slope of that relationship were 8.6212 and 0.8348x. Figure 3.40 depicts the relationship between biometric and model carbon stock in 2018.

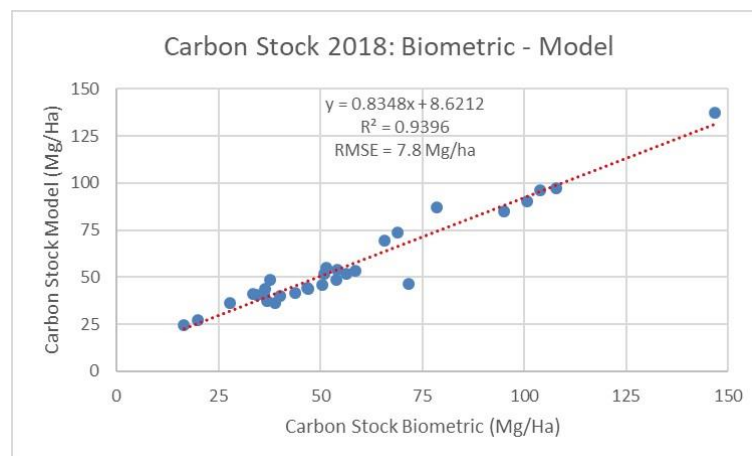


Figure 3.40 Relationship between biometric and modelled of carbon stock in 2018.

### 3.13.2 Comparison biometric and modelled of carbon stock 2017

Based on Figure 3.41, there was a difference between biometric and modelled carbon stock 2017, which was similar to carbon stock 2018 in plot 5, 17, 22, 26 and 27. While plot 6, 7, 21 and 38 were very close in the amount of carbon stock in 2017 both for biometric and model data. Overall, biometric data show more sequestration of carbon stock than the model in 2017, except in plots 1, 2, 3, 4, 9, 10, 11, 12, 18 and 29.

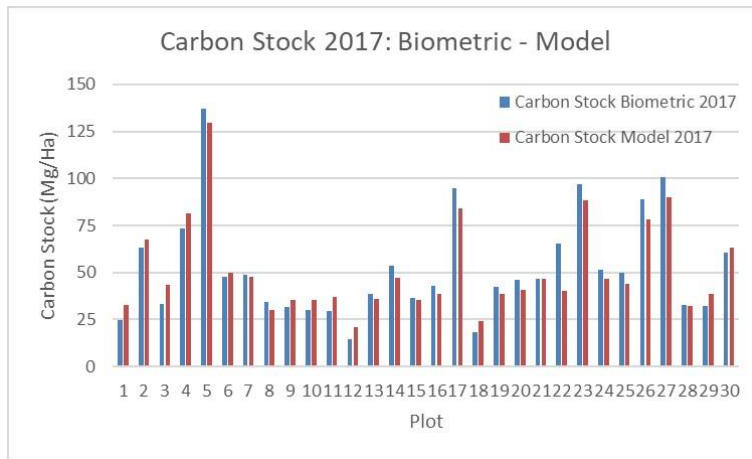


Figure 3.41 Comparison biometric and modelled of carbon stock in 2017.

R-square and RMS error of the relationship between carbon stock biometric and carbon stock modelled in 2017 were 0.93 and 7.71 respectively. While the intercept and slope are 6.9529 and 0.84x. Figure 3.42 presents the relationship between carbon stock biometric and modelled in 2017.

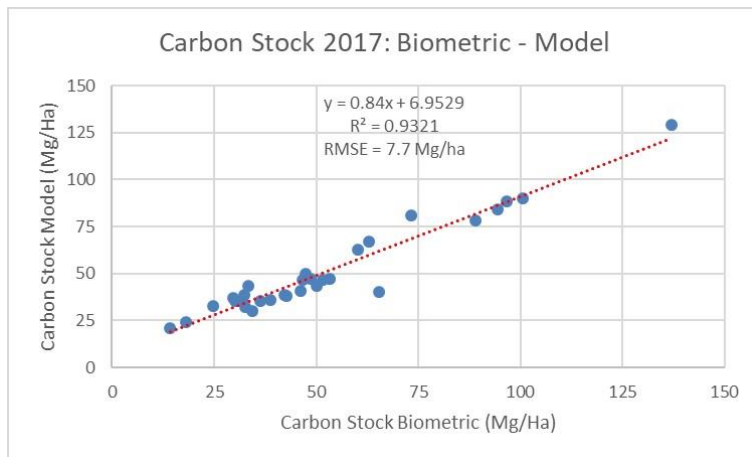


Figure 3.42 Relationship between biometric and modelled of carbon stock in 2017.

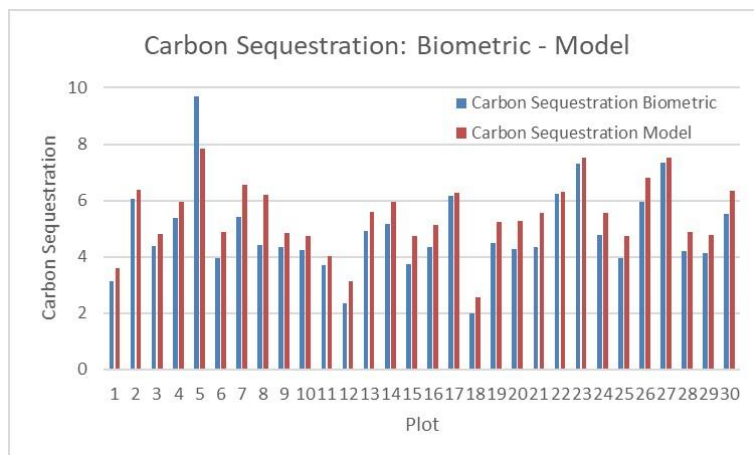


Figure 3.43 Comparison biometric and modelled of carbon sequestration.

### 3.13.3 Comparison biometric and modelled of carbon sequestration

In terms of carbon sequestration, the overall carbon stock model shows more carbon sequestered than the biometric. None of the model plots sequestered more than 10 Mg/ha/year, while in the biometric data of plot 5 carbon sequestration exceeded 8 Mg/ha/year. The majority of biometric and model data sequester carbon in the range 2 Mg/ha to 8 Mg/ha a year (Figure 3.43).

Figure 3.58 shows a significant relationship between carbon sequestration in biometric and modelled data. The R-square was 0.87, and the RMS error was 0.8 Mg/ha. Moreover, this relationship had an intercept and slope which of 1.7956 and 0.7526x, respectively.

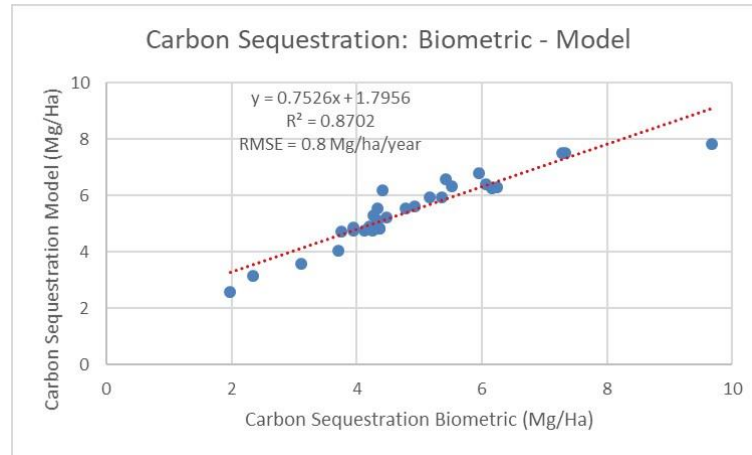


Figure 3.44 Relationship between biometric and modelled of carbon sequestration

## 4. DISCUSSION

### 4.1 Uncertainties of fieldwork data measurement

The non-destructive method becomes popular in forest inventory by a combination of earth observation and ground truth data rather than the destructive method by directly cutting and weighing the dry mass of the trees. Earth observation offers a variety of data to derive specific information related to forest inventory, such as using UAV, Lidar, Radar etc. While ground truth data is pivotal to access the accuracy of earth observation data. Fieldwork to retrieved data of forest structure in the field easy and fast and low-cost. However, it must consider some aspect, for instance, accessibility, security, data accuracy and the most important issue is data of the sample plot. Otherwise, the data does not represent the correct population.

Fieldwork data which contains the measurement of DBH, tree height measured or derived from diameter tape, Leica Disto D510 laser ranger, and tree height derived TLS RIEGL VZ 400 was right-skewed. The positive tail distribution or called right-skewed has a majority of large value in the left side (head) and a majority of small value in the right side (tail), generally is presented by a power law, a lognormal or an exponential function (Jiang, 2013). The fieldwork measurement presented positively skewed due to the restriction of DBH measurement. Tree with diameter = or >10 cm was measured since the data of trees < 10 cm DBH will not have a significant contribution to the biomass/carbon stock assessment of one sample plot (Brown, 2002). Otherwise, it gives a small portion to calculate biomass and difficult to identify its canopy cover in very height resolution image. Stem diameter of trees around 10cm also have relatively low height; this reason indicates that in tree height measurement using Leica Disto D510 laser ranger and TLS RIEGL VZ 400 also had the same distribution pattern (right-skewed) as DBH measurement.

Figure 3.3, Figure 3.5 and Figure 3.7 show that the histograms are asymmetrical between head in left side and tail in the right side. It means that the majority of 873 trees have a large percentage of small DBH and low altitude of tree height. However, in the normal distribution, data should be bell-shaped and has two tail. To deal with this issue, Doanne & Seward (2011), suggest taking into account the effect of binning and the role of sample size, while Jiang & Liu (2013), suggest dividing the mean of the value into two part, namely a high proportion in the tail and low percentage in the head. However, since we have collected the data from 10cm DBH and above because the insignificant contribution of small trees (Brown 2002), it is OK to have such a skewed distribution. Moreover, most of the trees in the area were planted 17-18 years ago. Therefore, such skewed distributions of the data are understandable.

Regarding sample size, purposive sampling using radii 12.62m of circular shape plot was chosen in this research due to the challenging working in the mangrove forest. The selection of sampling design, sampling frame and plot configuration must have been taken into account to select an appropriate design since statistics theory emphasize that accurate representation of the population would lead to accurate results in estimating AGB (Mcroberts et al., 1992).

Fieldwork measurement to retrieved DBH and tree height also produce an error. The result shows that tree height measured with Leica Disto D510 laser ranger was underestimated compared to tree height derived from TLS RIEGL VZ 400-point cloud. The average difference between tree height derived Leica Disto D510 laser ranger and tree height derived TLS RIEGL VZ was 1.1m, which shows a difference in the tree height measurement of, e.g., 13.3m and 14.4m respectively. The accuracy of tree height measurement also depends on the structure of the forest, tree height, terrain and topography, tree species, distance from the measurement trees, tree lean, instrument error and human error (Stereńczak et al., 2018). While measuring DBH in the mangroves, it has to take into account tree species, the structure of the tree, tree tilt and distance to measure diameter steam above the ground floor. For instance, measuring *Rhizophora* is more challenging than other mangroves, since *Rhizophora* has unique structure aerial root. Error measuring DBH affects calculate stem volume or estimate biomass/carbon stock.

Some research has been studied using TLS to measure DBH and tree height. The result shows that there was a significant relationship between measuring DBH derived TLS and direct measurement in the field with more than 0.98 of R-square (Heinzel & Huber, 2017; Bazezew, 2017). Moreover, Ghebremichael (2015), compared tree height derived TLS and tree height derived airborne Lidar, and the result shows the  $R^2$  was 0.87. Sadadi, (2016), showed the better result of  $R^2$  in the amount of 0.91 between tree height derive from TLS and tree height derive from Lidar data. This indicates that TLS has a promising application for forest inventory to obtain high accuracy for assessing tree height than using handheld Leica Disto D510 laser ranger.

Therefore, in this research TLS derived height was used as the ground truth to assess the accuracy of CHM UAV data. In the tropical inland forest, TLS may show some error in assessing trees height this is because lower canopy trees would block the laser beam from reaching the top of the upper canopy trees. However, in this research, the density of the mangrove trees was not high. Moreover, the structure of upper and lower canopy trees did not exist in these mangrove trees. Consequently, there was no problem for the laser beam of the TLS to reach the top of all trees of mangrove forest in this research (Bazezew, 2017). Therefore, TLS has assessed trees height accurately and it was used as the ground truth to assess the UAV CHM trees height.

#### **4.2 Quality of point cloud and orthophoto of UAV**

UAV data has several advantages such as very high spatial resolution, cost-effectiveness, reliable data quality, multi-temporal and the potential applications for forest inventory and management. The acquisition of UAV data in the field which comprised flight planning and set up of the devices which can take no more than an hour. While the flight which captured several hectares in our study area took less than 30 minutes.

Otero et al., (2018) has explained that, in the mangroves area, UAV can facilitate data collection to reach remote area due to difficulties to access, the drone can be launched from land or a boat. Moreover, UAV can improve forest monitoring by a combination of multi-temporal data acquisition and ground measurement. UAV does not disturb flora and fauna in the study area, as well as provides a historical record and unique insight related to near real-time reporting and validation of spatial changes and process in the forest area.

However, achieving the reliable quality of UAV image depends on flight height, flight pattern, overlap image, image rectification and point cloud. Effiom, (2018) examined the effect of flight height above the canopy on the calibration of the image which showed that flight height 60 m above ground level (AGL) gave 2.5 cm spatial resolution (GCD) with RMS error of geo-referencing in the amount of 1.4 cm and 81% images were calibrated. While increasing or using double flight height around 120 m, AGL had GCD image resolution, RMS error of geo-referencing and image calibration, namely 4.9 cm, and 100%, respectively.

This research also had the same result, when having two different flight height, which was 165 m AGL of UAV 2018 and 372 m AGL of UAV 2017. UAV 2018 which acquired images from 165 m above ground level gave better vision with GCD of 6.21 cm, while UAV 2017 obtained 9.29 cm of GCD. The RMS error of geo-referencing of UAV 2018 and 2017 was 4.7 cm and 30.2cm. Both data were 100% calibrated. Higher GCD of UAV othomosaic 2018 gave better vision to interpret the structure of trees, especially canopy cover. However, it is also influenced by the movement of the canopy due to wind condition since our mangrove area of Tani Baru is considered as seafront area. In some parts, the canopy cover of trees was blurred so that it was painful and more challenging to interpret and to delineate canopy cover using manual on-screen digitising. Take a close up look at Figure 2.9 and see the difference between the sharpness of the images of 2018 and 2017 and the effect of delineating CPA of trees.

Dandois et al., (2015) did research related to the effect of optimal altitude, overlap and weather condition of UAV to estimate forest structure using SfM. Percentage of the overlap of the images, especially forward overlap is essential to minimising canopy height error and spatial resolution of UAV.

The result of this research show that UAV 2018 had forward, and side overlap was 80% and 70%, while UAV 2017 had 70% of forwarding overlap and 60% side overlap. Figure 4.1 shows a comparison of the UAV 2018, which had a higher number of the overlapping image than UAV 2017 since the forward and side overlap of UAV 2018 was higher than UAV 2017. There were small red and the yellow area which represents low overlap in the UAV images of 2018. While UAV images of 2017 had a large red and yellow area. Yellow and red area affect the generation of the three-dimensional point cloud, othomosaic, digital surface model and digital terrain model.

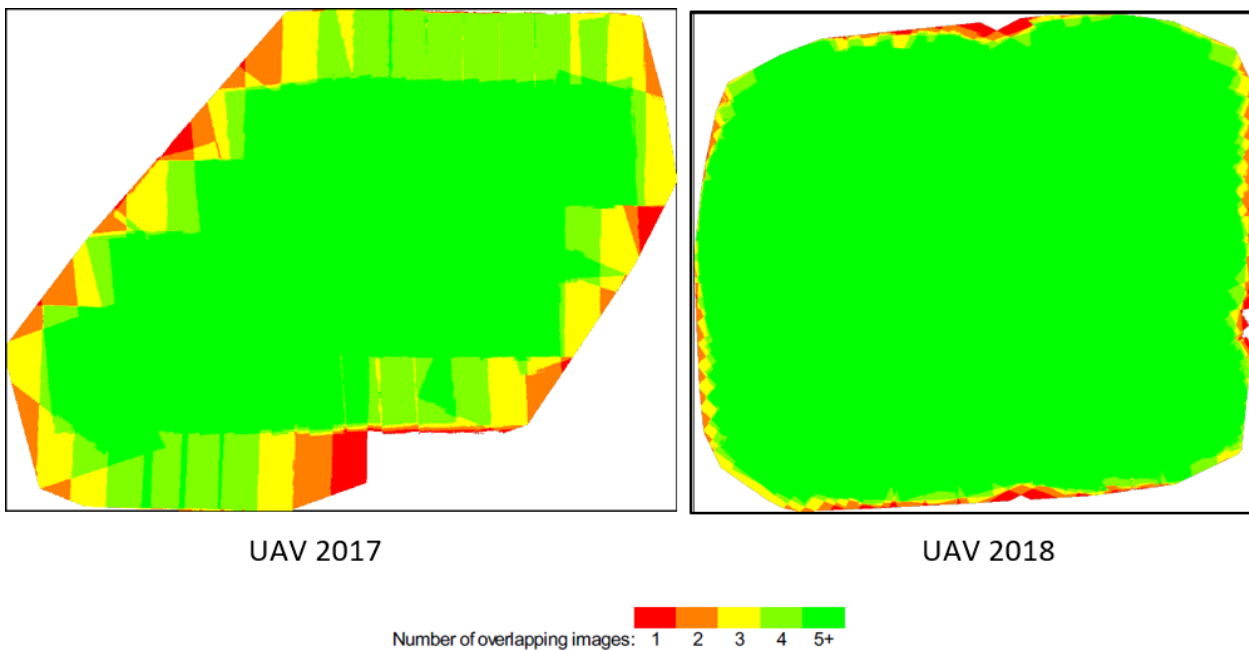


Figure 4.1 Number of overlapping images in UAV 2017 and UAV 2018.

The number of overlapping images computed for each pixel of the orthomosaic. Red and yellow areas indicate low overlap for which poor results may be generated. Green areas indicate an overlap of over five images for every pixel.

According to the density of three-dimensional point cloud, UAV 2018 is better than UAV 2017 in the amount of  $30.29 \text{ m}^3$  and  $29.63 \text{ m}^3$ . Point cloud density is also affected by flight height and image overlap. DSM and DTM derived from the point cloud, while the canopy height model is relative position between the digital surface model and digital terrain model which depends on the density of point cloud. The RMS error of Z-axis of 2018 was less than in 2017. Therefore, the quality of DSM and DTM were better than UAV 2017.

Otero et al., (2018) have suggested that when acquired UAV images, the time and tidal position must consider, which have their effects when generating orthomosaic and CHM. This study does not take into account tidal circulation, and the orthomosaic revealed that UAV 2017 collected on 25 October 2017 at 3:35 PM when the tide was low. Meanwhile, the UAV 2018 took on 18 December 2018 at 6:58 AM in inundated time of tide. This issue also affects generating CHM, while some part on orthomosaic was difficult to interpret and delineate since canopy cover was near to water body.

The time lag between retrieving image data and biometric trees properties in the field is as an exogenic factor that might have an influence on data quality as a result of ground truth in the interval of the time lag, while topography, off-nadir viewing and illumination angle make the visibility of crown size in the image different than the real tree size (Song et al., 2010). Therefore, planning a fieldwork data collection and UAV image acquisition can be challenging. Initially, UAV 2018 image acquisition did on 14 October 2018 and 13 to 24

October 2018, respectively. Nevertheless, the quality of the acquired UAV images was not reasonable. Then, a second flight campaign of UAV image collection of 2018 was taken on 18 December 2018. The time led between 2 months of data collection might have some effects on the data, particularly canopy cover and tree height since mangroves are in a tropical region where the growth is continuing 365 days a year.

To do this research two data sets of two years must be available. The data collected by University of Mulawarman in 2017 for the benefit of PERTAMINA Oil Company of Indonesia was used in this research. Without this data set of 2017, it would be impossible to do this work. The researcher had no other choice but to use this available UAV data set of 2017. Therefore, we had to use this data set and accept its quality.

### 4.3 Estimated DBH using the crown diameter

Trees canopy, which usually represents by crown projection area or crown diameter on a 2D remotely sensed data, is an important part of canopy structure of the trees which has a strong correlation to other tree parameters such as DBH, tree height and biomass/carbon stock (Song et al., 2010). Unlike stem diameter, which can be easily measured in the field, tree crown measurement is more difficult and challenging. In the field, the crown diameter is measured in two orthogonal/perpendicular direction (Figure 1.4), while the mean of the two measurements is taken as crown diameter. In addition, it also relatively subjective and influenced by a human error in assessing the edges of the canopy while measuring the crown diameter in the field. Dealing with this situation, this research used the crown projection area to derive crown diameter for individual trees by manual on-screen digitization crown canopy on orthomosaic UAV image. In this research, we did not use the CPA or the size of the canopy to model DBH. We have used crown diameter to model DBH. The results of the use of the modelled DBH from CD in the allometric equation to estimate biomass/carbon stock show higher accuracy of AGB estimation than using the modelled DBH from CPA.

The relationship between DBH and CD shows a strong correlation between DBH and CD of 2018 and 2017, in the range of 0.80 and 0.81 of  $R^2$ , respectively. Some research also examines the relationship between crown diameter and other tree structure, such as tree height dry weight and biomass, while other research also uses crown diameter as a proxy of DBH using remote sensing data (Hemery et al., 2005; Fu & Wu, 2011; Song et al., 2010; Popescu et al., 2003; Suhardiman et al., 2016; Domiciano et al., 2016). Those researches also stated that there is a significant relationship between crown diameter and other tree parameters. Figure 4.2 shows in A, the  $R^2$  of the relationship between DBH and CD is 0.92, while in B, there is a strong relationship between crown diameter and height to assess aboveground biomass in three different mangrove species, namely *Aegicerass corniculatum*, *Avicennia marina* and *Kandelia candel* (Figure 4.2)

Crown diameter has a significant relationship to predict aboveground biomass which is very suitable for multi-stem trees of mangroves and could be applied to those mangroves between multi stem and a single stem of mangrove (Fu & Wu, 2011). Based on the results of Fu & Wu, (2011), this method was applied to predict the DBH model using the relationship between crown diameter and DBH. The result shows that in modelled DBH 2018 the  $R^2$  was 0.80 while RME error was 1.46 cm. Furthermore, the  $R^2$  and RMS error of modelled or predicted DBH were 0.81 and 1.4 cm, respectively. The modelled DBH is also validated, and the result shows that RMS error was 2.50 cm for 2018 and 2.47 for 2017.

Based on the linear model of predicted DBH 2018 and 2017, some DBH models was underestimated, and others were overestimated. The modelled DBH had an equation to predict DBH in 2018 and 2017 and fitted line related to the relationship between crown diameter and diameter breast height. The data which is located above the best-fitted line would be underestimated of DBH, whereas overestimate DBH means the data situated under fitted line. In a few cases, predicted DBH 2017 were larger than predicted DBH 2017 since the crown diameter 2018 has nearly the same as crown diameter 2017. When applying that equation to predict DBH, the result shows that predicted DBH 2017 is larger than 2018.

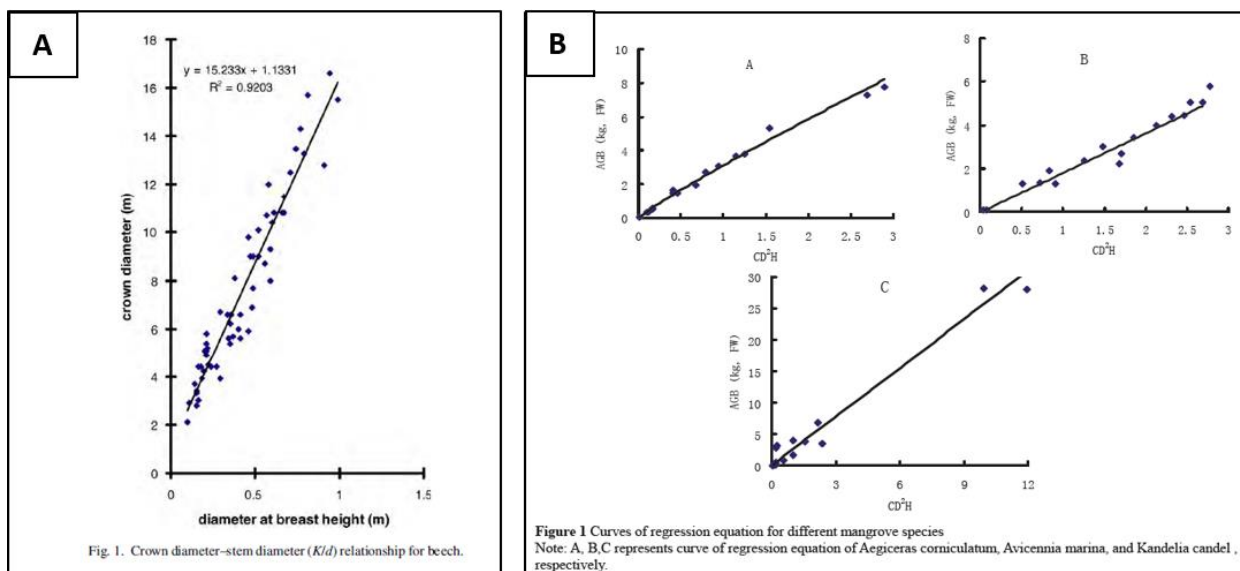


Figure 4.2 Relationship between crown DBH and CD (A), relationship between CD and biomass (B).

(Modified from Hemery et al., 2005; Fu & Wu, 2011)

#### 4.4 Estimated tree height using CHM

Three hundred one trees were used to perform the regression analysis between trees height measured or derived from the TLS point cloud and the UAV CHM. This was done before using the CHM as an input for modelling AGB with the modelled DBH from the crown diameter. The average of trees height derived from TLS in 2018 was higher than tree height derived from CHM UAV 2018, in the amount of 13.7 m and 13.4 m. The R2 of the TLS height and UAV CHM of 2018 and 2017 were 0.85 and 0.81 respectively. While the RMSE of the TLS height and UAV CHM of 2018 and 2017 were 0.5 m and 0.9 m respectively. Tree heights derived from TLS in 2017 has an average and standard deviation of 13.2 m and 2.3 respectively. Whilst the average and standard deviation of tree heights derived CHM 2017 were 11.9 m and 2.3.

Panagiotidis et al., (2017) did their research to determine tree height and crown diameter using high-resolution UAV image of two different areas of broadleaves forest in the Czech Republic. In plot 1, the mean of tree height field measurement was 24.2 m, while estimated height using CHM was 22.3. In plot 2, the mean of trees height field measurement was 27 m and the mean of tree height derived CHM 29.4 m.

Otero et al., 2018 have done their research on deriving trees height from UAV CHM in protective mangroves and productive mangrove in Matang Mangrove Forest Reserve in Peninsula Malaysia. There was a slight difference between the average tree height derived from CHM compared to field measurements in the productive zone in the amount of 14 m and 13.7 m respectively. Whereas in the protective zone, the average tree height derived from CHM was 15.5 m, and the average tree height of fieldwork measurements was 14.2 m. There was a similarity of the average of trees height of mangrove forest in the area of Matang Mangrove Forest Reserve in Peninsula Malaysia and our Mahakam Delta Indonesia in 2018. This research showed the difference between the average of trees height of 2018 from CHM is 13.4 m and TLS is 13.7 m. While in 2017 the average of trees height of CHM was 11.9 m and the TLS was 13.2 m. These results show that 2017 had high differences between CHM trees height and TLS backward prediction trees height. This means that there are errors in the CHM of 2017.

The biometric differences between the trees height using TLS in 2018 and the backward calculation of the height of the tree in 2017 should be somewhere between 0.34-0.55 m. However, the difference between CHM 2018 and CHM 2017 estimated trees height show a difference in a range from 11.9 m to 13.2 m. This difference is, of course, can be justified for many reasons. The first is that we did not measure the TLS

height in the field in 2017. We estimated according to the growth of different mangrove trees species in the study area according to Saenger & Siddiqi (1993) and Srivastava et al., (1988). However, these numbers are on average base and in some other specific areas. According to the local people, the growth in our areas is much higher than what these literature are showing. An example of the images of 2017 and 2018 that depicting the difference in the growth of mangrove trees is shown in Figure 4.3.



Figure 4.3 A comparison of the growth of mangrove trees in approximately one-year (A) 2017 and (B) 2018.

Moreover, the differences can be because of other imaging parameters of the two imaging campaigns of 2017 and 2018. The error can be rooted in flight height, overlap percentage of the sequential images, point cloud density, and geo-referencing. The flight height of UAV 2017 was double than flight height of UAV 2018. While forward and side overlap of UAV 2017 was 70% and 60% compared to 80% and 70% of forwarding overlap and side overlap of 2018.

The number is an overlapping image of more than five images in 2018 also greater than UAV 2017 (Figure 4.1). The density of the 3D point cloud also influences DSM and DTM, which were the source to generate CHM. The density of UAV 2018 point cloud was also higher than in UAV 2017. Moreover, the RMS error of geo-referencing UAV 2017 was also higher than in 2018. Regarding RMS error in Z-axis, UAV 2017 had 0.222 m compared 0.029 m of RMS error Z-axis of UAV 2018.

This research does not consider the annual tide circumstances which might affect CHM. UAV 2017 images which were acquired at 3:35 PM on 25 October 2017 with lower water level (LWS), whereas UAV 2018

images which were captured at 6:58 AM on 18 December 2018 which might be the inundated time of the daily tide.

The results illustrate the real phenomena in the study area. This mangrove area comprises of remnants of natural and planted mangroves. Before 1990, the study area was marginal land of mangrove forest, which converted into shrimp pond during 1990 – 2000. The fishermen still preserved some mangrove inside the area for shrimp ponds. Then, after the year 2000, the national oil and gas company (PT. PERTAMINA) has replanted the degraded mangroves with native mangrove species to show their efforts to improve the environment since they are extracting oil from this area.

#### 4.4.1 Mangrove Blue carbon sedimentation affecting the assessment of DTM

Mangrove sequestering carbon known as blue carbon. A lot of the blue carbon is sequestered by below-ground biomass. Because of the tidal activities and inundation, high tide water always brings sediments from rivers, waterways, deltas water and the sea to deposit the soil on top of the mangrove roots, aerial roots and Pneumatophores. This sedimentation process can bring 20 to 29 mm annually (Woodroffe et al., 2016) to be deposit soil on to on the mangrove ground. This extra sedimentation or soil deposit of approximately 2 cm annually would rias the mangrove floor, and the digital terrain model would increase (Figure 4.5).

During the process of SfM to produce the mosaic of UAV images DSM, DTM and consequently the CHM would be generated. Basically, the CHM is the height of the trees. Therefore, this soil deposit or sedimentation would have a significant effect on DTM and thus on the assessment of CHM. Since the time difference between the imaging campaign of 2017 and 2018 is about 14 months. It is believed that this soil deposit or sedimentation can have an effect on assessing CHM and might have affected the trees height assessment.



Figure 4.4 Soil deposit and sedimentation on top of the mangrove floor.

#### 4.5 AGB/Carbon stock estimation

The average aboveground biomass model in 2018 and 2017 was 112.5Mg/ha and 101.6 Mg/ha while the average aboveground biomass biometric (i.e., estimated from measurements in the field or the reference ground truth) was 114.1 Mg/ha in 2018 and 104.4 Mg/ha in 2017. This result is nearly similar to Arifanti et al., (2019), in which they calculate land-use carbon footprint and carbon dynamic in mangroves-converted aquaculture in Mahakam Delta, Indonesia. The dominant mangrove species were *Avicennia alba*, *Bruguiera*

*sexangula*, and *Rhizophora apiculata* which had a diameter in the range 5 – 10 cm. The average aboveground biomass of mangroves was 118 Mg/ha.

Comparison between aboveground biomass biometric and the modelled AGB in 2018 and 2017 show that there are variabilities of above ground biomass in both data. Above ground biomass of biometric data is higher than the model in plots which have a high amount of biomass, namely plot 5, 17, 13, 26 and 27. It happens because the majority of large DBH when predicted by DBH model, were underestimated. It also influenced by trees height derived from CHM, since the average of trees height derived CHM is lower than the average of trees height derived from TLS.

An example of high biomass plots is shown in Figure 4.5. This plot shows the biomass of 293 Mg/ha. This plot shows big trees in size and high-density mangrove trees. While Plot 22 is was the only plot where the difference between the modelled AGB and the biometric AGB is high. The AGB biometric in 2018 and 2017 were 143 Mg/ha and 130 Mg/ha. While the modelled AGB in 2018 and 2017 were 92.7Mg/ha and 80.1Mg/ha. We believe that the source of error in assessing the AGB in this plot was because of error in the assessment of CPA and height of the trees in this plot both in 2018 and 2017. Although the difference between the AGB of two years was reasonable (e.g. 13 and 12 Mg/ha in the biometric and the modelled AGB), but still the AGB was not assessed accurately. The plot has 16 *Avicennia* trees and 14 of *Rhizophora* which show small CPA but the reasonable size of stem. Consequently, the modelling of AGB shows an error. Moreover, the majority of trees AGB in plots 1, 3, 4, 5, 11, 12, 18, 29 were overpredicted because trees height derived from CHM were higher than trees height derived from TLS and predicted DBH were also overpredicted.



Figure 4.5 Plot-5 as an example of high biomass plots that show high-density big trees.

Error in aboveground biomass estimation can be influenced by many factors such as an inappropriate allometric equation, inaccurate measurement of variable, instrument and calibration error (Petrokofsky et al., 2012) while this research used a general allometric equation of mangroves, which contains diameter breast height, tree height and wood density.

Moreover, the likely source of errors for collecting ground truth data in the field (i.g. measuring DBH, tree height, location and species) to calculate aboveground biomass to are human error and instrument error. As a result of the lack of information related to mangrove species, identification of mangroves was classified into tree species which did not represent the real specific species of mangroves. In some case, the recorded location of trees using GPS handheld were shifting, since GPS did not receive appropriate signals when measuring location due to occlusion of high density canopy cover of mangrove forest.

## 4.6 Carbon sequestration estimation

The average carbon sequestration of the model was 5.5 Mg/ha/year, while the average carbon sequestration of biometric was 4.9 Mg/ha/year. There was a difference of approximately 11% between model and biometric. This result is close to 4.71 Mg/ha/year of annual increment of carbon sequestration based on DBH in Sundarbans, Bangladesh (De et al., 2011). Alongi, 2012 assessed globally the overall carbon sequestration which is 13.5 Mg/ha/year of carbon sequestration of mangrove forest, which comprised above ground and below ground biomass. Knowing that mangrove forest trees sequester carbon 2-3 times of the trees in the tropical in-land forest (Alongi 2002), our modelled carbon sequestration is one-third of the total AGB plus belowground biomass.

Above ground carbon stock is generally calculated as 0.5 the amount of AGB biomass. In the study area, carbon sequestration model is higher around 0.6 Mg/ha than carbon sequestration biometric. All of the plots except plot 5, the carbon sequestration modelled were higher than the biometric. In plot 5, the majority of predicted DBH were underestimated, and there was a small difference between CHM 2018 and CHM 2017. Therefore, modelled AGB and consequently, carbon shows less carbon sequestration than in the biometric data. Carbon sequestration modelled in Plot 7 and eight were more than the biometric data since the difference in trees height of CHM 2018 and 2017 were around 1.5 m. The average annual increment of tree height in biometric was 43 cm only (Saenger & Siddiqi 1993; Srivastava et al., 1988). Therefore, in those plots, tree height shows it affects three to four times in the allometric equation. Consequently, the modelled biomass and carbon stock were higher than the biometric data.

The advantages of UAV to capture a consecutive overlapping image with fine resolution has the opportunity to retrieve the structure of an object in single-level. UAV can use regularly capture the same area to monitor forest system. This is evidence that UAV can be employed to estimate biomass/carbon stock and carbon sequestration in the mangrove forest.

This research work was done in response to the call of the REDD+ MRV program for new applications of remotely sensed data to assess biomass/ carbon stock and carbon sequestration. The world needs new methods and techniques using remotely sensed data to be presented as an example for a practical, less expensive, reasonably accurate and operational methods to assess carbon sequestration in tropical in-land forests and mangrove forests. Looking at the previous and current literatures, there is no literature on the use of UAV data to assess AGB/carbon stock and carbon sequestration. We believe that this research work is a reasonable, innovative example of the applications of multitemporal UAV images and SfM to assess AGB/ carbon stock and carbon sequestration.

## 4.7 Limitation

The limitations of this research are:

1. Trees which had DBH equal and greater ( $\Rightarrow$ ) than 10 cm were measured in the field.
2. The lack of information related to species of mangroves had an effect to identify the correct species.
3. Purposive sampling plot might not represent the real mangrove forest of the study area.
4. Backward prediction of biometric 2017 might not represent the real annual growth rate of specific trees in specific ages.
5. Wood density using literature review might not be accurate.
6. UAV image acquisition did not consider optimum flight height, image overlap, flight speed, weather, wind speed, tide cycles, sun-angle, and illumination.
7. GCP did not well distributed in the whole area due to the accessibility and difficulties to find open area when measuring GCP using GNSS RTK in the field.
8. Crown diameter derived CPA using manual on-screen digitation might be influenced by the human error, and this way to retrieve crown diameter might not represent a real condition in the field.
9. The general allometric equation for mangrove might not be sufficient to calculate specific mangrove.

## 5. CONCLUSION

The study used UAV (Unmanned Aerial Vehicle) images of two different years December 2018 and October 2017 to estimate aboveground biomass/carbon stock and carbon sequestration in mangrove forest, Mahakam Delta, Indonesia. The conclusion was made based on the research questions and objectives.

### **Research question 1.**

*What is the relationship between crown diameter derived from CPA of UAV images and DBH of ground truth data?*

There was a significant relationship between crown diameter derived from CPA of UAV images and DBH of ground truth data in 2018 and 2017. The  $R^2$  and RMS error of 2018 were 0.80 and 1.5 cm, while in 2017 the  $R^2$  was 0.81 and the RMS error was 1.4 cm. Therefore,  $H_0$  is rejected since there is a significant relationship between crown diameter derived from CPA of UAV image and DBH ground truth data.

### **Research question 2.**

*What is the relationship between trees height derived from CHM of UAV images and trees height derived from TLS point clouds data?*

There was a significant relationship between trees height derived from CHM of UAV images and tree height derived from TLS point cloud data both in 2018 and 2017. The relationship between trees height derived from CHM of UAV images and trees height derived from TLS in 2018 shows an  $R^2$  and RMS error of 0.85 and 0.5 m respectively. Whereas, the relationship between trees height derived from CHM of UAV images and trees height derived from TLS in 2017 showed an  $R^2$  of 0.81 and RMS error of 0.9 m. Therefore,  $H_0$  is rejected since there is a strong relationship between trees height derived from CHM of UAV image and trees height driven from TLS.

### **Research question 3.**

*What are AGB/carbon stock modelled from UAV images in 2017 and 2018 in the study area and how accurate are these results compared to the biometric data?*

The average AGB/carbon stock modelled from UAV images in 2017 and 2018 were 101 Mg/ha and 112 Mg/ha, while the average of AGB/carbon stock of the biometric data (ground truth) was 104 Mg/ha and 114 Mg/ha in 2017 and 2018 respectively. There was a significant relationship between AGB/carbon stock modelled from UAV images and biometric data in 2017 and 2018. The relationship between AGB/carbon stock modelled from UAV images and biometric data in 2017 was significant with an  $R^2$  of 0.93 and an RMS error of 15 Mg/ha. While in 2018, the  $R^2$  and RMS error of the significant relationship AGB/carbon stock between modelled from UAV images and biometric data were 0.93 and 15 Mg/ha. Therefore,  $H_0$  is rejected since there is a significant relationship between the AGB/carbon stock modelled from UAV images of 2017 and 2018 and the biometric data of the two years.

### **Research question 4.**

*What is the carbon sequestration modelled from UAV images of the years 2017 and 2018 and how accurate is it?*

Carbon sequestration modelled from UAV images of 2017 and 2018 was 6 Mg/ha/year compared to 5 Mg/ha/year of the biometric carbon sequestration of the years 2017 and 2018. There was a significant relationship between carbon sequestration modelled from UAV images of the years 2017 and 2018 and carbon sequestration of the biometric data which showed an  $R^2$  and RMS error of 0.87 and 1 Mg/ha/year, respectively. Therefore,  $H_0$  is rejected since there is a significant relationship between carbon sequestration modelled from UAV images of the years 2017 and 2018 and carbon sequestration of the biometric data of 2017 and 2018.

## LIST OF REFERENCES

---

- Adame, M. F., Cherian, S., Reef, R., & Stewart-Koster, B. (2017). Mangrove root biomass and the uncertainty of belowground carbon estimations. *Forest Ecology and Management*, 403(August), 52–60. <https://doi.org/10.1016/j.foreco.2017.08.016>
- Alongi, D. M. (2002). Present state and future of the world's mangrove forests. *Environmental Conservation*, 29(3), 331–349. <https://doi.org/10.1017/S0376892902000231>
- Alongi, D. M. (2012). Carbon sequestration in mangrove forests. *Carbon Management*, 3(3), 313–322. <https://doi.org/10.4155/cmt.12.20>
- Arifanti, V. B., Kauffman, J. B., Hadriyanto, D., Murdiyarso, D., & Diana, R. (2019). Carbon dynamics and land use carbon footprints in mangrove-converted aquaculture: The case of the Mahakam Delta, Indonesia. *Forest Ecology and Management*, 432(August 2018), 17–29. <https://doi.org/10.1016/j.foreco.2018.08.047>
- Baccini, A., Goetz, S. J., Walker, W. S., Laporte, N. T., Sun, M., Sulla-Menashe, D., ... Houghton, R. A. (2012). Estimated carbon dioxide emissions from tropical deforestation improved by carbon-density maps. *Nature Climate Change*, 2(3), 182–185. <https://doi.org/10.1038/nclimate1354>
- Barbier, E., Hacker, S., Kennedy, C., Stier, A., & Silliman, B. (2011). The value of estuarine and coastal ecosystem services. *Ecological Monographs*, 81(2), 169–193. Retrieved from <http://www.esajournals.org/doi/abs/10.1890/10-1510.1>
- Bazew, N. M. (2017). Integrating Airborne Lidar and Terrestrial Laser Scanner Forest Parameters for Accurate Estimation of Aboveground Biomass/ Carbon in Ayer Hitam Tropical Forest Reserve, Malaysia. *M.Sc. Thesis. ITC University of Twente*, (2017), 96.
- Blaschke, T. (2010). Object based image analysis for remote sensing. *ISPRS Journal of Photogrammetry and Remote Sensing*, 65(1), 2–16. <https://doi.org/10.1016/j.isprsjprs.2009.06.004>
- Boehm, H. D. V., Liesenberg, V., & Limin, S. H. (2013). Multi-temporal airborne LiDAR-survey and field measurements of tropical peat swamp forest to monitor changes. *IEEE Journal of Selected Topics in Applied Earth Observations and Remote Sensing*, 6(3), 1524–1530. <https://doi.org/10.1109/JSTARS.2013.2258895>
- Boudreau, J., Nelson, R. F., Margolis, H. A., Beaudoin, A., Guindon, L., & Kimes, D. S. (2008). Regional aboveground forest biomass using airborne and spaceborne LiDAR in Québec. *Remote Sensing of Environment*, 112(10), 3876–3890. <https://doi.org/10.1016/j.rse.2008.06.003>
- BPS. (2018). *Kutai Kartanegara Dalam Angka 2018*. BPS Kabupaten Kutai Kartanegara (Vol. 91).
- Brown, S. (2002). Measuring carbon in forests: Current status and future challenges. *Environmental Pollution*, 116(3), 363–372. [https://doi.org/10.1016/S0269-7491\(01\)00212-3](https://doi.org/10.1016/S0269-7491(01)00212-3)
- Brown, S., Pearson, T., Slaymaker, D., Ambagis, S., Moore, N., Novelo, D., & Sabido, W. (2005). Creating a virtual tropical forest from three-dimensional aerial imagery to estimate carbon stocks. *Ecological Applications*, 15(3), 1083–1095. <https://doi.org/10.1890/04-0829>
- Chave, J., Réjou-Méchain, M., Búrquez, A., Chidumayo, E., Colgan, M. S., Delitti, W. B. C., ... Vieilledent, G. (2014a). Improved allometric models to estimate the aboveground biomass of tropical trees. *Global Change Biology*, 20(10), 3177–3190. <https://doi.org/10.1111/gcb.12629>
- Chave, J., Réjou-Méchain, M., Búrquez, A., Chidumayo, E., Colgan, M. S., Delitti, W. B. C., ... Vieilledent, G. (2014b). Improved allometric models to estimate the aboveground biomass of tropical trees. *Global Change Biology*, 20(10), 3177–3190. <https://doi.org/10.1111/gcb.12629>
- Colomina, I., & Molina, P. (2014). Unmanned aerial systems for photogrammetry and remote sensing: A review. *ISPRS Journal of Photogrammetry and Remote Sensing*, 92, 79–97. <https://doi.org/10.1016/j.isprsjprs.2014.02.013>
- Cunliffe, A. M., Brazier, R. E., & Anderson, K. (2016). Ultra-fine grain landscape-scale quantification of dryland vegetation structure with drone-acquired structure-from-motion photogrammetry. *Remote Sensing of Environment*, 183, 129–143. <https://doi.org/10.1016/j.rse.2016.05.019>
- Dandois, J. P., Olano, M., & Ellis, E. C. (2015). Optimal altitude, overlap, and weather conditions for computer vision uav estimates of forest structure. *Remote Sensing*, 7(10), 13895–13920. <https://doi.org/10.3390/rs71013895>
- De, T. K., Chowdhury, C., Mukhopadhyay, S. K., Das, S., Mandal, S. K., Ganguly, D., ... Jana, T. K. (2011). Carbon sequestration and annual increase of carbon stock in a mangrove forest. *Atmospheric Environment*, 45(28), 5016–5024. <https://doi.org/10.1016/j.atmosenv.2011.04.074>
- Díaz-Varela, R. A., de la Rosa, R., León, L., & Zarco-Tejada, P. J. (2015). High-resolution airborne UAV imagery to assess olive tree crown parameters using 3D photo reconstruction: Application in

- breeding trials. *Remote Sensing*, 7(4), 4213–4232. <https://doi.org/10.3390/rs70404213>
- Disney, M. I., Boni Vicari, M., Burt, A., Calders, K., Lewis, S. L., Raunonen, P., & Wilkes, P. (2018). Weighing trees with lasers: Advances, challenges and opportunities. *Interface Focus*, 8(2). <https://doi.org/10.1098/rsfs.2017.0048>
- Doanne, D. ., & Seward, L. E. (2011). Measuring Skewness. *Journal of Statistics*, 19(2), 1–18.
- Domiciano Galvancio, J., & Popescu, S. C. (2016). Measuring Individual Tree Height and Crown Diameter for Mangrove Trees with Airborne Lidar Data. *International Journal of Advanced Engineering, Management and Science (IJAEEMS) Infogain Publication (Infogainpublication.Com)*, 2(5), 2454–1311. <https://doi.org/2454-1311>
- Donato, D. C., Kauffman, J. B., Murdiyarto, D., Kurnianto, S., Stidham, M., & Kanninen, M. (2011). Mangroves among the most carbon-rich forests in the tropics. *Nature Geoscience*, 4(5), 293–297. <https://doi.org/10.1038/ngeo1123>
- Dube, T., & Mutanga, O. (2015). Evaluating the utility of the medium-spatial resolution Landsat 8 multispectral sensor in quantifying aboveground biomass in uMgeni catchment, South Africa. *ISPRS Journal of Photogrammetry and Remote Sensing*, 101, 36–46. <https://doi.org/10.1016/j.isprsjprs.2014.11.001>
- Esong Effiom, A. (2018). UAV-RGB and Multispectral Pleiades images, for tree species identification and forest carbon estimation in Amtsvenn, Germany. <https://doi.org/10.13140/RG.2.2.13484.77444>
- FAO. (2007). The world's mangroves 1980-2005. *FAO Forestry Paper*, 153, 89. <https://doi.org/978-92-5-105856-5>
- Feng, Y., Li, Z., & Tokola, T. (2010). Estimation of stand mean crown diameter from high-spatial-resolution imagery based on a geostatistical method. *International Journal of Remote Sensing*, 31(2), 363–378. <https://doi.org/10.1080/01431160902887867>
- Fu, W., & Wu, Y. (2011). Estimation of aboveground biomass of different mangrove trees based on canopy diameter and tree height. *Procedia Environmental Sciences*, 10(PART C), 2189–2194. <https://doi.org/10.1016/j.proenv.2011.09.343>
- Ghebremichael, Z. M. (2015). Airborne LiDAR and terrestrial laser scanner (TLS) in assessing above ground biomass / carbon stock in tropical rainforest of Ayer Hitam forest reserve, Malaysia (Master's Thesis), 67. Retrieved from [http://www.itc.nl/library/papers\\_2016/msc/nrm/ghebremichael.pdf](http://www.itc.nl/library/papers_2016/msc/nrm/ghebremichael.pdf)
- Gibbs, H. K., Brown, S., Niles, J. O., & Foley, J. A. (2007). Monitoring and estimating tropical forest carbon stocks: Making REDD a reality. *Environmental Research Letters*, 2(4). <https://doi.org/10.1088/1748-9326/2/4/045023>
- Giri, C., Ochieng, E., Tieszen, L. L., Zhu, Z., Singh, A., Loveland, T., ... Duke, N. (2011). Status and distribution of mangrove forests of the world using earth observation satellite data. *Global Ecology and Biogeography*, 20(1), 154–159. <https://doi.org/10.1111/j.1466-8238.2010.00584.x>
- Giri, C., Pengra, B., Zhu, Z., Singh, A., & Tieszen, L. L. (2007). Monitoring mangrove forest dynamics of the Sundarbans in Bangladesh and India using multi-temporal satellite data from 1973 to 2000. *Estuarine, Coastal and Shelf Science*, 73(1–2), 91–100. <https://doi.org/10.1016/j.ecss.2006.12.019>
- Gonzalez de Tanago, J., Lau, A., Bartholomeus, H., Herold, M., Avitabile, V., Raunonen, P., ... Calders, K. (2018). Estimation of above-ground biomass of large tropical trees with terrestrial LiDAR. *Methods in Ecology and Evolution*, 9(2), 223–234. <https://doi.org/10.1111/2041-210X.12904>
- Gopal, B. (2013). Future of wetlands in tropical and subtropical Asia, especially in the face of climate change. *Aquatic Sciences*, 75(1), 39–61. <https://doi.org/10.1007/s00027-011-0247-y>
- Gschwantner, T., Schadauer, K., Vidal, C., Lanz, A., Tomppo, E., Di Cosmo, L., ... Lawrence, M. (2009). Common tree definitions for national forest inventories in Europe. *Silva Fennica*, 43(2), 303–321. <https://doi.org/10.14214/sf.463>
- Hadush Berhe, T. (2018). *Towards a UAV based Standalone System for Estimating and mapping Aboveground Biomass/ carbon Stock in Berkelah Tropical Fain Forest, Malaysia (M.Sc Thesis)*. Enschede: ITC University of Twente. Retrieved from <https://ezproxy.utwente.nl:2315/library/2018/msc/nrm/berhe.pdf>
- Hairiah, K., Dewi, S., Agus, F., Velarde, S., Ekadinata, A., Rahayu, S., & Van Noordwijk, M. (2011). *Measuring Carbon Stock Across Land Use Systems Measuring Carbon Stocks Across Land Use Systems Disclaimer and Copyright*. Retrieved from <http://www.worldagroforestry.org/sea/Publications/files/manual/MN0050-11/MN0050-11-1.pdf>
- Heinzel, J., & Huber, M. O. (2017). Tree stem diameter estimation from volumetric TLS image data. *Remote Sensing*, 9(6), 1–11. <https://doi.org/10.3390/rs9060614>
- Hemery, G. E., Savill, P. S., & Pryor, S. N. (2005). Applications of the crown diameter-stem diameter relationship for different species of broadleaved trees. *Forest Ecology and Management*, 215(1–3), 285–

294. <https://doi.org/10.1016/j.foreco.2005.05.016>
- Hirata, Y., Tabuchi, R., Patanaponpaiboon, P., Pongparn, S., Yoneda, R., & Fujioka, Y. (2014). Estimation of aboveground biomass in mangrove forests using high-resolution satellite data. *Journal of Forest Research*, 19(1), 34–41. <https://doi.org/10.1007/s10310-013-0402-5>
- Iizuka, K., Yonehara, T., Itoh, M., & Kosugi, Y. (2018). Estimating Tree Height and Diameter at Breast Height (DBH) from Digital surface models and orthophotos obtained with an unmanned aerial system for a Japanese Cypress (*Chamaecyparis obtusa*) Forest. *Remote Sensing*, 10(1). <https://doi.org/10.3390/rs10010013>
- IPCC. (2006). 2006 IPCC Guidelines for National Greenhouse Gas Inventories Volume 4: Agriculture, Forest and Other Land Use. *2006 IPCC Guidelines for National Greenhouse Gas Inventories.*, 4(2), 4.1-4.83. <https://doi.org/10.1016/j.phrs.2011.03.002>
- Jiang, B. (2013). Head/Tail Breaks: A New Classification Scheme for Data with a Heavy-Tailed Distribution. *Professional Geographer*, 65(3), 482–494. <https://doi.org/10.1080/00330124.2012.700499>
- Jiang, B., & Liu, X. (2013). Scaling of geographic space from the perspective of city and field blocks and using volunteered geographic information. *Big Data Computing*, 8816, 483–500. <https://doi.org/10.1201/b16014>
- Kauffman, J. B., & Donato, D. C. (2012). Protocols for the measurement, monitoring and reporting of structure, biomass and carbon stocks in mangrove forests. *Book*, 50. <https://doi.org/10.17528/cifor/003749>
- Kershaw, J. A., Ducey, M. J., Beers, T. W., & Husch, B. (n.d.). *Forest mensuration*. Retrieved from <https://ezproxy.utwente.nl:3808/lib/itc/reader.action?docID=4731589&query=>
- Komiyama, A., Ong, J. E., & Pongparn, S. (2008). Allometry, biomass, and productivity of mangrove forests: A review. *Aquatic Botany*, 89(2), 128–137. <https://doi.org/10.1016/j.aquabot.2007.12.006>
- Kuenzer, C., Bluemel, A., Gebhardt, S., Quoc, T. V., & Dech, S. (2011). *Remote sensing of mangrove ecosystems: A review. Remote Sensing* (Vol. 3). <https://doi.org/10.3390/rs3050878>
- Laar, A. van, & Akca, A. (2007). *Forest Mensuration*. Springer. <https://doi.org/10.15713/ins.mmj.3>
- Larjavaara, M., & Muller-Landau, H. C. (2013). Measuring tree height: A quantitative comparison of two common field methods in a moist tropical forest. *Methods in Ecology and Evolution*, 4(9), 793–801. <https://doi.org/10.1111/2041-210X.12071>
- Le Toan, T., Quegan, S., Woodward, I., Lomas, M., Delbart, N., & Picard, G. (2004). Relating radar remote sensing of biomass to modelling of forest carbon budgets. *Climatic Change*, 67(2–3), 379–402. <https://doi.org/10.1007/s10584-004-3155-5>
- Lee, S. Y., Primavera, J. H., Dahdouh-Guebas, F., Mckee, K., Bosire, J. O., Cannicci, S., ... Record, S. (2014). Ecological role and services of tropical mangrove ecosystems: A reassessment. *Global Ecology and Biogeography*, 23(7), 726–743. <https://doi.org/10.1111/geb.12155>
- Liang, X., Kankare, V., Hyypä, J., Wang, Y., Kukko, A., Haggren, H., ... Vastaranta, M. (2016). Terrestrial laser scanning in forest inventories. *ISPRS Journal of Photogrammetry and Remote Sensing*, 115, 63–77. <https://doi.org/10.1016/j.isprsjprs.2016.01.006>
- Mcroberts, R. E., Tomppo, E. O., & Czaplowski, R. L. (1992). Sampling Designs for National Forest Assessments, 1–19. Retrieved from <http://www.fao.org/forestry/44859-02cf95ef26dfdcb86c6be2720f8b938a8.pdf>
- Mohan, M., Silva, C. A., Klauberg, C., Jat, P., Catts, G., Cardil, A., ... Dia, M. (2017). Individual tree detection from unmanned aerial vehicle (UAV) derived canopy height model in an open canopy mixed conifer forest. *Forests*, 8(9), 1–17. <https://doi.org/10.3390/f8090340>
- Nagelkerken, I., Blaber, S. J. M., Bouillon, S., Green, P., Haywood, M., Kirton, L. G., ... Somerfield, P. J. (2008). The habitat function of mangroves for terrestrial and marine fauna: A review. *Aquatic Botany*, 89(2), 155–185. <https://doi.org/10.1016/j.aquabot.2007.12.007>
- Nex, F. (2017). UAV for Earth Observation Structure from Motion - SfM: Powerpoint slides. Retrieved from [blackboard.utwente.nl/bbcswebdav/pid-1059942-dt-content-rid-2617656\\_2/courses/M17-EOS-104/04\\_SfM.pdf](http://blackboard.utwente.nl/bbcswebdav/pid-1059942-dt-content-rid-2617656_2/courses/M17-EOS-104/04_SfM.pdf)
- Nex, F. (2018). Unmanned Aerial Vehicles for Earth Observation 2018. Retrieved from <http://www.ncl.ac.uk/ceser/research/observation/uav-ese-applications/%5Cnhttp://www.ncl.ac.uk/ceser/researchprogramme/observationmonitoring/uavsfo-reseapplications/>
- Nex, F., & Remondino, F. (2014). UAV for 3D mapping applications: A review. *Applied Geomatics*, 6(1), 1–15. <https://doi.org/10.1007/s12518-013-0120-x>
- Odia, B. E. (2018). (Uav) Datasets for Retrieval of Forest Parameters and Estimation of Aboveground Biomass in Berkelah Tropical.

- Otero, V., Van De Kerchove, R., Satyanarayana, B., Martínez-Espinosa, C., Fisol, M. A. Bin, Ibrahim, M. R. Bin, ... Dahdouh-Guebas, F. (2018). Managing mangrove forests from the sky: Forest inventory using field data and Unmanned Aerial Vehicle (UAV) imagery in the Matang Mangrove Forest Reserve, peninsular Malaysia. *Forest Ecology and Management*, 411(December 2017), 35–45. <https://doi.org/10.1016/j.foreco.2017.12.049>
- Panagiotidis, D., Abdollahnejad, A., Surový, P., & Chiteculo, V. (2017). Determining tree height and crown diameter from high-resolution UAV imagery. *International Journal of Remote Sensing*, 38(8–10), 2392–2410. <https://doi.org/10.1080/01431161.2016.1264028>
- Persoon, G. A., & Simarmata, R. (2014). Undoing “marginality”: The islands of the Mahakam Delta, East Kalimantan (Indonesia). *Journal of Marine and Island Cultures*, 3(2), 43–53. <https://doi.org/10.1016/j.imic.2014.11.002>
- Petrokofsky, G., Kanamaru, H., Achard, F., Goetz, S. J., Joosten, H., Holmgren, P., ... Wattenbach, M. (2012). Comparison of methods for measuring and assessing carbon stocks and carbon stock changes in terrestrial carbon pools. How do the accuracy and precision of current methods compare? A systematic review protocol. *Environmental Evidence*, 1(1), 1. <https://doi.org/10.1186/2047-2382-1-6>
- Pham, T. D., Yokoya, N., Bui, D. T., Yoshino, K., & Friess, D. A. (2019). Remote Sensing Approaches for Monitoring Mangrove Species, Structure, and Biomass: Opportunities and Challenges. *Remote Sensing*, 11(230), 1–24. <https://doi.org/10.3390/rs11020230>
- Phil Wilkes, Alvaro lau, Mathias Disney, Kim Calders, Andrew Burt, Jose Gonzales de Tanago, Harm Bartholomeus, Benjamin Brede, M. H. (2017). Data acquisition consideration for Terrestrial Laser Scanning of forest plots. *Remote Sensing of Environment*, 196(11 May 2017), 21.
- Pix4d. (2019). Pix4D User Manual. Retrieved from <https://support.pix4d.com/hc/en-us/articles/204272989-Offline-Getting-Started-and-Manual-pdf>
- Popescu, S. C., Wynne, R. H., & Nelson, R. F. (2003). Measuring individual tree crown diameter with lidar and assessing its influence on estimating forest volume and biomass. *Canadian Journal of Remote Sensing*, 29(5), 564–577. <https://doi.org/10.5589/m03-027>
- Pouliot, D. A., King, D. J., Bell, F. W., & Pitt, D. G. (2002). Automated tree crown detection and delineation in high-resolution digital camera imagery of coniferous forest regeneration. *Remote Sensing of Environment*, 82(2–3), 322–334. [https://doi.org/10.1016/S0034-4257\(02\)00050-0](https://doi.org/10.1016/S0034-4257(02)00050-0)
- Pretzsch, H., Biber, P., Uhl, E., Dahlhausen, J., Rötzer, T., Caldentey, J., ... Pauleit, S. (2015). Crown size and growing space requirement of common tree species in urban centres, parks, and forests. *Urban Forestry and Urban Greening*, 14(3), 466–479. <https://doi.org/10.1016/j.ufug.2015.04.006>
- Prieditis, G., Šmits, I., Arhipova, I., Dağis, S., & Dubrovskis, D. (2012). Tree diameter models from field and remote sensing data. *International Journal of Mathematical Models and Methods in Applied Sciences*, 6(6), 707–714.
- Rahman, M. Z. A., Bakar, M. A. A., Razak, K. A., Rasib, A. W., Kanniah, K. D., Kadir, W. H. W., ... Latif, Z. A. (2017). Non-destructive, laser-based individual tree aboveground biomass estimation in a tropical rainforest. *Forests*, 8(3). <https://doi.org/10.3390/f8030086>
- Remondino, F., Spera, M. G., Nocerino, E., Menna, F., & Nex, F. (2014). State of the art in high density image matching. *The Photogrammetric Record*, 29(146), 144–166. <https://doi.org/10.1111/phor.12063>
- Sadadi, O. (2016). Accuracy of Measuring Tree Height Using Airborne Lidar and Terrestrial Laser Scanner and Its Effect on Estimating Forest Biomass and Carbon Stock in Ayer Hitam Tropical Rain Forest Reserve, Malaysia, 77. Retrieved from [http://www.itc.nl/library/papers\\_2016/msc/nrm/ojoatre.pdf](http://www.itc.nl/library/papers_2016/msc/nrm/ojoatre.pdf)
- Saenger, P., & Siddiqi, N. A. (1993). Land from the sea: The mangrove afforestation program of Bangladesh. *Ocean and Coastal Management*, 20(1), 23–39. [https://doi.org/10.1016/0964-5691\(93\)90011-M](https://doi.org/10.1016/0964-5691(93)90011-M)
- Schreuder, H. T., Gregoire, T. G., & Weyer, J. P. (2001). For what applications can probability and non-probability sampling be used? *Environmental Monitoring and Assessment*, 66(3), 281–291. <https://doi.org/10.1023/A:1006316418865>
- Selkowitz, D. J., Green, G., Peterson, B., & Wylie, B. (2012). A multi-sensor lidar, multi-spectral and multi-angular approach for mapping canopy height in boreal forest regions. *Remote Sensing of Environment*, 121, 458–471. <https://doi.org/10.1016/j.rse.2012.02.020>
- Shen, X., Cao, L., Chen, D., Sun, Y., Wang, G., & Ruan, H. (2018). Prediction of Forest Structural Parameters Using Airborne Full-Waveform LiDAR and Hyperspectral Data in Subtropical Forests. *Remote Sensing*, 10(11), 1729. <https://doi.org/10.3390/rs10111729>
- Sidik, A. (2010). The change of mangrove ecosystem in Mahakam Delta, Indonesia : a complex social

- environmental pattern of linkages in resources utilization. *Borneo Research Journal*, 4(November 2008), 27–46.
- Soares, M. L. G., & Schaeffer-Novelli, Y. (2005). Above-ground biomass of mangrove species. I. Analysis of models. *Estuarine, Coastal and Shelf Science*, 65(1–2), 1–18.  
<https://doi.org/10.1016/j.ecss.2005.05.001>
- Song, C., Dickinson, M. B., Su, L., Zhang, S., & Yaussey, D. (2010). Estimating average tree crown size using spatial information from Ikonos and QuickBird images: Across-sensor and across-site comparisons. *Remote Sensing of Environment*, 114(5), 1099–1107.  
<https://doi.org/10.1016/j.rse.2009.12.022>
- Srivastava, P. B. L., Guan, S. L., & Muktar, A. (1988). Progress of Crop in Some Rhizophora Stands before First Thinning in Matang Mangrove Reserve of Peninsular Malaysia. *Perlanika*, 11(3), 365–374.
- Stereńczak, K., Mielcarek, M., Wertz, B., Bronisz, K., Zajączkowski, G., Jagodziński, A. M., ... Skorupski, M. (2018). Factors influencing the accuracy of ground-based tree-height measurements for major European tree species. *Journal of Environmental Management*, 231(June 2018), 1284–1292.  
<https://doi.org/10.1016/j.jenvman.2018.09.100>
- Stickler, C. M., Nepstad, D. C., Coe, M. T., McGrath, D. G., Rodrigues, H. O., Walker, W. S., ... Davidson, E. A. (2009). The potential ecological costs and cobenefits of REDD: A critical review and case study from the Amazon region. *Global Change Biology*, 15(12), 2803–2824.  
<https://doi.org/10.1111/j.1365-2486.2009.02109.x>
- Suhardiman, A., Tsuyuki, S., & Setiawan, Y. (2016). Estimating Mean Tree Crown Diameter of Mangrove Stands Using Aerial Photo. *Procedia Environmental Sciences*, 33, 416–427.  
<https://doi.org/10.1016/j.proenv.2016.03.092>
- Suhardiman, A., Tsuyuki, S., Sumaryono, M., & Sulistioadi, Y. B. (2013). Geostatistical Approach for Site Suitability Mapping of Degraded Mangrove Forest in the Mahakam Delta, Indonesia. *Journal of Geographic Information System*, 05(05), 419–428. <https://doi.org/10.4236/jgis.2013.55040>
- Tian, J., Wang, L., Li, X., Gong, H., Shi, C., Zhong, R., & Liu, X. (2017). Comparison of UAV and WorldView-2 imagery for mapping leaf area index of mangrove forest. *International Journal of Applied Earth Observation and Geoinformation*, 61(May), 22–31. <https://doi.org/10.1016/j.jag.2017.05.002>
- Torresan, C., Berton, A., Carotenuto, F., Di Gennaro, S. F., Gioli, B., Matese, A., ... Wallace, L. (2016). Forestry applications of UAVs in Europe: a review. *International Journal of Remote Sensing*, 38(8–10), 1–21. <https://doi.org/10.1080/01431161.2016.1252477>
- Tuan, V. Q., Kuenzer, C., Quang Minh, V., Moder, F., & Oppelt, N. (2012). Review of valuation methods for mangrove ecosystem services. *Ecological Indicators*, 23, 431–446.  
<https://doi.org/10.1016/j.ecolind.2012.04.022>
- US Agency for International Development. (2014). REDD+ Measurement, Reporting and Verification (MRV) Manual Version 2.0 : Overview, (December), 41.
- Wallace, L., Lucieer, A., Malenovsky, Z., Turner, D., & Vopěnka, P. (2016). Assessment of forest structure using two UAV techniques: A comparison of airborne laser scanning and structure from motion (SfM) point clouds. *Forests*, 7(3), 1–16. <https://doi.org/10.3390/f7030062>
- Wannasiri, W., Nagai, M., Honda, K., Santitamnont, P., & Miphokasap, P. (2013). Extraction of mangrove biophysical parameters using airborne LiDAR. *Remote Sensing*, 5(4), 1787–1808.  
<https://doi.org/10.3390/rs5041787>
- Warren-Rhodes, K., Schwarz, A. M., Boyle, L. N., Albert, J., Agalo, S. S., Warren, R., ... Duke, N. (2011). Mangrove ecosystem services and the potential for carbon revenue programmes in Solomon Islands. *Environmental Conservation*, 38(4), 485–496. <https://doi.org/10.1017/S0376892911000373>
- Woodroffe, C. D., Rogers, K., McKee, K. L., Lovelock, C. E., Mendelssohn, I. A., & Saintilan, N. (2016). Mangrove Sedimentation and Response to Relative Sea-Level Rise. *Annual Review of Marine Science*, 8(1), 243–266. <https://doi.org/10.1146/annurev-marine-122414-034025>
- World Agroforestry Center, Nairobi, K. (n.d.). World Agroforestry Center 2018 Database. Retrieved February 16, 2019, from <http://db.worldagroforestry.org/wd/>
- Wu, J., Yao, W., Choi, S., Park, T., & Myneni, R. B. (2015). A Comparative Study of Predicting DBH and Stem Volume of Individual Trees in a Temperate Forest Using Airborne Waveform LiDAR. *IEEE Geoscience and Remote Sensing Letters*, 12(11), 2267–2271. <https://doi.org/10.1109/LGRS.2015.2466464>
- Zahawi, R. A., Dandois, J. P., Holl, K. D., Nadwodny, D., Reid, J. L., & Ellis, E. C. (2015). Using lightweight unmanned aerial vehicles to monitor tropical forest recovery. *Biological Conservation*, 186, 287–295. <https://doi.org/10.1016/j.biocon.2015.03.031>
- Zarco-Tejada, P. J., Diaz-Varela, R., Angileri, V., & Loudjani, P. (2014). Tree height quantification using

very high resolution imagery acquired from an unmanned aerial vehicle (UAV) and automatic 3D photo-reconstruction methods. *European Journal of Agronomy*, 55, 89–99.  
<https://doi.org/10.1016/j.eja.2014.01.004>

Zhang, J., Hu, J., Lian, J., Fan, Z., Ouyang, X., & Ye, W. (2016). Seeing the forest from drones: Testing the potential of lightweight drones as a tool for long-term forest monitoring. *Biological Conservation*, 198(November), 60–69. <https://doi.org/10.1016/j.biocon.2016.03.027>

# APPENDICES

**Appendix 1:** Table sheet of fieldwork data collection

**DATA COLLECTION FORM FOR MAHAKAM DELTA, INDONESIA**

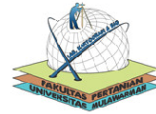
Plot No : ..... Date : .....  
 X : ..... Name of recorder : .....  
 Y : ..... Plot Radius Size : .....

Tree No	Species	DBH (cm)	Height (m)	Crown Diameter (m)	X-coordinate	Y-coordinate
1						
2						
3						
4						
5						
6						
7						
8						
9						
10						
11						
12						
13						
14						
15						
16						
17						
18						
19						
20						
21						
22						
23						
24						
25						
26						
27						
28						
29						
30						
31						
32						
33						
34						
35						

## Appendix 2: Ground control points (GCPs)



**LABORATORIUM KARTOGRAFI DAN SIG**  
**JURUSAN AGROTEKNOLOGI**  
**FAKULTAS PERTANIAN UNIVERSITAS MULAWARMAN**  
Jl. Tanah Grogot, Gedung Lab. Pertanian Terpadu Fakultas Pertanian UNMUL  
Telp. 0541 – 9019973 Email : [sig.fpunmul@gmail.com](mailto:sig.fpunmul@gmail.com)



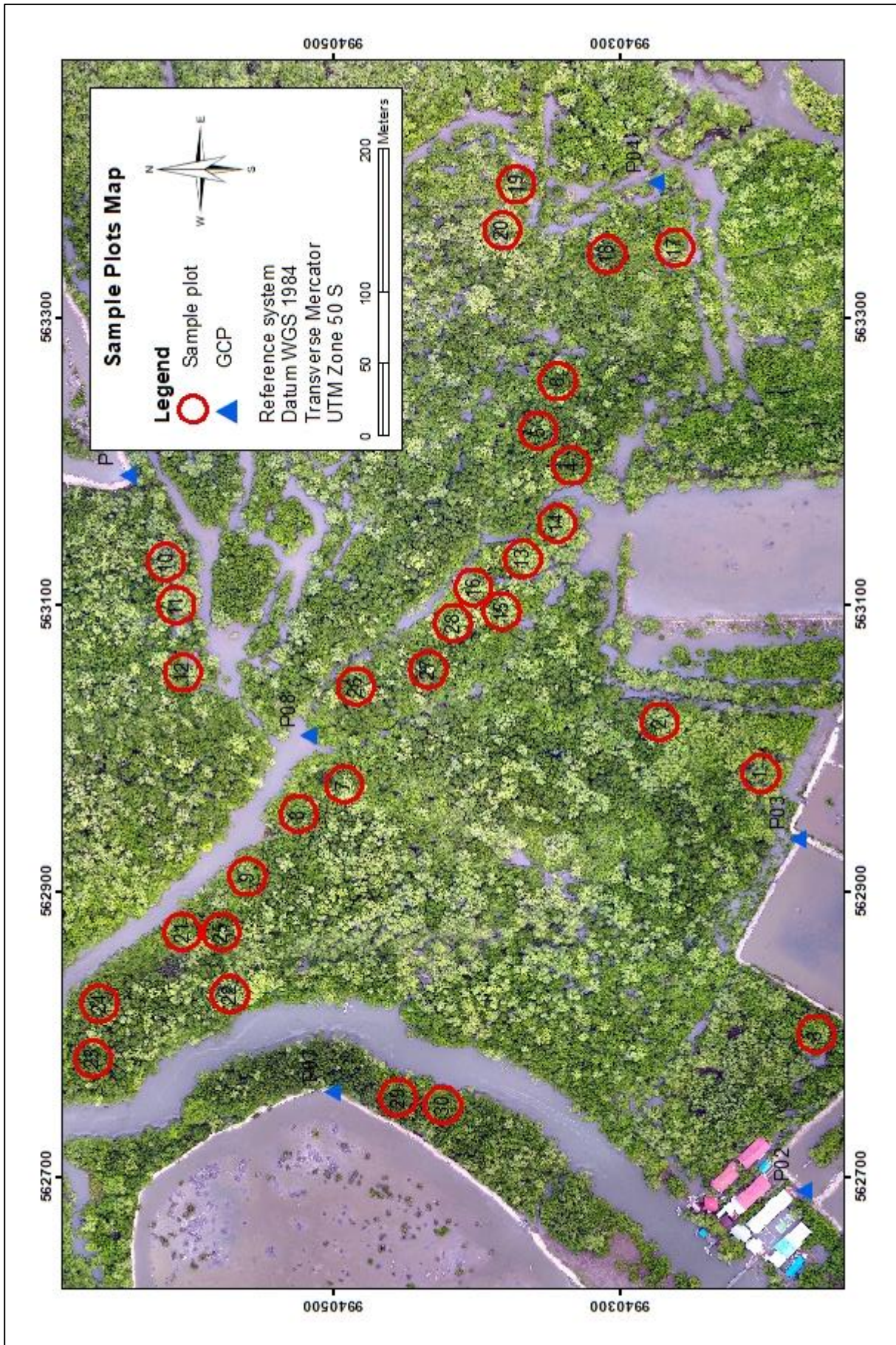
### Project Summary

Project name : Desa Tani Baru Kecamatan Anggana  
Surveyor : Lab. Kartografi dan SIG  
Linear unit : Meter  
Projection : WGS 1984 UTM Zone 50 S: 114E to 120E  
Geoid : egm2008

GCP	Grid South (m)	Grid Easting (m)	Elevation Ellipsoid (m)	Elevation Geoid (m)
P1	9940224.608	562524.875	57.125	2.536
P2	9940172.075	562690.730	55.216	0.622
P3	9940175.416	562936.649	55.745	1.145
P4	9940275.153	563395.743	57.363	2.752
P5	9940085.885	563193.727	55.544	0.938
P7	9940501.433	562760.572	59.291	4.695
P8	9940517.480	563008.710	56.701	2.099
P10	9940449.869	563584.217	55.680	1.063
P11	9940643.957	563190.955	58.282	3.674
P12	9940868.161	563102.093	56.540	1.934
P13	9940817.526	563516.187	57.653	3.036
P14	9940886.404	563680.670	62.659	8.038

Ditetapkan di : Samarinda  
Pada tanggal : 15 Oktober 2018  
Kepala,  
Lab. Kartografi dan SIG  
Fakultas Pertanian Unmul  
Donny Dhonanto, SP., M.Sc  
NIP. 19760325 200501 1 002

Appendix 3: Sample plots location



#### Appendix 4: Boxplot of the result

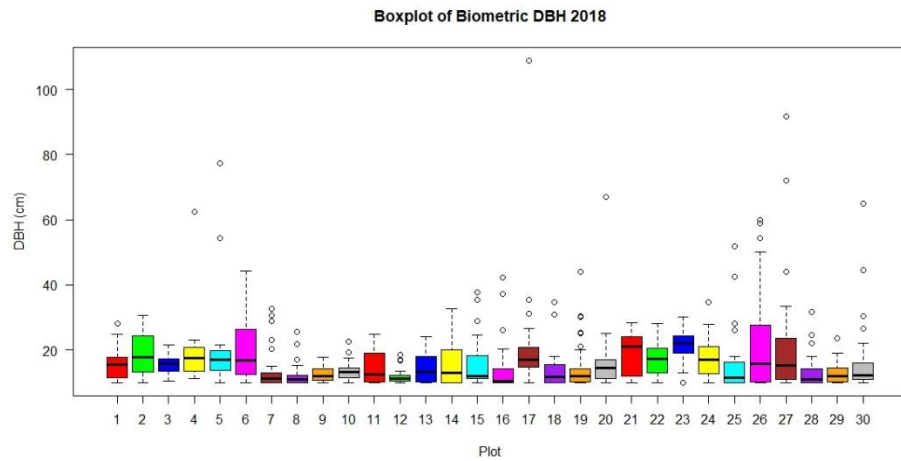


Figure 1 Boxplot of biometric DBH distribution of all 30 plots collected in this study.

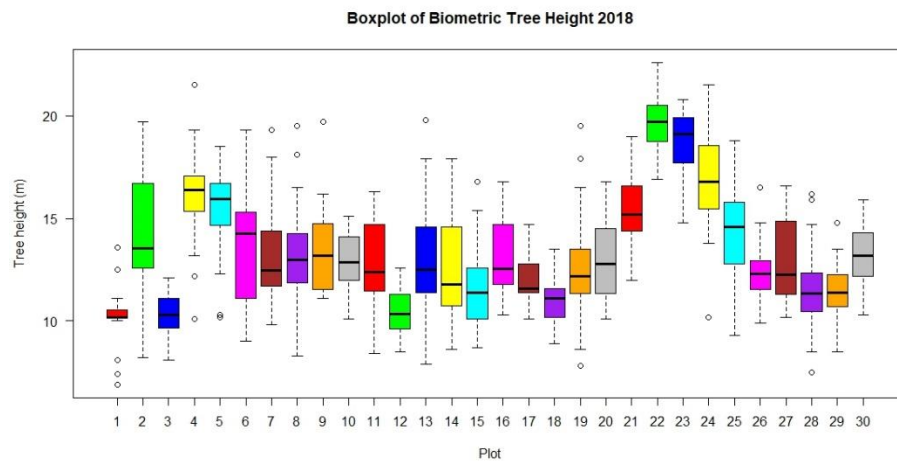


Figure 2 Boxplot of biometric trees height measured in the field using Leica DISTO D510 laser Ranger.

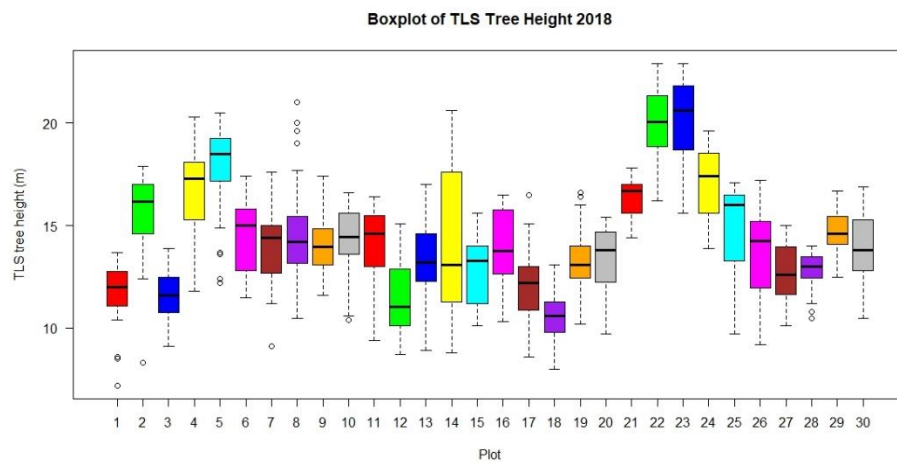


Figure 3 Boxplot of trees height derived from TLS point clouds data.

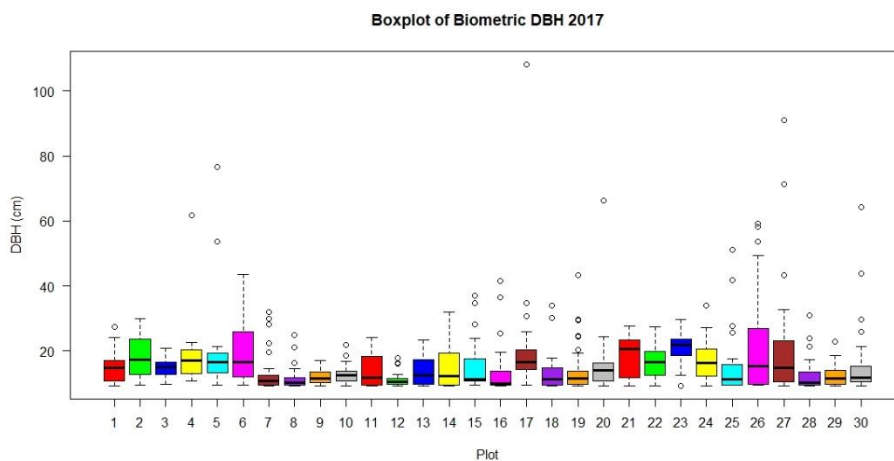


Figure 4 Boxplot of DBH of 2017 calculated using backward prediction.

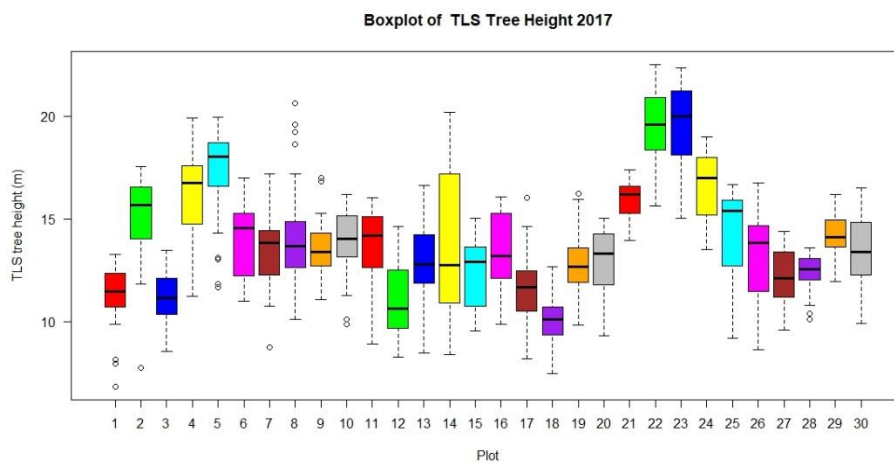


Figure 5 Boxplot of TLS trees height in 2017 calculated using backward prediction

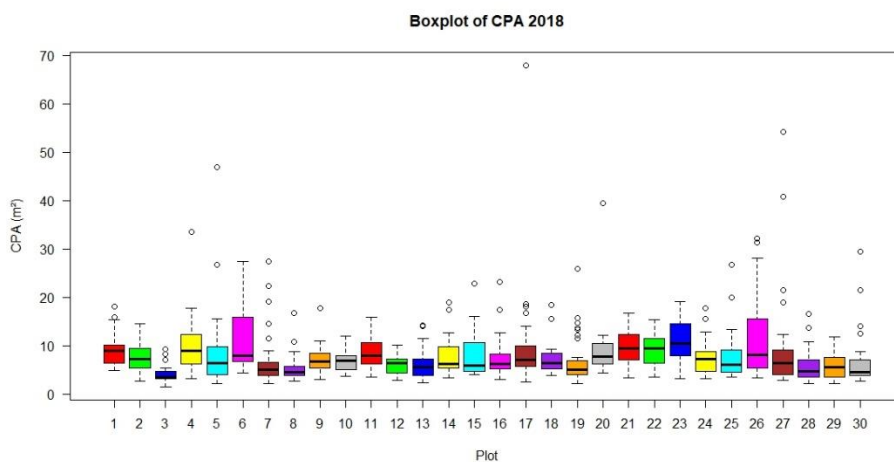


Figure 6 Boxplot of the crown projection area in 2018.

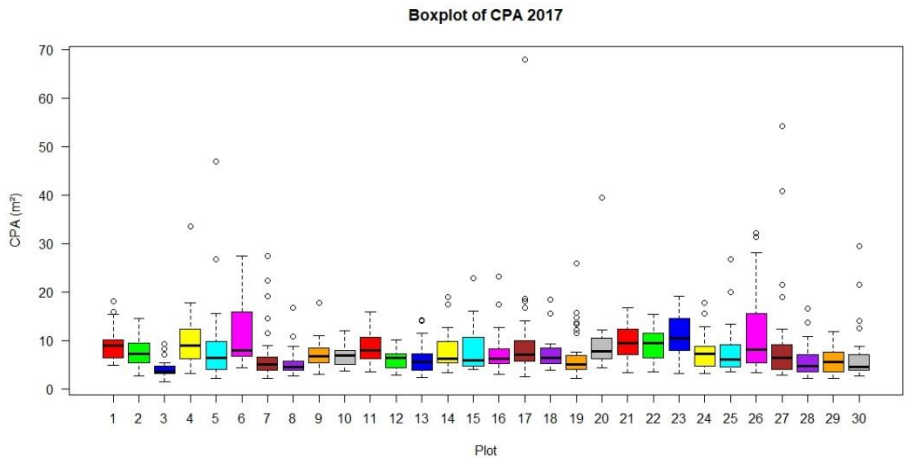


Figure 7 Boxplot of the trees crown projection area in 2017.

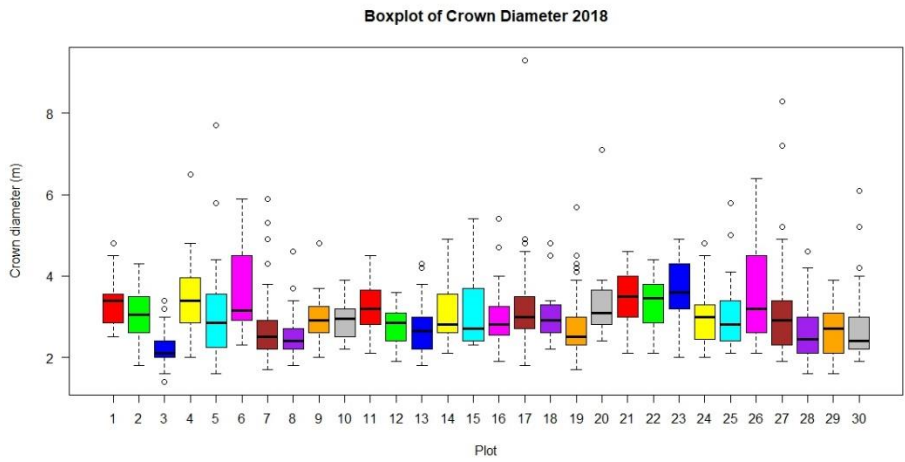


Figure 8 Boxplot of crown diameter of trees in 2018.

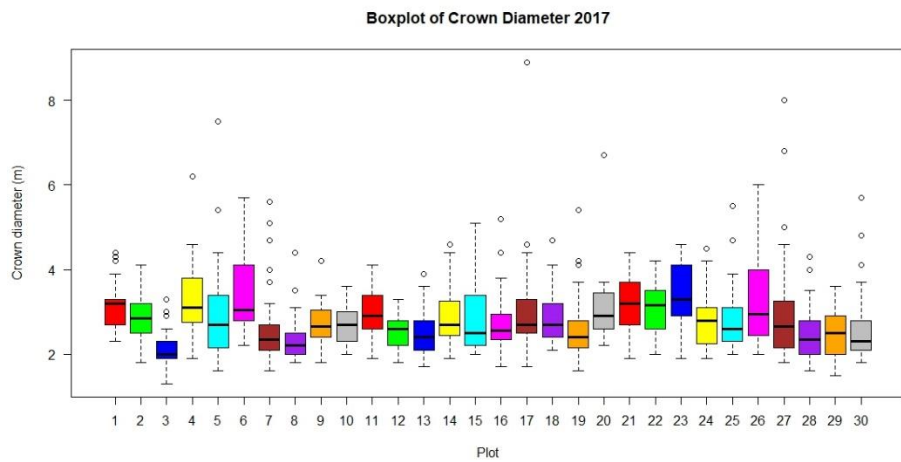


Figure 9 Boxplot of trees crown diameter in 2017.

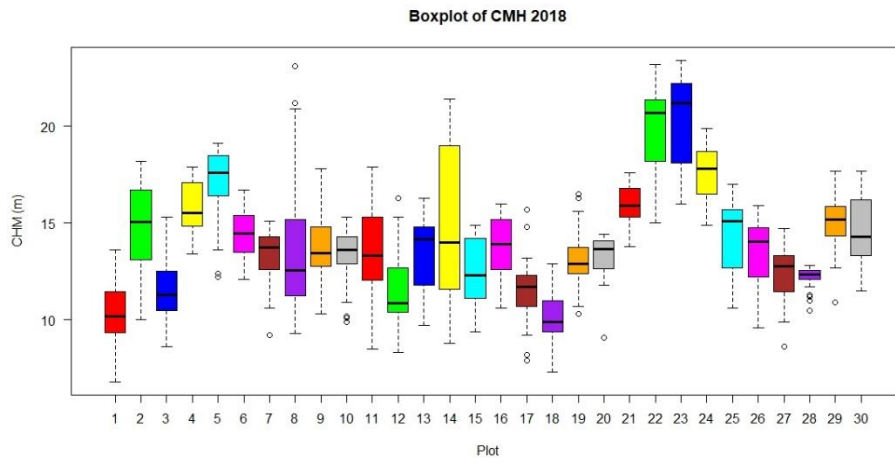


Figure 10 Boxplot of CHM 2018.

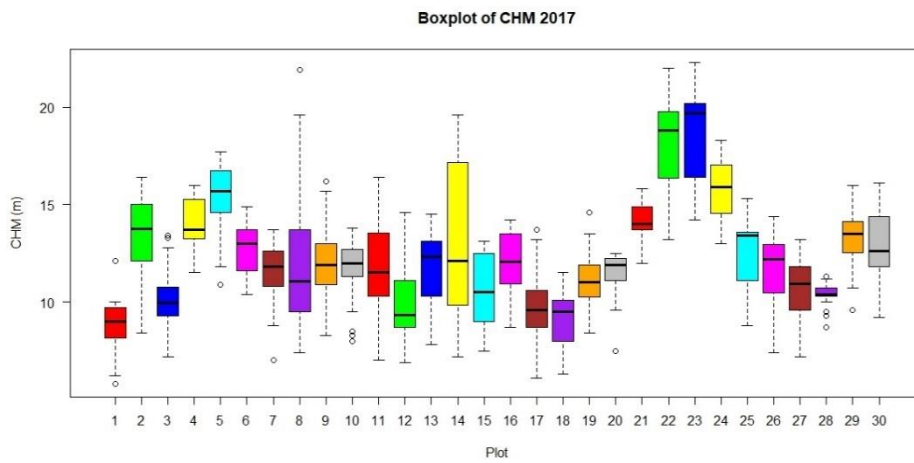


Figure 11 Boxplot of CHM 2018.

Appendix 5: Aboveground biomass per plot

Plot	AGB Biometric (Mg/ha)			AGB Model (Mg/ha)		
	2018	2017	Sequestration	2018	2017	Sequestration
1	55.6	49.4	6.2	72.6	65.4	7.2
2	138.0	125.9	12.1	147.3	134.5	12.8
3	75.2	66.5	8.7	96.6	87.0	9.6
4	157.0	146.3	10.7	174.3	162.4	11.9
5	293.3	273.9	19.4	274.4	258.7	15.7
6	102.8	94.9	7.9	109.5	99.7	9.7
7	108.4	97.5	10.9	108.0	94.9	13.1
8	77.8	68.9	8.8	72.8	60.4	12.4
9	72.3	63.6	8.7	80.6	70.9	9.7
10	69.0	60.5	8.5	80.5	71.0	9.5
11	66.9	59.5	7.4	82.4	74.3	8.1
12	33.2	28.5	4.7	48.5	42.2	6.3
13	87.5	77.7	9.8	83.5	72.3	11.2
14	117.2	106.8	10.3	106.3	94.4	11.9
15	80.3	72.8	7.5	80.3	70.8	9.4
16	94.0	85.3	8.7	87.0	76.7	10.2
17	201.4	189.1	12.3	180.9	168.3	12.5
18	40.1	36.1	4.0	53.7	48.6	5.1
19	93.7	84.7	9.0	88.1	77.6	10.5
20	101.1	92.6	8.5	92.0	81.5	10.6
21	102.0	93.3	8.7	104.0	92.9	11.1
22	143.2	130.7	12.5	92.7	80.1	12.6
23	208.0	193.4	14.6	192.1	177.1	15.0
24	112.6	103.0	9.6	104.0	92.9	11.1
25	107.9	100.0	7.9	96.9	87.4	9.5
26	190.1	178.2	11.9	170.4	156.8	13.6
27	215.8	201.2	14.7	195.0	180.0	15.0
28	73.9	65.5	8.4	74.6	64.8	9.8
29	72.8	64.5	8.3	87.2	77.7	9.5
30	131.6	120.6	11.0	138.6	125.9	12.6

Appendix 6: Carbon stock per plot

Plot	AGB Biometric (Mg/ha)			AGB Model (Mg/ha)		
	2018	2017	Sequestration	2018	2017	Sequestration
1	27.8	24.7	3.1	36.3	32.7	3.6
2	69.0	62.9	6.1	73.6	67.2	6.4
3	37.6	33.3	4.4	48.3	43.5	4.8
4	78.5	73.2	5.4	87.1	81.2	5.9
5	146.6	137.0	9.7	137.2	129.3	7.8
6	51.4	47.5	4.0	54.7	49.9	4.9
7	54.2	48.8	5.4	54.0	47.4	6.6
8	38.9	34.5	4.4	36.4	30.2	6.2
9	36.1	31.8	4.4	40.3	35.4	4.8
10	34.5	30.2	4.3	40.2	35.5	4.7
11	33.5	29.8	3.7	41.2	37.2	4.0
12	16.6	14.3	2.3	24.3	21.1	3.1
13	43.8	38.8	4.9	41.8	36.2	5.6
14	58.6	53.4	5.2	53.2	47.2	5.9
15	40.2	36.4	3.7	40.1	35.4	4.7
16	47.0	42.7	4.3	43.5	38.4	5.1
17	100.7	94.5	6.2	90.4	84.2	6.3
18	20.0	18.1	2.0	26.9	24.3	2.6
19	46.8	42.3	4.5	44.0	38.8	5.2
20	50.5	46.3	4.3	46.0	40.7	5.3
21	51.0	46.7	4.3	52.0	46.5	5.5
22	71.6	65.4	6.2	46.4	40.1	6.3
23	104.0	96.7	7.3	96.1	88.6	7.5
24	56.3	51.5	4.8	52.0	46.5	5.5
25	54.0	50.0	3.9	48.4	43.7	4.8
26	95.1	89.1	6.0	85.2	78.4	6.8
27	107.9	100.6	7.3	97.5	90.0	7.5
28	37.0	32.8	4.2	37.3	32.4	4.9
29	36.4	32.3	4.1	43.6	38.8	4.8
30	65.8	60.3	5.5	69.3	63.0	6.3